Diplomarbeit

Biomarkers in Melanoma Patients Treated with Immune-Checkpoint Inhibitors

Evaluation of Mismatch Repair Deficiency, Microsatellite Status and Total Mutation Load and Their Relationship with Prognosis and Treatment Response.

eingereicht von

Maximilian Christian Köller

zur Erlangung des akademischen Grades

Doktor(in) der gesamten Heilkunde

(Dr. med. univ.)

an der

Medizinischen Universität Graz

ausgeführt am

Diagnostik & Forschungsinstitut für Pathologie

unter der Anleitung von

Univ. FÄ Priv. Doz.in Dr.med.univ. Ariane Aigelsreiter

und

Univ.-Prof.in Priv.-Doz.in Dr.med.univ. Erika Richtig

Graz, am 08.11.2020

Eidesstattliche Erklärung

Ich erkläre ehrenwörtlich, dass ich die vorliegende Arbeit selbstständig und ohne fremde Hilfe verfasst habe, andere als die angegebenen Quellen nicht verwendet habe und die den benutzten Quellen wörtlich oder inhaltlich entnommenen Stellen als solche kenntlich gemacht habe.

Graz, am 08.11.2020 *Maximilian Christian Köller eh*

Danksagungen

Eingangs möchte ich meinen Diplomarbeitsbetreuerinnen Frau Univ.-FÄ Priv.-Doz.in Dr.med.univ Ariane Aigelsreiter sowie Univ.-Prof.in Priv.-Doz.in Dr.med.univ. Erika Richtig für Ihre langjährige Betreuung, auch über den Rahmen der Diplomarbeit hinweg herzlich danken!

Weiters meiner gesamten Familie und insbesondere meinen Eltern, welche mich stets auf meinem bisherigen Lebensweg emotional, strukturell, unvoreingenommen und bedingungslos unterstützt haben!

Auch möchte ich an dieser Stelle noch eine ausgewählte Liste an Freunden nennen, mit welchen ich die Freude und das Glück hatte, gemeinsam meinen bisherigen Lebens- und Bildungsweg zu beschreiten:

Dr.med.univ. Rüdiger Hochstätter, MSc, Markus Krainz, BSc, Dr.med.univ. Dino Mehic, Dr.med.univ. Gregor Senekowitsch, Martin Stadler, MSc und Dr.med.univ. Sebastian Wrighton

Vielen Dank an jeden von Euch!

Abschließend möchte ich mich besonders bei meiner Lebensgefährtin Christiane Wakonig, BA für die wundervollen vergangenen gemeinsamen Jahre sowie für all ihre Energie, Stunden und aufmunternden Worte bedanken, welche Sie mir durchwegs, aber im Besonderen gegen Ende der Fertigstellung dieser Arbeit gespendet hat!

Table of Content

Abbreviations

For readability and clarity all defined abbreviations or terms within this thesis will be written in italic letters. Italic letters will only be used for abbreviated or defined terms and direct quotes.

Symbols

:= defined as:

Persons

AA := Univ. FÄ Priv.-Doz.in Dr.med.univ. Ariane Aigelsreiter[1]
EJ := Dr.med.univ. Elmar Janek[4]
ER := Univ.-Prof.in Priv.-Doz.in Dr.med.univ. Erika Richtig[3]
ES := Mag.a rer.nat. Dr.scient.med. Elke Stadelmayer[2]
EW := Elke Winter[2]
KK := Priv.-Doz. Mag. Dr.phil. Karl Kashofer[2]
MB := Dr.med.univ. Marina Berger[3]
MK := Maximilian Köller[1]
SE := Stefan Eder[1]

Terms abbreviated within this Study

AUC := area under the curve
bp := base pair
CBG := clinical benefit group
chr := chromosome
CI := confidence interval
CM := cutaneous melanoma
CR := complete remission
CTLA-4 := cytotoxic T-lymphocyte-associated antigen-4
dMMR := defective mismatch repair
EXO1 := exonuclease 1
HNPCC := non-polyposis colorectal cancer kindreds
ICI := immune-checkpoint inhibitors
IHC := immunohistochemistry
IQR := inter quartile range
irAE := immune-related adverse event
ISH := in-situ hybridization
LDH := lactic dehydrogenase
LOH := loss of heterozygosity
max := maximum
Mb := mega bases
min := minimum
MM := malignant melanoma
MMR := DNA mismatch repair
MS := microsatellites
MSI := microsatellite instability
MSI-H := *MSI*-high
MSI-L := *MSI*-low
MSS := microsatellite stable

mut/mB :=	mutations per mega base
NGS :=	next generation sequencing
non-CBG :=	clinical non-benefit group
nt :=	nucleotide
ORR :=	overall response rate
OS :=	overall survival
oTR :=	objective treatment response
PCR :=	polymerase chain reaction
PD :=	progression of disease
PDL-1:=	programmed-death-receptor 1 ligand
PD1 :=	programmed-death-receptor 1
PFS :=	progress free survival
PNCA :=	proliferating cellular nuclear antigen
Pol δ :=	DNA polymerase δ
PR :=	partial response
RECIST 1.1 :=	response evaluation criteria in solid tumors 1.1
RFC :=	replication factor C
SD :=	stable disease
sd :=	standard deviation
SNVs :=	short nucleotide variants
TMB :=	tumor mutational burden
TML :=	total mutation load
TR :=	treatment response
UP :=	melanoma of unknown primum
WES :=	whole exome sequencing

Institutions

[1]*DRI-Patho* :=	Diagnostic and Research Institute of Pathology of the Medical University of Graz
[2]*Molecular Diagnostic Lab* :=	Molecular Diagnostic Lab at the *DRI-Patho*
[3]*Dep.Derm.* :=	Department of Dermatology of the Medical University of Graz
[4]*Dep.Rad.* :=	Department of Radiology of the Medical University of Graz
BioBank Graz :=	BioBank of the Medical University of Graz

List of Figures

All figures have been created by using either of the following software (Inkscape [Version 0.92.4]), R [Version 3.6.1].

List of Tables

Zusammenfassung

Wissenschaftlicher Hintergrund:

Immun-Checkpoint Inhibitoren (:= *ICI*), wirksame Melanom (:= *MM*)-Therapeutika, sind mit schweren Nebenwirkungen und hohen Kosten verbunden. Daher ist die Entwicklung von validen Biomarkern von besonderer Relevanz.

Die Anzahl der Mutationen pro Mega-Base (:= *mut/Mb*) ist ein valider *ICI*-Biomarker im *MM*. Weiters bedingt eine defiziente Mismatch Repair (:= *dMMR*) eine Erhöhung der *mut/Mb* im Mausmodell und tritt in *MM* von Patienten/innen, welche von einer *ICI* profitieren, auf.

Methodik:

Studien-Kohorte: Patienten/innen mit *MM* (kutanem, unbekannten Ursprungs), welche zwischen 2012-2016 an der Abteilung für Dermatologie der Medizinischen Universität mit *ICI* behandelt wurden.

Archiviertes Tumorgewebe wurde mit folgenden Methoden untersucht:

dMMR: Immunhistochemie (MLH1, MSH2, MSH6 und PMS2) in 23, Polymerase Chain Reaction gekoppelter Fragment-Analyse in fünf Patienten/innen;

mut/Mb: Oncomine TML Assay (Thermo Scientific) in 14 Patienten/innen, welche in Gruppen, in Abhängigkeit des Therapieansprechens (sehr gutes Ansprechen (n = 6), kein Ansprechen (n = 7), unterteilt wurden.

Ergebnisse:

Es wurde kein Verlust der Proteinfärbung beobachtet (0 % (0/23), 95% *CI*: 0.00 – 14.81 %). Alle *MM* wiesen einen microsatelliten-stabilen Phänotyp auf (100 % (0/5)) mit Verlust der Heterozygotie in 40 % (2/5) am Mikrosatelliten Locus Penta-D.

Die *mut/Mb* war signifikant höher (einseitiger Mann-Whittney-U Test: p-value = 0.03671, n = 13) in Patienten/innen mit sehr gutem *ICI* Ansprechen. Die *mut/Mb* besaß gute prädiktive Mächtigkeit in der Vorhersage des *ICI*- Ansprechens (Receiver Operative Curve: Area under the curve = 0.810 (*CI* 0.561 – 1.00), Cut-Off = Youden's J 9.51 [*mut/Mb*] (100 % Sensitivität, 57.1 % Spezifität)).

Es bestand kein Zusammenhang zwischen dem Prozentsatz positiv gefärbter Tumorzellen und der *mut/Mb*.

Es bestand eine signifikante Differenz des Prozentsatzes an MLH1-positiv gefärbten Tumorzellen zwischen *MM* welche sehr gut und nicht auf *ICI* ansprachen (zweiseitiger Mann-Whitney-U Test: p-value = 0.00168, n = 14).

Konklusion:

Wir schließen aus der Literatur und unseren Ergebnissen, dass *dMMR*: -nur in einer kleinen Teilmenge von mit *ICI* behandelten *MMs* vorkommt, -nur eine geringe Rolle in der Pathogenese von *MMs* mit erhöhter *mut/Mb* einnimmt;

Unsere Studie validiert die Nutzung des Oncomine *TML* Assay als *ICI*-Biomarker im *MM*.

Die beobachtete Relation des Prozentsatzes MLH1-positiver Zellen und des *ICI*-Ansprechens sollte in weiteren Studien überprüft werden.

Abstract

Scientific Background

The occurrence of severe adverse events and high expenses in the immune checkpoint inhibitor (:= *ICI)* treatment of malignant melanoma (:= *MM*) prompts the necessity of reliable biomarkers for the clinical practice.

The rate of mutations per mega base (:= *mut/Mb*) is a viable *ICI*-biomarker in *MM*. An increase of novel mutations due to defective mismatch repair (:= *dMMR*) occurs in *MM* mouse models and *dMMR* has been observed in *MM* patients benefitting from *ICI*.

Methods

Patients: *MM* patients (cutaneous, unknown primary) treated with *ICI* between 2012-2016 at the Department of Dermatology of the Medical University of Graz.

Archived tissues samples were investigated using:

dMMR: Immunohistochemistry (MLH1, MSH2, MSH6 and PMS2) in 23, polymerase chain reaction-based microsatellite fragment length analysis assay in 5 patients;

mut/Mb: Oncomine TML Assay (Thermo Scientific) in 14 patients, grouped into a clinical benefit (n = 6) and a clinical non-benefit group (n = 7) (:= *CBG, non-CBG,* respectively).

Results

No loss of protein staining was detected (0% (0/23) *CI*: 0.00 – 14.81%). A microsatellite stable phenotype was observed in all tumors (100% (5/5)), with 40 % (2/5) showing loss of heterozygosity at the Pent-D locus.

The *mut/Mb* was significantly higher in *MM* of the *CBG* (one-sided Wilcoxon test: p-value = 0.03671, n = 13). The *mut/Mb* was a feasible predictive biomarker (Receiver Operative Curve: Area under the curve = 0.810 (*CI* 0.561 – 1.00), Cut-Off = Youden's J 9.51 [*mut/Mb*] (100 % sensitivity, 57.1 % specificity)).

No correlation between the *mut/Mb* and the percentage of positively stained cells was found.

A significant difference in the percentage of MLH1-positively stained tumor cells between the *CBG* and *non-CBG* (two-sided Wilcoxon test: p-value = 0.00168, n = 14) was found.

Conclusion

We infer from the literature and our findings that *dMMR*: -occurs in a small subset of *MM* treated with *ICI*, -plays a minor role in the pathogenesis of *MMs* with increased *mut/Mb*;

Our study validates the use of the *TML*-assay as a predictive *ICI*-biomarker in *MM*.

The observed relationship between the percentage of MLH1-positive tumor cells and treatment outcome should be validated by further studies.

Declaration of Previous Publications

Some findings of this Thesis have already been presented at the European Congress of Pathology 2018 and an abstract was published:

Koeller M, Berger M, Eder S, Richtig G, Richtig E, Pichler M, et al. Is microsatellite-instability a prognostic factor in melanoma patients treated with immune-checkpoint inhibitors? VIRCHOWS Arch. 2018 Sep;473(1):S9–10.

1 Introduction

The introduction of this thesis is conceptually structured in three main parts, starting with the relevant background information and current scientific knowledge about the research field. Proceeding with the motivation to conduct new research in this area and lastly the hypotheses, inferred from the current evidence that underly this study, and the research questions.

1.1 *Scientific Background*

1.1.1 Malignant Melanoma

Definition

Considering the Medical Subject Headings (MeSH®)(1), provided by the U.S. National Library of Congress, *malignant melanoma* (:= *MM*) is defined as:

> *"A malignant neoplasm derived from cells that are capable of forming melanin, which may occur in the skin of any part of the body, […]"* (2)

This definition will be adopted within this thesis. Furthermore, the term *cutaneous melanoma* (:= *CM*) will be used for *MM* originating from the skin. And the term *melanoma of unknown primum* (:= *UP*) refers to all *MM* for whom the origin of their primum is unknown.

Etiology

There is great consensus about the risk of developing *MM* being closely related to a set of constitutional, acquired and post-expositional factors (3).

Constitutional factors comprise the individual Fitzpartick skin type and the existence of large (> 20 [cm]) congenital nevi whereas acquired factors are the number of newly acquired melanocytic nevi, positive family history, clinical atypical areas of pigmentation, and previous *MM* in the patient's medical history (3). The most important post-expositional factor seems to be the exposure to sun light (3).

For a long time, hypotheses regarding this factor (i.e. UV light) have been based solely on epidemiologic studies and the fact that DNA damage can be caused by UV-light (4).

However, the evidence strengthening this hypothesis on a molecular basis is growing, as most of the somatic base substitutions in cell lines of metastatic *MM* were observed to be C>T/G>A transitions, which have been linked to UV-light exposure (5). Furthermore, BRAF mutations occur significantly more often on skin areas with intermittent sun exposure, than

on areas of chronic or no exposure (6). This is of importance, as between 50 – 60 % of *MM* seem to have mutations of the BRAF gene (7).

Furthermore, considering the positive family history, there also is molecular evidence that the risk of developing a *MM* can be explained by inherited genetical changes, especially mutations within the CDKN2A gene (8,9).

Epidemiology

The incidence of *MM* has been raising worldwide since the 1950s (10). This could also be shown for Austria, were the age-standardized incidence rates increased significantly from 4.9 in 1983 to 10.5/100.000 in 2008 (11). However, the actual rates might be substantially higher since an active reevaluation of *MM* incidence rates of the year 2011 showed a world age-standardized rate of 25/100.000 per inhabitants (10). In general, men seem to have a greater life time risk to develop a *MM* compared to women (11).

Considering geographic factors in Austria, it has been shown that incidence rates are associated to altitude (increase in rates per 10 m altitude) and whether a person lives in rural or urban areas (higher rates for the latter) (12).

Classification

Considering the UICC TNM Classification of Malignant Tumors *MM* of the skin is classified and staged as follows (13):

pTNM Pathological Classification

pT – Primary Tumor

pTx :=	Primary tumor cannot be assessed (this includes shave biopsies and regressed melanomas)
pT0 :=	No evidence of primary tumor
pTis :=	Melanoma in situ (Clark level 1) (atypical melanocytic hyperplasia, severe melanocytic dysplasia, not an invasive malignant lesion)
pT1 := pT1a := pT1b :=	Tumor 1 mm or less in thickness 0.8 mm or less in thickness without ulceration 0.8 mm in thickness with ulceration **or** more than 0.8 mm but no more than 1 mm in thickness, with or without ulceration
pT2 :=	Tumor more than 1 mm but not more than 2 mm in thickness

pT2a :=	Without ulceration
pT2b :=	With ulceration

pT3 :=	Tumor more than 2 mm but not more than 4 mm in thickness
pT3a :=	Without ulceration
pT3b :=	With ulceration
pT4 :=	Tumor more than 4 mm in thickness
pT4a :=	Without ulceration
pT4b :=	With ulceration

pN – Regional Lymph Node

pNX :=	Regional lymph nodes cannot be assessed
pN0 :=	No regional lymph node metastasis Histological examination of a regional lymphadenectomy specimen will ordinarily include 6 or more lymph nodes. If the lymph nodes are negative, but the number ordinarily examined is not met, classify as pN0. Classification based solely on sentinel node biopsy without subsequent axillary lymph node dissection is designated (sn) for sentinel node, e.g. (p)N1(sn).
pN1 :=	Metastasis in one regional lymph node or intratympanic regional metastasis without modal metastases
pN1a :=	Only microscopic metastasis (clinically occult)
pN1b :=	Macroscopic metastasis (clinically apparent)
pN1c :=	Satellite or in-transit metastasis without regional nodal metastasis
pN2 :=	Metastasis in two or three regional lymph nodes or intratympanic regional metastasis with lymph node metastases
pN2a :=	Only microscopic metastasis (clinically occult)
pN2b :=	Macroscopic metastasis (clinically apparent)
pN2c :=	Satellite or in-transit metastasis with only one regional nodal metastasis
pN3 :=	Metastasis in four or more regional lymph nodes, or matted metastatic regional lymph nodes, or satellite(s) or in-transit metastasis with metastasis in two or more regional lymph node(s)
pN3a :=	Only microscopic metastasis (clinically occult)
pN3b :=	Macroscopic metastasis (clinically apparent)
pN3c :=	Satellite(s) or in-transit metastasis with two or more regional nodal metastasis

pM – Distant Metastasis

M0 :=	No distant metastasis (**CAVE:** pM0 is not a valid category)
pM1 :=	Distant metastasis Suffixes: - (0) := lactic dehydrogenase (:= *LDH*) – not elevated - (1) := *LDH* – elevated No suffix is used if *LDH* is not recorded or unspecified.
pM1a :=	Skin, subcutaneous tissue or lymph node(s) beyond the regional lymph nodes
pM1b :=	Lung
pM1c :=	Other non-central nervous system sites
pM1d :=	Central nervous system

Pathological Stage

Stage	pT	pN	pM
0 :=	pTis	pN0	M0
I :=	pT1	pN0	M0
IA :=	pT1a	pN0	M0
	pT1b	pN0	M0
IB :=	pT2a	pN0	M0
IIA :=	pT2b	pN0	M0
	pT3a	pN0	M0
IIB :=	pT3b	pN0	M0
	pT4b	pN0	M0
IIC :=	pT4b	pN0	M0
III :=	Any pT	pN1, pN2, pN3	M0
IIIA	pT1a, pT1b, pT2a	pN1a, pN2a	M0
IIIB	pT1a, pT1b, pT2a	pN1b, pN1c, pN2b	M0
	pT2b-pT3a	pN1, pN2a, pN2b	M0
IIIC	pT1a, pT1b, pT2a, pT2b, pT3a	pN2c, pN3	M0
	pT3b, pT4a	pN1, pN2	M0
	pT4b	pN, pN2	M0
IIID	pT4b	pN3	M0
IV	Any pT	Any N	pM1

1.1.2 Immune Checkpoint Inhibitors in Malignant Melanoma

Immune checkpoint inhibitors (:= *ICI*) are a novel group of therapeutic agents used in the treatment of *MM* that comprises a set of monoclonal antibodies blocking co-inhibitory molecules expressed on T-lymphocytes (14). The *ICI* currently used in the therapeutic setting are directed against cytotoxic T-lymphocyte-associated antigen-4 (:= *CTLA-4*) expressed on activated $CD4^+$ and $CD8^+$ effector T-cells and regulatory T-cells, programmed-death-receptor 1 (:= *PD1*) also expressed on activated effector T-cells, as well as its ligand (:= *PDL-1*) expressed on dendritic cells, activated T-cells and tumor cells (14).

These new agents seem to be a feasible new therapeutic regiment, especially in metastatic *CM*, as a meta-analysis conducted by Yun et al. (15) was able to show that *ICIs* are associated with higher 6-month progress free survival (:= *PFS*), 1-year overall survival (:= *OS*) and overall response rate (:= *ORR*) in patients with metastatic *CM* compared to the control groups (15).

However, these agents do come with some drawbacks, as they exhibit a range of grade 3/4 immune-related adverse events (:= *irAE*) most commonly related to the endocrine system (e.g. disorders of the thyroid, pituitary and adrenal dysfunction), gastrointestinal tract (e.g. diarrhea, colitis and nausea), lung (pneumonitis), skin (e.g. rash, pruritus and vitiligo) and musculoskeletal apparatus (e.g. arthralgia and myalgia) (16). Furthermore, therapeutic regiments incorporating *ICIs* are, at the current state, rather expensive (17).

Lastly, it seems that there are differences in the treatment outcome of *ICIs* that depend on the sex of the patients since a meta-analysis conducted by Wu et al. (18) showed that males benefitted more from *ICI* treatment than females. However, both sexes did benefit from *ICI* when compared to the control group, with only one exception of a treatment with nivolumab (an *CTLA-4* inhibitor) in which females did not benefit from the treatment regimen (18). A similar effect was observed for *PFS,* as males exhibit longer *PFS* than females after *ICI* treatment, albeit both sexes had longer *PFS* compared to chemotherapy (18).

1.1.3 DNA Mismatch Repair and its Relation to Human Melanoma

1.1.3.1 DNA Mismatch Repair

The major role of the DNA mismatch repair (:= *MMR*) system is to correct DNA base mismatches and insertion/deletion loops that occur during DNA replication, repair and recombination (19). Therein, providing genomic stability during these processes, however, it also plays additional roles during meiosis and immunoglobulin maturation/-diversification in eukaryotes and mammals, respectively (19).

A set of proteins has been related to the *MMR* system in eukaryotes (i.e. MSH2, MSH3, MSH6, MLH1, MLH3, PMS1, PMS2, exonuclease 1 (:= *EXO1*), DNA polymerase δ (:= *Pol δ*), proliferating cellular nuclear antigen (:= *PNCA*), replication factor C (:= *RFC*)), of which certain proteins form protein complexes serving specific functions within the *MMR* system (i.e. MutSα (MSH2-MSH6), MutSβ (MSH2-MSH3), MutLα (MLH1-PMS2), MutLβ (MLH1-PMS1), MutLγ (MLH1-MLH3) (20).

As MutSα and MutLα are of immediate interest within this thesis, the molecular mechanisms of the *MMR* system in eukaryotic cells will only be discussed in terms of these protein complexes.

The mechanism during which these proteins interact, resulting in the repair of DNA mismatches, is thought to consist of a sequence of steps starting with recognition of the mismatch site followed by removal of the wrongly synthesized sequence on the nascent strand and re-synthesis of an correct nucleotide sequence (20). The sequence is initialized by MutSα, which recognizes mismatches (primarily base mismatches or small insertions or deletions up to 3 nucleotides) on double-strand DNA (19). Subsequently MutSα recruits MutLα forming a tetrameric complex (19). Next, MutLα, harboring a latent endonuclease, is able to introduce an incision into the double-stranded DNA with its endonuclease, which is thought to be stochastically activated by *PNCA* (19). *PNCA* is also thought to serve as the strand discrimination signal as the asymmetry of *PNCA* bound to the DNA may direct the incision only on the nascent strand (19). In a next step *EXO1* is recruited at the incision site and activated by MSH2 and/or MLH1 and excises the nascent strand (19). The resulting gap is re-synthesized by *Pol δ* and lastly ligated to the preexisting strand by DNA ligase 1 (19).

Considering the chromosomal location of the four *MMR* proteins (i.e. MSH2, MSH6, MLH1 and PMS2) investigated within this study, two of them are found on chromosome (:= *chr*) 2

(MSH2: *chr* 2p21, MSH6: *chr* 2p15.3) one on chromosome 3 (MLH1: *chr* 3p22.2) and one on chromosome 7 (PMS2: *chr* 7p22.2) (20).

1.1.3.2 Genetic Mutations, mRNA Expression, Protein Expression and Protein Staining of MSH2, MSH6, MLH1 and PMS2 in Melanoma

This subchapter starts by summarizing the current literature on the proteins MSH2, MSH6, MLH1 and PMS2 in melanoma. It will start by providing information on which mutations of these genes occur, the methylation status of their genes, what is known about their mRNA expression, how these proteins are expressed and in the end their staining properties will be discussed. For each subsequent topic, the occurrence, the factors that have been shown to have an effect on them, their interrelation (i.e. effect of gene mutation of mRNA expression etc.) as well as impact on *MMR* activity in melanoma will be discussed.

Genetic Mutations of MSH2, MSH6, MLH1 and PMS2 in Melanoma

Given the research questions of this thesis, the existence of disturbances in the *MMR* system in melanoma is a necessary condition for any subsequent reasoning.

Indeed mutations of MSH2, MSH6 and MLH1 have been found in melanoma patients or melanoma cell lines (21–28). The type of the observed mutations are base substitutions (23–28), exonic insertions (28) and exonic deletion (21,22). Considering the base substitution mutations they constituted of missense mutations in MSH6 (23), MSH2 (26) and MLH1 (25), as well as nonsense mutations in MSH2 (25) and MSH6 (23). Furthermore, splice donor site mutations of MSH2 (28) and splice acceptor site mutations of MLH1 (24,26) have been observed. These findings give putative evidence that the *MMR* system has disruptive changes that might result in loss of *MMR* proteins or expression of altered proteins which eventually cause defective *MMR*. However, melanoma also harbor silent mutations of MSH2 and MLH1 (27). Of note: the observed mutations (MSH2/MLH1) of Ponti et al. (28) were germline mutations, raising the question of the impact of *MMR* protein mutations on the pathogenesis in human melanoma. However, this will not be discussed in this thesis.

So far, the impact of UV light, considering its relevance in melanoma pathogenesis (3), as etiologic factor in melanoma *MMR* gene mutagenesis, remain inconsistent, as mutational pattern indicative of UV light could not be found in melanoma brain metastases (25), however, Hussein et al. was able to show that silent mutations can be induced in melanoma cell lines, derived from radial growth melanoma through UV radiation (27). This indicates

that *MMR* gene mutations can appear as a result of UV radiation in principle. Nevertheless, it remains unclear if this mechanism also results in mutations affecting the *MMR* activity. Another factor that has been linked to *MMR* mutagenesis are alkylating agents, as Sharma et al. (25) were able to show that the mutational pattern of MLH1 and MSH2 was indicative of being caused by these agents. As chemotherapeutic agents seem to have an impact on the *MMR* system, these will be discussed in more detail later in this thesis (see 1.1.3.3).

Considering the mRNA expression and its relation to *MMR* genes, it has been found that the intronic splice acceptor site mutation of exon 16 of the MLH1 genes in the presence of a chromosomic deletion of 3p21-p24 (the MLH1 gene has been mapped to 3p21.3), resulted in the expression of an aberrant MLH1 mRNA molecule harboring an in frame exon skipping of exon 16 (24). Providing empirical evidence that disruptions of the *MMR* system observed on the gene level, is sufficient to translate to the mRNA expression level in human *MM*.

In line with the preceding findings it could be shown that the missense mutation and nonsense mutations found on different alleles of the MSH6 gene imply a loss of MSH6 protein expression in cell lines derived from metastatic melanoma (23). Furthermore, the observed loss of MLH1 in the cell line PR-Mel (29) seems due to biallelic somatic mutations (i.e. exonic deletion of 3p21-24 (locus of the MLH1 3p21.3) and a G > A base substitution at the intronic splice acceptor site of intron 15 of the MLH1 gene), which has been identified within the same cell line (24). Interestingly, this genotype also resulted in a concomitantly loss of protein expression status of PMS2 (24). This might be due to destabilization of PMS2 in the absence of MLH1 (24). However, only chromosomic loss of 7p22 (PMS2 is located within this region) was assessed and no sequence analysis of the PMS2 gene was performed in the study (24). Hence, since this has yet not explicitly been shown in melanoma, the relationship of MLH1 gene mutation and PMS2 protein staining remains unclear. Nevertheless, these findings provide evidence that the types of *MMR* gene mutations occurring in human melanoma can result in the disruption of the *MMR* system on a protein basis.

As proteins expressed in a given cell, can be visualized by immunohistochemistry (:= *IHC*), the relationship of *MMR* mutations and *MMR* protein staining will be discussed next. The result of an *IHC* experiment can be evaluated and communicated as percent of positively stained cells (=: $\%_{IHC\_pos}$, herein) of a given specimen or as an binary status (IHC_{pos} := positive, stained or IHC_{neg} : = negative, not stained), therefore, the newly introduced terms

will be used concisely and consciously from this point on to avoid inconsistencies. If the staining was interpreted differently (e.g. by a histoscore incorporating staining intensity and $\%_{IHC\_pos}$ the concrete score will be stated).

Consistent with the previous mentioned findings, biallelic mutations of MSH6 has also shown to result in an IHC_{neg} status of MSH6 in the corresponding tissue sample of which the cell line was established (23). Furthermore, the biallelic mutation of MLH1 has been shown to result in an IHC_{neg} status of the corresponding protein within the tissue sample of the primary tumor of the same patient (24). Therefore, the proposed hypothesis regarding the effect of *MMR* mutations hold robust, also under incorporating *MMR IHC* staining experiments, for missense, nonsense, intron splice acceptor site and chromosomal deletions mutations. However, the proposed relationship seems to fall when considering exonic deletion, since it has been shown that exonic deletion of MSH2 or MLH1 does not imply a IHC_{neg} status of MSH2 or MLH1 in primary cutaneous melanoma, although it can occur (21). Furthermore, no exonic deletion of MSH2 and MLH1 did also not imply an IHC_{pos} status in any of these proteins (21). Questioning the *MMR* gene mutations status as necessary as well as sufficient condition for the loss of *MMR* protein expression, at least in all mutation types. Interestingly, the observed relation between intronic splice acceptor site mutation has also been found for MSH2 germline mutations of melanoma patients, who did also show an IHC_{neg} status of MSH2 in their primary cutaneous melanoma as well as corresponding colon carcinoma (28). However, germline mutation of the exonic insertion type in MLH1 did not result in IHC_{neg} status of MLH1 in primary cutaneous melanoma, even if corresponding colon carcinoma did show a concomitant IHC_{neg} status (28). This might be due to the two hit model proposed by Knudson et al. (30), in which a secondary mutation of the other allele is necessary for complete loss of function of an given protein. Evidence supporting this hypothesis is that both, either the intronic splice acceptor site mutation of MLH1 as well as the missense mutation of MSH6 resulted in an IHC_{neg} status, only in the presence of either an chromosomal loss or an nonsense mutation of the other allele, respectively (23,24). Another question that arises is whether the mutation of *MMR* genes results in the expression of aberrant *MMR* proteins with subsequent cellular accumulation and staining of these aberrant proteins via *IHC* similarly as what has been observed for TP53 (31). Therefore, the effect of *MMR* mutations on $\%_{IHC\_pos}$ status as well as histoscore measures will be discussed next.

So far this relationship has, to our knowledge, only been investigated by Korabioska et al. (21) who found that the exonic deletion mutation of MSH2 or MLH1 results in an reduction of $\%_{IHC\_pos}$ status of these proteins. Interestingly, while in MSH2 the number and type of exon (1 vs. 2, exon 12 vs. 13) deleted had no effect on $\%_{IHC\_pos}$ status of MSH2, there was a relation between the number and type of exon (1 vs. 2, exon 15 vs. 16) deleted in MLH1 (21).

To our knowledge, there are no studies today who did investigate the histoscore or staining intensity of *MMR* proteins and their relation to *MMR* mutations status in human *MM*.

Lastly, Alvino et al. (29) was able to demonstrate an imparted *MMR* activity in the cell line PR-Mel, which has shown to harbor biallelic mutations of MLH1 (24), implicating that disruptive changes of genes related to the *MMR* system are sufficient to translate into impairments of the MMR system on a functional level.

Methylation Status of MSH2, MSH6, MLH1 and PMS2 Genes in Melanoma

As has been discussed in the previous subchapter, *MMR* gene mutation status alone is not sufficient to explain the loss of *MMR* protein staining in all human melanoma (21). Therefore, especially given the relevance of *MMR* gene methylation in entities known to harbor disturbances of the *MMR* system (i.e. colon cancer) (32–34), it seems reasonable to discuss the relevance of *MMR* gene methylation status in melanoma next.

So far, changes in methylation status of *MMR* genes (promotor hypermethylation of MLH1) has only been found in primary *CM* of patients being hereditary non-polyposis colorectal cancer kindreds (:= *HNPCC*) (28). However, being a *HNPCC* kindred did not imply a hypermethylation of the MLH1 promotor, and even further, MLH1 promotor hypermethylation did also not imply a IHC_{neg} of MLH1 in their primary *CM*, even if an IHC_{neg} status in their corresponding colon carcinoma was observed (28). Yet again, this could be due to some sort of second hit similar to what has been proposed for gene mutations (30) (or inconsistencies in the reported data, since it was not entirely clear if the methylation status was tested in the primary melanoma, the colon carcinoma or both). However, there is evidence that altered *MMR* gene methylation status plays rather a minor role in disruptive *MMR* if any. Since all studies that, to our knowledge, investigated *MMR* gene methylation (29,35,36) in human *MM* of non *HNPCC* kindreds did not find any changes in methylation status of the *MMR* genes investigated (i.e. MLH1 (29,35,36) or MSH2 (35)) whatsoever. Of

note is that all of these studies were conducted on cell lines only investigating one (29,35) or a rather small sample (n = 16) (36). Nevertheless, they were able to show that the observed reduction of *MMR* mRNA expression (i.e. MLH1 or MSH2) as well as corresponding reduction of protein expression of the same proteins, after acquired resistance to chemotherapeutic agents, was not caused by promotor hyper or hypo-methylation of MLH1 or MSH2 (35). This provides evidence that alteration of MLH1 and MSH2 methylation status is no necessary condition for *MMR* mRNA and protein level changes observed in human *MM*. Further evidence regarding this hypothesis was found by Alvino et al. (29) who showed that no promotor hypermethylation of MLH1 does not imply an IHC_{pos} status of MLH1 and PMS2. In the end it has to be pointed out that although Tellez et al. (36) did not find any melanoma cell lines with altered methylation status of MLH1, the true rate of altered methylation status occurring in melanoma patients might be between 0 – 20.59% (Clopper & Pearson Confidence Interval (:= *CI*) (37), self-calculated using R) assuming that the individual cell lines were uniformly, randomly drawn, from 16 different *MM* patients. As this cannot robustly stand as basis for any subsequent reasoning, it shows the necessity for studies comprised of larger sample sizes, to answer the relevance of *MMR* gene methylation status in human melanoma more properly. As none of the mentioned studies did investigate the *MMR* activity, we are not able to draw conclusions about its relation to *MMR* gene methylation in melanoma on an empirical basis.

Expression of MSH2, MSH6, MLH1 and PMS2 mRNA in Melanoma

So far loss of mRNA expression of *MMR* genes has been found for MSH2 and MLH1 in metastatic *MM* (38). However, no loss of mRNA expression was found by Seifert et al. (39) in a subset of primary *MM* (n = 18) and metastatic *MM* (n = 11) as well as that the mRNA expression level of MSH2 is distributed over a wide range in primary and metastatic lesions. Additionally they were able to show that the mRNA level was significantly increased by a mean fold of 6.8 and 7.7 in cell lines of primary and metastatic *MM* compared to benign nevi, respectively (39). Furthermore, Rass et al. (40) showed that no definitive conclusion regarding the mRNA expression level of *MM* cells compared to HaCat cells can be drawn for MSH2, as the mRNA level did and did not differ significantly within the tested cell lines. However, the observed inhomogeneous widespread mRNA expression distribution could be due to factors related to the mRNA expression for whom both studies might not have controlled for. Furthermore, it has been shown that the mRNA expression measured via in-

situ hybridization (:= *ISH*), is lost in MLH1 and MSH2 in 23.7 % (14/59) and 3.6 % (8/59) in primary *MM* (41).

Today, there are a set of factors have been related to the mRNA expression of *MMR* genes comprising of either tissue or cell specific as well as environmental or iatrogenic factors (35,39,42). Tissue or cell specific factors that have been correlated to mRNA expression of MLH1 (41), MSH2 (41,42), MSH6 (42) are the Breslow thickness and or pT-stage of a primary *MM* as well as the mitotic rate of a given tumor specimen (42). Of note: it is not entirely clear if these two factors comprise two independent factors, as it has been shown that the mitotic rate is positively correlated to the Breslow thickness as well (43). The subset of environmental or iatrogenic factors comprises of UV-light affecting MSH2 mRNA expression (39) and the resistance status of chemotherapeutic agents that has been shown to be related to changes in the mRNA expression of MLH1 (35,42), MSH2 and MSH6 (35).

Considering the relations between *MMR* mRNA and protein expression it has been shown, that the change of MSH2 mRNA via RNA interference resulted in a delayed, yet clearly observable change in MSH2 protein (39). However, no global direct or indirect correlation of *MMR* gene mRNA expression level with protein expression has been observed in melanoma cell lines resistant to chemotherapeutic agents (35).

Additionally, it has been shown that the results by *ISH* and *IHC* of the *MMR* proteins of MLH1 and MSH2 are significantly correlated and highly concordant (41). Indicating that the *MMR* mRNA expression status can be deduced by the corresponding *IHC* status and/or $\%_{IHC\_pos}$ and vice versa.

The Protein Expression of MSH2, MSH6, MLH1 and PMS2 in Melanoma

This subchapter will solely focus on the current evidence regarding the protein expression of the *MMR* proteins measured via western blot analysis. Protein staining using *IHC* will be discussed in the following subchapter.

Loss of protein expression of *MMR* proteins has so far been found in four different melanoma cell lines, with loss of MLH1 and PMS2 in the cell line PR-Mel (29,44), loss of MSH6 in the cell line MR-Mel (23) and PD-Mel (44), and an expression of MSH2 and MSH6 on the boarder of detection in the cell line M27 (45). As previously mentioned only Castiglia et al. examined the mutation status of the investigated cell line, and found a biallelic mutation within the gene of the lost protein (23,24). Naumann et al. (45) as well as Pepponi et al. (44) did not provide any information on the cause of the observed protein expression on the

boarder of detection, or loss of protein expression, respectively, as they did not perform any genetic sequencing nor methylation assays.

Considering the interrelation of *MMR* protein expression status it has been shown that a loss of MLH1 occurs together with an loss of PMS2 (29,44). As mentioned above, this has been speculated to be due to an biallelic alteration of the MLH1 gene in this cell line (23). This gives rise to the hypothesis that the loss of both proteins is caused by a biallelic mutation of MLH1 rather than two biallelic mutations of MLH1 and PMS2, and therefore proposing a concomitant relation of PMS2 to the MLH1 expression status. This hypothesis is strengthened by the finding of Castiglia et al. (24) who did also observe a concomitant IHC_{neg} status of MLH1 and PMS2 in cells harboring biallelic mutations of the MLH1 gene. Again this might be due to destabilization of the PMS2 protein in the absence of MLH1 (24), however, all studies observing an concomitant loss of MLH1 and PMS2 expression did not investigate the mutation status of the corresponding genes (29,44), making definitive conclusion of the relationship between the mere protein expression status of MLH1 and PMS2 impossible. While the relationship of protein expression status of MLH1 and PMS2 remains unclear, a protein expression of MSH6 on the boarder of detection has been observed together with a protein expression of MSH2 on the boarder of detection (45) as well as an isolated loss of MSH6 protein expression in the absence of loss of protein expression in any other *MMR* protein (23,44). This leads to the conclusion that the loss of protein expression of MSH6 is not sufficient to cause loss of protein expression of any other *MMR* protein. However, it remains unclear if the observed concomitant loss of protein expression of MSH2 and MSH6 is due a single cause of one protein (e.g. mutation or hypermethylation of one gene) resulting in the loss of protein expression with subsequent loss of protein expression of the other protein solely based on protein degradation similarly as what has proposed by Castiglia et al. (24) for MLH1 and PMS2 or if two independent causes (e.g. mutation/hypermethylation of both genes) result in the loss of protein expression of MSH2 and MSH6 in melanoma.

As it can be argued that the observed alteration in the *MMR* protein expression might have occurred spontaneously within the cell lines after the corresponding tumor was removed, not reflecting the actual in vivo expression status, this seems rather unlikely in the case of the cell line PR-Mel (29) and MR-Mel (23) as in both cases the corresponding tumor tissue showed an concomitant IHC_{neg} status of the proteins with loss of expression observed in the cell lines.

To our knowledge the only factor that has been related to *MMR* protein expression is the resistance status to chemotherapeutic agents (35,44,45). However, this will be discussed in the corresponding chapter in greater detail (1.1.3.3).

Considering the relationship of *MMR* protein expression and protein staining, it has been shown that the loss of protein expression in melanoma cell lines occurred if and only if loss of protein staining for MSH6 (23) as well as MLH1 and PMS2 (29) in their corresponding tumor tissues was observed. Furthermore, no loss of protein expression of MSH2, MSH6, MLH1 or PMS2 in melanoma cell lines did also occur if and only if no loss of protein staining of the corresponding protein within the corresponding tumor tissue was observed (29). Therefore, given the current evidence, it can be inferred that the protein staining status of a given protein is indicative for its protein expression status, and vice versa.

The relationship of the *MMR* activity and protein expression has to our knowledge only been investigated explicitly by three studies (29,44,45). So far two studies were able to show that the loss of protein expression of MLH1 and PMS2 in the cell line PR-Mel was associated with an significantly impaired *MMR* activity compared to the cell lines without loss of *MMR* protein expression (29,44). Additionally, Pepponi et al. (44) did show that the loss of protein expression of MSH6 was also associated with an impaired *MMR* activity compared to the cell lines without loss of *MMR* protein expression. Furthermore, Naumann et al. (45) were able to demonstrate that the level of MutSα bound to G/T mismatch-containing oligonucleotides was reduced in the cell line (MZ) with a protein expression of MSH2 and MSH6 on the boarder of detection compared to cell lines without *MMR* protein alterations. However, it shall be noted that the *MMR* activity did show substantial variation between cell lines expressing no loss of *MMR* gene expression (29,44). Based on these findings it can be inferred that loss of protein expression of *MMR* genes is sufficient to cause impairment of *MMR* activity. Furthermore, that no loss of protein expression of *MMR* genes is a necessary condition for unimpaired *MMR* activity, however, the mere positive expression status of *MMR* genes is not sufficient to explain the level of *MMR* activity in melanoma cells.

The Protein Staining Properties of MSH2, MSH6, MLH1 and PMS2 in Melanoma

This paragraph will start by discussing the IHC_{neg}-*Status* of the MSH2, MSH6, MLH1 and PMS2 proteins, the interrelation of the IHC_{neg}-*Status* within *MMR* proteins. Subsequently we will discuss the $\%_{IHC\_pos}$ as well as the relation of $\%_{IHC\_pos}$ and IHC_{neg}-*Status.* The paragraph ends with the discussion of the effect of $\%_{IHC\_pos}$ and IHC_{neg}-*Status* on *MMR* activity.

An IHC_{neg}-*Status* of the MSH2, MSH6, MLH1 and PMS2 proteins has been observed by several studies (21,23,24,26,28,29,41,46–50). So far an IHC_{neg}-*Status,* has been observed for MSH2 (21,26,28,41,46,48–50), MSH6 (23,47,51), MLH1 (26,41,46,48–50) and PMS2 (50). A concomitant IHC_{neg}-*Status* of MLH1 and PMS2 was found by Alvino et al. (29) as well as Castiglia et al. (24) while no IHC_{neg}-*Status* of the remaining proteins (MSH2 and MSH6) was observed. From this it can be inferred that the IHC_{neg}-*Status* of MLH1 or PMS2 does not imply an IHC_{neg}-*Status* of MSH2 or MSH6. Similarly, the presence of an IHC_{neg}-*Status* of MLH1 and no concomitant IHC_{neg}-*Status* has been observed for MSH2 (21,41,46,48–50) and MSH6 (49) in other studies. The same could be observed for the IHC_{neg}-*Status* of PMS2 and MSH2 (26,50). Further evidence regarding this hypothesis for PMS2 and its relation to MSH6 is lacking as no study that observed a IHC_{neg}-*Status* of PMS2 other than Alvino et al. (29) as well as Castiglia et al. (24) did simultaneously investigate the *IHC* expression of MSH6 (26,50) to our knowledge. In contrast to the aforementioned observations stands the finding of Garcia et al. (49) who did observe a concomitant IHC_{neg}-*Status* of MLH1, MSH2 and MSH6. This leads to the conclusion that even though an IHC_{neg}-*Status* of MLH1 or PMS2 does not imply an IHC_{neg}-*Status* of MSH2 or MSH6 it still can occur. Given the observed concomitant IHC_{neg}-*Status* of MLH1 and PMS2 it has previously been mentioned that Castiglia et al. (24) proposed that the IHC_{neg}-*Status* of PMS2 might be due to protein degradation of PMS2 in the absence of MLH1. However, this question cannot adequately been answered based on the current studies in which an MLH1 as well as PMS2 IHC_{neg}-*Status* was observed, since both studies did only state pooled percentages and did not depict the individual staining statuses (26,50).

Since the staining status of a given tumor tissue can also be descripted in terms of its $\%_{IHC\_pos}$ the current evidence regarding its properties for *MMR* protein will be discussed next. Today there are to our knowledge only seven studies (21,24,26,40,41,47,52) that investigated the $\%_{IHC\_pos}$ of *MMR* protein in human melanoma.

Interestingly, the observed distributions of $\%_{IHC\_pos}$ did vary considerably for the observed proteins as has been depicted in Table 1:

Protein	mean (± *sd*) %	median %	*min* %	*max* %	Author
MSH2	-	19	0	(43, 72)	Korabiowska, König et al. 2004 (26)
	-	(2.5, 15, 21, 31)	(0, 17)	(9, 29, 34, 70)	Korabiowska, Cordon et al. 2004 (41)
	67.2 (± 7.7)	-	-	-	Hussein et al. 2002 (52)
	(2.47, 2.94) (-)	-	-	-	Rass et al. 2001 (40)
	-	-	-	80	Castiglia et al. (24)
	-	-	-	98	Korabiowska et al. 2006 (21)
	-	[71, 80]	[0,10]	[91, 100]	Alvino et al. 2014 (47)
MSH6	-	36	(0, >0)	(53, 58)	Korabiowska, König et al. 2004 (26)
	76.6 (±2.1)	-	-	-	Hussein et al. 2002 (52)
	-	[11, 20]	[0, 10]	[71, 80]	Alvino et al. 2014 (47)
MLH1	-	(20,31)	0	(65,82)	Korabiowska, König et al. 2004 (26)
	-	(7, 16, 21, 45)	(0, 18)	(19, 32, 39, 74)	Korabiowska, Cordon et al. 2004 (41)
	75.6 (±3.4)	-	-	-	Hussein et al. 2002 (52)
	-	-	-	96	Korabiowska et al. 2006 (21)
	-	[81, 90]	[41, 49]	[9, 100]	Alvino et al. 2014 (47)
PMS2	-	[81, 90]	[21, 30]	[91, 100]	Alvino et al. 2014 (47)

Table 1 Overview of the $\%_{IHC\_pos}$ of *MMR* Proteins Found in Human Melanoma.
This table depicts the $\%_{IHC\_pos}$ observed in human melanoma by various studies. The numbers in parentheses are values found in different subsets of human melanoma grouped by different attributes (i.e. pT stage (41)*, brain metastases vs. primary melanoma* (26)*), if only one value is stated in the corresponding reference this is either due to lacking information or the same value for each subset. The numbers in brackets relate to intervals of $\%_{IHC\_pos}$ values* (47)*. (Abbreviations: sd := standard deviation, min := minimum, max := maximum, % := percentage of positively stained cells, >0 :=greater than zero, however, not exact value was stated, - := values were not stated within the study)*

These variations might partially be explained by factors that have been shown to be related to the $\%_{IHC\_pos}$ of *MMR* protein. These constitute a tumor intrinsic factor (i.e. mutations (21)) as well as factors that can be associated with melanoma stage (i.e. pT-stage (41), Breslow Thickness (47), ulceration (47), mitotic rate (47)). As it could be shown that the $\%_{IHC\_pos}$ of MLH1 and MSH2 are significantly related to exonic deletions of the MLH1 (exon 15, exon 16) and MSH2 (exon 12, exon 13) genes respectively (21). Regarding the pT stage Korabiowska et al. (41) found a significant difference of $\%_{IHC\_pos}$
of MLH1 and MSH2 for distinct combinations of pT stages:

- $\%_{IHC\_pos}$ of MLH1: pT1 > pT4, pT2 > pT3, pT2 > pT4, pT3 > pT4; (41)
- $\%_{IHC\_pos}$ of MSH2: pT1 > pT4, pT2 > pT4, pT3 > pT4; (41)

Furthermore, Alvino et al. (47) found a significant overall association of the Breslow Thickness, ulceration, mitotic rate and AJCC clinical stage with a binary status {high, low} of $\%_{IHC\_pos}$ of MSH2 (cut off: 20% $\%_{IHC\_pos}$). Of note is that the finding of Korabiowska et

al. (41) could not be reproduced by Alvino et al. (47) as they did not observe an overall association of the $\%_{IHC\_pos}$ of MLH1 nor MSH2 with Breslow Thickness. However, this might be due to the study design, as Alvino at al. (47) investigated, as mentioned, a binary status of $\%_{IHC\_pos}$ of *MMR* proteins (cut off: 80% for MLH1, MSH2 and PMS2), performing an overall $\chi 2$ or Fisher exact test for the binary status and Breslow Thickness classes {≤1.00 mm, 1.01-2.00 mm, 2.01-4.00 mm, >4.00 mm}, whereas Korabiowska et al. (41) used the raw $\%_{IHC\_pos}$ conducting a Mann-Whitney U test to evaluate differences in the pT-stage {pT1, pT2, pT3, pT4}. Nevertheless, even considering these facts, Korabiowska et al. (41) was also not able to show a total order of the $\%_{IHC\_pos}$ of MLH1 nor MSH2 in relation to the pT-stage. This leads to the conclusion that even if the observed relation exists, it is not linearly decreasing, but either specific for each combination.

Considering the observed association of MSH6 by Alvino et al. (47) it must be stated that all these factors (mitotic rate, pT-stage, AJCC clinical stage, ulceration) might be internally interrelated. Which obviously can be assumed for the Breslow Thickness and the AJCC clinical stage as they are formally related (13), but also for the Breslow Thickness and the mitotic rate as it has been shown that these two factors are highly significantly related to each other [$r = + 0.8$, $p < 0.001$) (43). Furthermore, Rass et al. (40) was not able to show a correlation of the $\%_{IHC\_pos}$ of MSH2 and Ki-67 in primary as well as metastatic *MM*. Questioning an relationship of the mitotic rate and MSH6, especially as it has been shown that the $\%_{IHC\_pos}$ MSH2 and MSH6 are significantly positively related in human melanocytic lesions (53). However, Alvino et al. (47) did hypothesize, since the observed expression pattern of MSH6 resembled those being reported for Ki-67 in previous studies that MSH6 as in contrast to MSH2, MLH1 and PMS2, is primarily expressed in proliferating cells, however this has to our knowledge never explicitly been investigated in human melanoma.

Beside the previously mentioned direct relationship of MSH2 and MSH6 (52), the $\%_{IHC\_pos}$ of MSH2 has also been shown to be directly related to MLH1 (41,50).

Considering the exact distribution of the $\%_{IHC\_pos}$ of *MMR* proteins in human melanoma, this has to our knowledge only been explicitly stated by Alvino et al. (47) and is depicted in Figure 1.

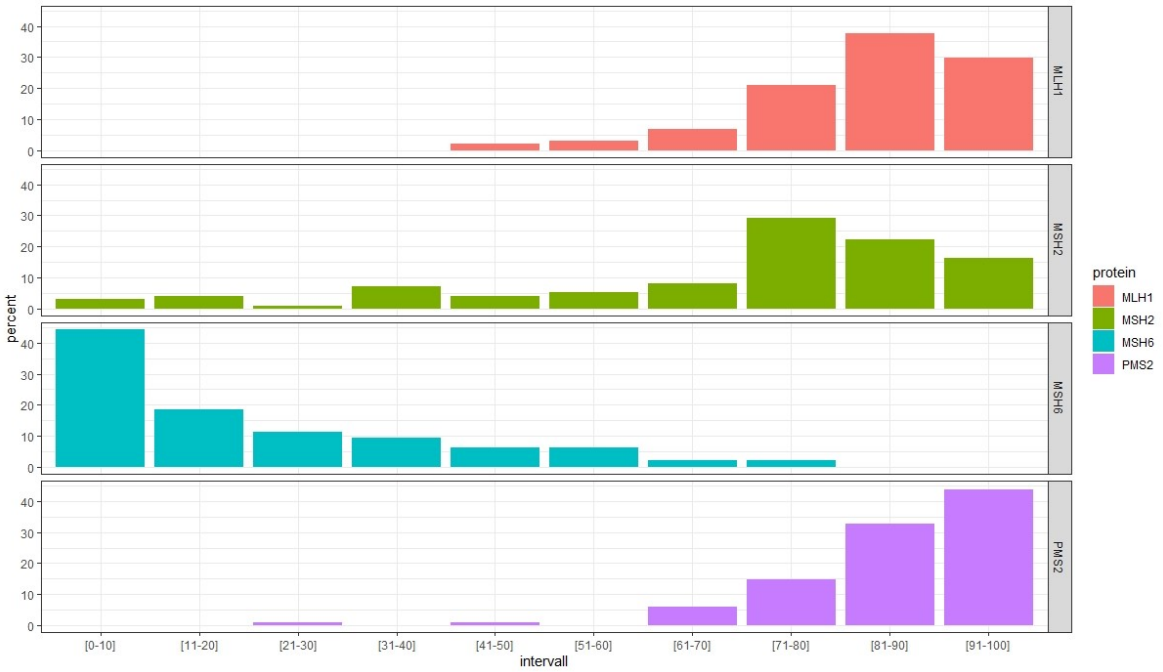

Figure 1 Distribution of the *%IHC_pos* of *MMR* Proteins in Human Primary Melanoma.
This figure has been drawn based on the data published by Alvino et al. (47)

This chapter will proceed by discussing the *IHC$_{neg}$-Status* and *%IHC_pos* of *MMR* proteins and their relations to *MMR* activity. To our knowledge, only the *IHC$_{neg}$-Status* of *MMR* proteins and *MMR* activity has been investigated so far (29). Where a *IHC$_{neg}$-Status* of MLH1 and PMS2 was observed together with an highly reduced *MMR* activity (29). However, concomitant results were observed as previously reported for protein expression of *MMR* proteins, as no *IHC$_{neg}$-Status* of either of the *MMR* proteins resulted in a variably level of *MMR* activity in the observed cell lines (29). From these findings it can be inferred that in the same manner as for loss of protein expression of *MMR* genes, the *IHC$_{neg}$-Status* of *MMR* proteins is sufficient to cause impairment of *MMR* activity. Furthermore, that no *IHC$_{neg}$-Status* of *MMR* proteins is a necessary condition for unimpaired *MMR* activity, however, the mere positive expression status is not sufficient to explain the level of *MMR* activity in melanoma cells.

1.1.3.3 The Relationship of Chemotherapeutic Agents and the *MMR* System in Melanoma

As has been mentioned in the previous subchapters, chemotherapeutic agents and their resistance status have been to be related to disruptive changes in the *MMR* system. The set of chemotherapeutic agents investigated in this regard consist to our knowledge of Cisplatin (35,54), Etoposide (35), Fotemustine (35,55), Vindesine (35), Vemurafenib (55) and Temozolomide (44,45,54,55). This subchapter will proceed by discussing each agent, respectively.

The resistance to Cisplatin and its relation to the *MMR* system has been investigated in the human melanoma cell lines MeWo (lymph node metastasis) (35) and M14 (melanoma metastasis) (54). MeWo cells resistant to Cisplatin showed a reduced relative expression of mRNA of the *MMR* proteins MSH2, MLH1 and MSH6 (PMS2 was not investigated), with MSH2 showing the greatest reduction (35). Interestingly, while a dose dependent relative reduction of MSH2 and MLH1 was observed (1 µg/ml vs. 0.01 µg/ml, 0.7 vs. 0.2, 0.8 vs. 0.6, respectively) no dose dependent relative reduction was observed for MSH6 (0.9 each) (35). Furthermore, the observed dose dependent reduction did not translate to protein expression level as MSH2 as well as MLH1 did show a relative reduction, however not dose dependent, whereas MSH6 did show a dose dependent relative reduction (0.7 vs. 0.6) (35). Regarding the relative reduction of *MMR* mRNA expression the authors did not find any changes in methylation status of any of the genes investigated (35). In contrast to these findings are the findings observed by Fontijn et al. (54) as they were not able to detect altered expression levels of MLH1, MSH2 and MSH6 in M14 melanoma cells resistant to Cisplatin. However, these cells where transfected with bFGF and where shown to overexpress bFGF, hence the resistance might be due to some relations of bFGF and Cisplatin (54). However, this will not be further discussed in this thesis. Given these facts it can be inferred that relatively reduced expression of *MMR* mRNA as well as concomitant relatively reduced protein expression can occur in the presence of resistance to Cisplatin (35), however, relatively reduced protein expression does not seem to be necessary to develop resistance to Cisplatin, at least in metastatic melanoma (54). Furthermore, it remains unclear if the observed relative reduction is due to structural changes of the *MMR* genes, post transcriptional and/or post translational processes, or altered gene regulation since this has to our knowledge not been investigated in human melanoma.

Regarding Etoposide the discrepancies between the relative mRNA and protein expression have been found to be even greater (35). As the relative mRNA expression did neither show

an overall stable reduction nor a dose dependent (i.e. 0.1 vs. 1.0 µg/ml Etoposide) increase or decrease (MSH2: 0.9 vs. 1.5, MSH6: 0.8 vs. 1.0, MLH1: 1.0 vs. 0.2, relative to non-resistant MeWo cells) (35). However, the protein expression of MSH2, MSH6 and MLH1 showed a marked relative reduction of all three proteins in MeWo cells resistant to Etoposide when compared to non-resistant cells (35). Furthermore, there seemed to be a dose dependent decrease in the relative expression of MSH2 (0.5 vs. 04) and MLH1 (0.7 vs. 0.6), whereas not for MSH6 (0.3 vs. 0.4) (35). Again, no promotor hypermethylations were observed in MeWo cell lines resistant to Etoposide (35). These findings indicate that the resistance to Etoposide might be due to a decrease in protein expression of *MMR* proteins (i.e. MSH2, MSH6 and MLH1), however, the reduction of protein expression could not be explained by reduced mRNA expression or promotor hypermethylation (35). Hence, the exact cellular mechanism causing these findings remain unknown.

So far, no consistent directional changes in the mRNA expression of MSH2, MSH6 and MLH1 could be observed in melanoma cells resistant to Fotemustine (35). Furthermore, the protein expression of these proteins was almost equivalent in all investigated proteins, regardless of the resistance status (35). From this it can be inferred that disruptive changes of the *MMR* system are not necessary for resistance to Fotemustine. In addition, it has been shown that Fotemustine still elicits adequate apoptosis in the human melanoma cell line MZ7 (splenic metastasis), which showed impairments of the MutSα complex (i.e. MSH2/MSH6 protein expression on the boarder of detection, reduced molecular weight of MutSα bound to an G/T mismatch-containing oligonucleotide) (45). This indicates that disruptive changes of the *MMR* systems are also not sufficient to produce resistance against this agent.

Similar to Fotemustine, MeWo cells resistant to Vindesine showed no consistent directional change in mRNA expression of MSH2, MSH6 and MLH1 compared to non-resistant cells (35). However, the protein expression level of the investigated proteins (i.e. MSH2, MSH6 and MLH1) showed marked relative reduction of all proteins tested in MeWo cells resistant to Vindesine (35). While MSH2 and MLH1 showed a dose dependent decrease (0.5 vs. 5.0 ng/ml; MSH2: 0.6 vs. 0.5, MLH1: 0.5 vs. 0.4), this was not observed in MSH6 (0.6 vs. 0.6) (35). Therefore, it can be assumed that reduced protein expression due to Vindesine contributes to resistance against this agent in human melanoma.

Roos et al. (55) did investigate the relationship of Vemurafenib therapy/resistance and the *MMR* system in $BRAF^{V600E}{}_{positive}$ human melanoma cells (cell line A375) and found no difference in protein expression of MSH2, MSH6, MLH1 and PMS2 between resistant and non-resistant cells. However, they observed an increase in nuclear staining of MSH2, MSH6

and PMS2 after Vemurafenib treatment of non-resistant cells (55). Of note: resistance to Vemurafenib had no effect on the resistance status of Fotemustine and Temozolomide, within these cell lines (55). These findings indicate that alterations of the *MMR* system are not necessary for resistance against Vemurafenib.

Lastly the relationship of temozolomide and the *MMR* system has to our knowledge been investigated by four studies (44,45,54,55). So far resistance to temozolomide has been found in three different cell lines harboring disruptive changes of the *MMR* system (i.e. PR-Mel (44), PD-Mel (44), M27 (45)). Furthermore, it has been shown that in the absence of O^6-alkylguanine-DNA alkyl transferase (an enzyme, removing small alkyl groups from O^6-guanine by transferring it to an internal cysteine residue) activity, the IC_{50} concentration (concentration producing 50% inhibition of cell growth) of temozolomide is inversely related to the *MMR* activity (44). This gives putative evidence that disruptions of the *MMR* system are sufficient to induce resistance against temozolomide. However, resistance against temozolomide has also been found in cells of the melanoma cell line M14 transfected to overexpress bFGF, which did not show an altered protein expression of MLH1, MSH2 and MSH6 (54), indicating that disruptive changes of the *MMR* system are no necessary condition for temozolomide resistance.

1.1.3.4 The *MMR* System and Overall Survival in Human Melanoma

So far there are four types of measures of the *MMR* system that have been investigated in relation to the *OS* of melanoma patients, comprising of mutation status (21), the IHC_{neg}-*Status* (51), the $\%_{IHC\_pos}$ (47,50,56) and a histoscore measure (the study used the tissue studio image analysis program, Definiens AG, München, Germany) (57), which will be discussed in this subchapter.

Considering the mutation status of *MMR* genes it has been shown that the *OS* is significantly reduced in primary melanoma harboring exonic deletion of MSH2 (exon 12 and exon 13) or MLH1 (exon 15 and exon 16) (21).

Ponti et al. (51) was able to show that a patient with subungual melanoma and an IHC_{neg}-*Status* of MSH6 showed an marked increase of *OS* as well as *PFS* after anti PD-1 therapy when compared to patients without an IHC_{neg}-*Status* of MSH2, MSH6, MLH1 or PMS2 (2546 and 956 days vs. 542 and 290 days, respectively).

Another relation between *MMR* proteins and *OS* was observed by Alvino et al. (47) who could show that a $\%_{IHC\_pos}$ low status of MSH6 ($\%_{IHC\_pos} < 20\%$) was an independent predictive factor for melanoma survival, even after controlling for age, sex, Breslow Thickness and ulceration using a multivariate cox proportional hazard model (relative risk: 3.76, 95% *CI*: 1.12 – 12.70, p = 0.03). Furthermore, the $\%_{IHC\_pos}$ of MLH1 and MSH2 has shown to be related to *OS* in human melanoma (50). Whereas the finding for MSH2 could not be reproduced by Meyer et al. (56) using a Univariate Cox proportional hazard regression model (p = 0.588), they were also able to show a significant association of MLH1 and *OS* (Hazard ratio: 1.290, 95% *CI*: 1.086 – 1.531, p = 0.004). Furthermore, Song et al. (57) was also not able to show an significant association between MSH2 and *OS* (p = 0.5) using the aforementioned histoscore measure within a Cox proportional hazard model.

1.1.4 Microsatellites and their Relation to Human Melanoma

1.1.4.1 Description and Definition of Microsatellites and Microsatellite Instability

Microsatellites (:= MS) are defined as DNA sequences of DNA motifs in the length between 1-6 base pairs (:= *bp*) that are repeating tandemly in a given genome at defined loci (58,59). The term satellites dates back to the 1960s and did originate from observations that a fraction of sheared DNA in density gradient centrifugation showed a distinct buoyant density and was detectable as a "satellite peak". These peaks where then identified as large centromeric tandem repeats. Subsequently, shorter tandem repeats (10-30 bp) have been found and were named minisatellites. In the same manner the term *microsatellites* was coined after the discovery of tandem iterations of simple sequence motifs (60).

MS are ubiquitously found in the genomes of eukaryotes at varying rates (58). Considering the human genome (assembly hg38) they constitute about 2% of the covered genome and can be classified according to their specific sequence motif (e.g. ATC vs. ATT and all corresponding palindromes, := *motif class* within this thesis) and the length of the sequence (e.g. A vs. AAA, mono vs. tri respectively, := *motif type* within this thesis) (58). Using this classification it can be shown that these classes are non-randomly distributed within the entire human genome with *MS* of the hexa *motif type* (see Figure 2A) and the A *motif class* (see Figure 2B) being the most abundant in the entire genome (58).

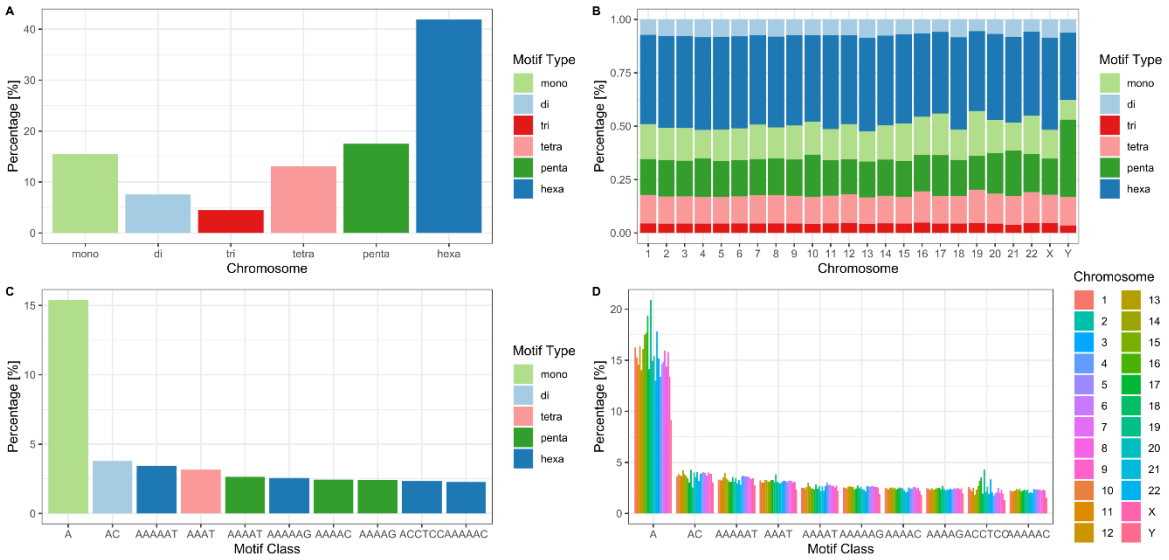

Figure 2: Distribution of *Microsatellite* Classes of the Human Genome.
This figure depicts subfigures of self-calculated summary statistics of MS data within the MS database provided by Avvaru et al. (58).

The distribution shapes, for *motif class* and *motif type* respectively, seem to be rather constant for all chromosomes, with only the Y chromosome showing significant changes (see Figure 2, Figure 3) where *MS* of the penta *motif type* and AATGG *motif class* are the most abundant (58).

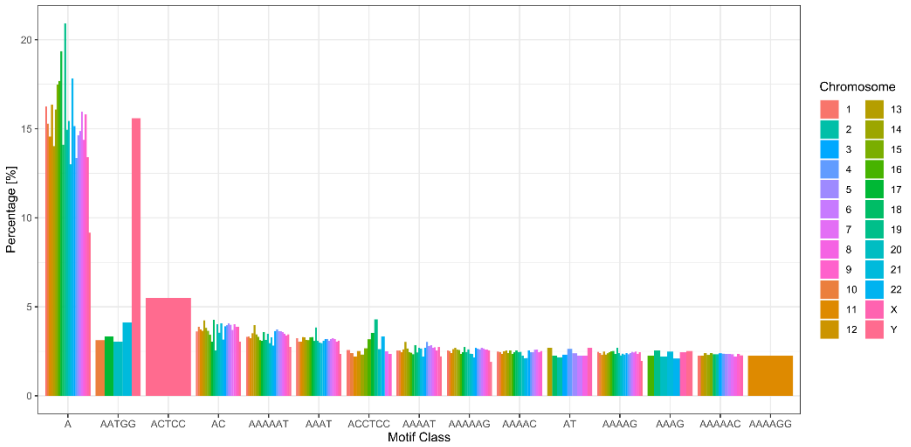

Figure 3: Distribution of the Ten Most Abundant *Microsatellite Motif Classes* of Each Chromosome.
This figure depicts a self-calculated summary statistic of MS data within the MS database provided by Avvaru et al. (58).

The *bp* length of *MS* ranges between 12 – 35 *bp* in the vast majority (58). Correspondingly only few *MS* show a repetition numbers higher then 35 (see Figure 4) (58).

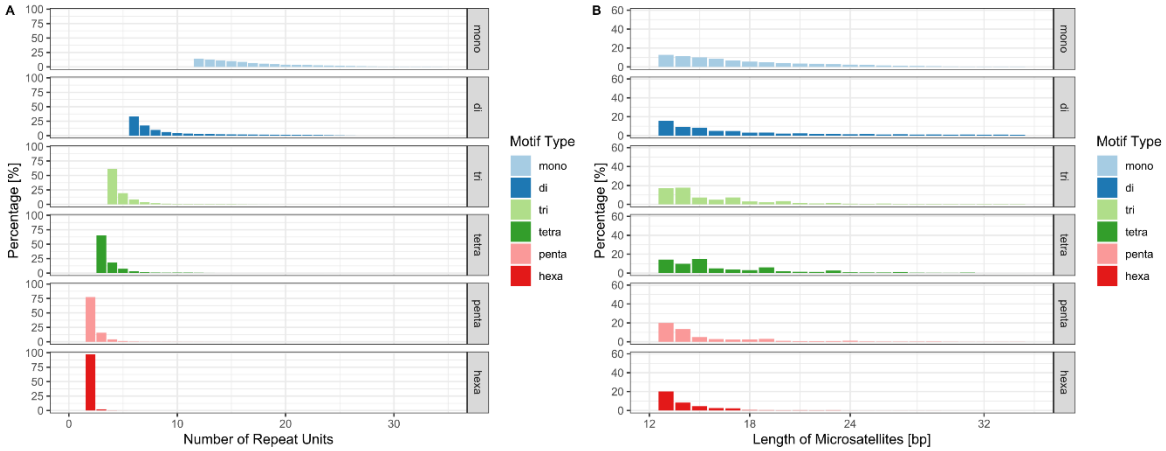

Figure 4: Distribution of *Microsatellite* Length and Number of Repeat Units.
This figure depicts subfigures of self-calculated summary statistics of MS data within the MS database provided by Avvaru et al. (58).

The rate of *MS* varies in relation to a given chromosome (58). However, this variation seems to be due to the differences in chromosome length, as it can be shown that when the *MS* count of a given chromosome is plotted against its length, the relationship appears to be rather constant (see Figure 5).

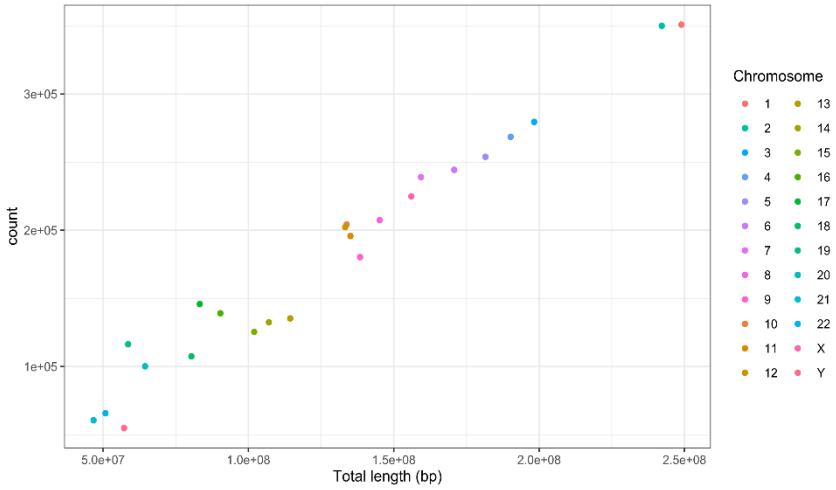

Figure 5: Chromosomal *Microsatellite* Count Plotted Against its Length for All Human Chromosomes.
This figure was created by plotting the total count of MS of a given chromosome obtained from the MS database provided by Avvaru et al. (58) against its total length (bp). The data for chromosomal length was retrieved from the website of the genome reference consortium and refers to the GRCh38.p13 (https://www.ncbi.nlm.nih.gov/grc/human/data, last retrieval 13.10.2020).

Regarding the location, *MS* are found mostly in non-coding regions of the human genome, which holds true even after subsetting for chromosome and *motif type* (see Figure 6) (58).

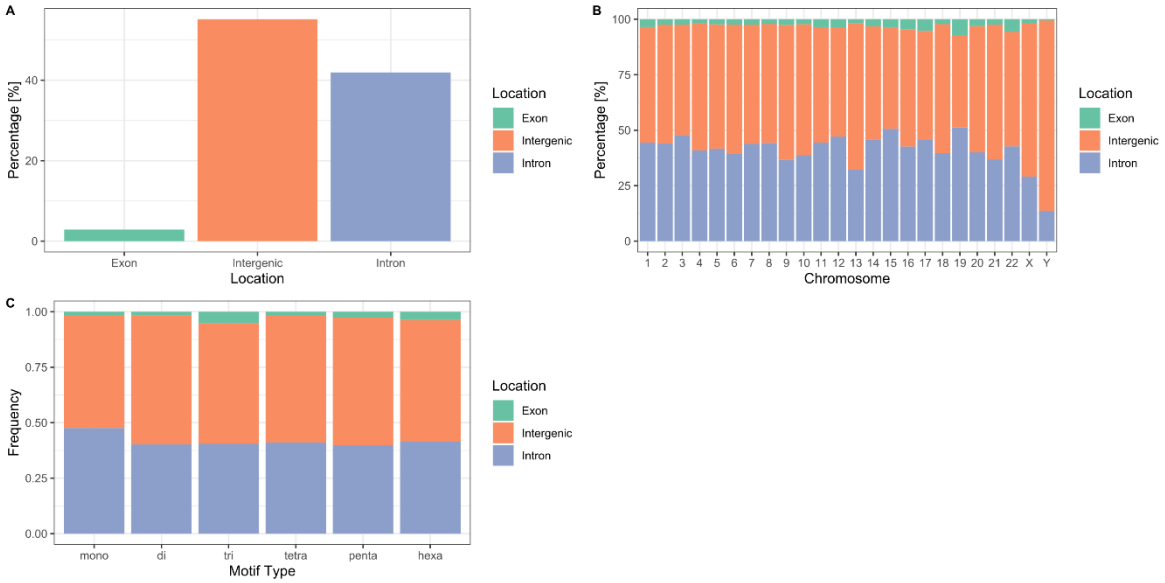

Figure 6: Location of *Microsatellites* within the Human Genome.
This figure depicts subfigures of self-calculated summary statistics of MS data within the MS database provided by Avvaru et al. (58).

MS became of special scientific interest as they are among the most variable types of DNA sequences in the human genome (61,62). This resulted in the use of *MS* as markers in association studies, population genetics, forensics and cancer diagnostics (59).
Interestingly, the mutability of *MS* does vary between loci in vivo and can be partly explained by considering the *motif type*, the number of repeats and the length of a given locus (63).

This holds true for ex vivo shuttle vector studies as well as for in vitro polymerase experiments (59).

One model thought to explain the mutagenesis in *MS,* resulting in alteration of repeat length, is the "*slipped strand mispairing model*". In this model the alteration occurs due to the stop of the DNA polymerase and a subsequent dissociation of the nascent from the template strand. Followed by the rehybridization of a wrongly aligned sequence motif and formation of an interspersed DNA loop consisting of one or more repeating motifs. When the DNA polymerase starts its replication process again, the number of repeating motifs is increased or decreased depending whether the loop was formed on the nascent or template strand respectively (59,60,64).

1.1.5 Microsatellite Instability, Defective *MMR* System, and their Relationship

As the number of repeats of a given *MS* is highly polymorphic within the human population, a given individual can harbor a specific *MS* genotype (number of repeat at this locus) at a given locus, which can either be homozygous or heterozygous (two distinct numbers of repeats at that given locus on each chromosome) (65). This genotype is, in principle, thought to be the same for every cell within a given individual (65).

At the end of the last century comparative studies in patients suffering from colorectal carcinoma did reveal that the number of repeats at a given *MS* locus did show differences (increase and/or decrease of the repetition number) between the tumor tissue and matched normal tissue of these patients (59). This phenomenon lead to the introduction of a new descriptive term by which these tumors were classified, namely *microsatellite instability* (:= *MSI*) (59). Since then a tumor had been classified as *MSI*, when the tumor exhibited two or more alleles with different *MS* repetition length at a given locus compared to the patients normal tissue (65). It became clear that this phenomenon can be caused by defective *MMR* (:= *dMMR*) (e. g. inactivation, mutational and/or epigenetic silencing of *MMR* genes). (66) As it has been shown that the insertion/deletion loops formed during *MS* mutagenesis (see preceding subchapter) are effectively corrected by the *MMR* system during DNA replication (59).

However, it became apparent that not all *MS* must be affected by *dMMR* in a given tumor, prompting the necessity to investigate more than one *MS* to accurately detect tumors with *dMMR* (65). Therefore, in 1998 a standardized diagnostic test was proposed during a National Cancer Institute workshop, which later became known as the Bethesda panel that

was designed to specifically detect *dMMR* (59). This test comprises five distinct *MS* markers (i.e. two markers of the mono *motif type* (A/T *motif class*) and three markers of the di *motif type* (GT/CA *motif class*) (59).

After adopting the classification of colorectal cancers according to *MSI* it became evident that the number of *MS* classified as *MSI* can vary considerably within a given tumor with some tumors showing no *MS* of the *MSI* type coined microsatellite stable (:= *MSS*), some exhibiting the *MSI* phenotype only at low percentage, as well as some showing the *MSI* phenotype in a high percentage of the *MS* tested (66). Therefore, the *MSI* phenotype was subdivided into an MSI-low (:= *MSI-L*) and MSI-high (:= *MSI-H*) phenotype, with either exhibiting the *MSI* phenotype in < 30-40% or only one marker, when using the Bethesda panel, or ≥ 30-40% or more than one marker, of the tested *MS*, respectively (59).

As *dMMR* generally display the *MSI-H* phenotype and *MS* markers of the mono *motif type* have been shown to be more sensitive and specific for detecting the *MSI-H* phenotype a new panel has been proposed by the revised Bethesda guidelines incorporating only *MS* markers of the mono *motif type*, which is today widely adopted to investigate the *dMMR* status (59).

In contrast to the *MSI-H* phenotype, the etiology, and the pathologic significance of the *MSI-L* phenotype are not as thoroughly understood (59). Since it is not entirely clear if the *MSI-L* constitutes an experimental artifact, reflects spontaneous mutation events at *MS* markers, reflects a damage-induced phenotype or is a distinct subgroup of moderate defects in replication and repair (59).

1.1.5.1 Microsatellite Instability in Human Melanoma

So far the occurrence of *MSI* has been restricted solely to non-benign melanocytic lesions and it seems that there are differences in the prevalence of *MSI* considering the specific *MSI* phenotype as well as the type of malignant melanocytic lesions as is depicted in Table 2.

The prevalence of *MSI* seems to increase with the malignant potential of a given melanocytic lesions, as the prevalence of *MSI* in at least one examined locus is significantly higher in dysplastic nevi as well as primary *CM* compared to benign nevi (53). Furthermore, the prevalence of *MSI* in at least one examined locus has also been observed to be significantly higher in dysplastic nevi harboring mild as well as severe atypia compared to dysplastic nevi with moderate atypia (53). Additionally Richetta et al. (67) did also find a higher prevalence of *MSI* in at least one examined locus in metastases compared to primary *MM*.

These findings may indicate that some mechanisms (e.g. *dMMR*) involved during tumorigenesis in an early stage, serve as constant factors that increase the possibility of *MS* mutagenesis, thus resulting in a higher prevalence of *MSI* in at least one locus in consecutive melanoma conversion classes (e.g. dysplastic nevi > primary melanoma > metastasis).

This hypothesis is strengthened by the findings that: *MSI* at a given locus can develop in metastases of a primum formerly devoid of *MSI* at that locus (68,69), the prevalence of *MSI* is higher in the set of metastases compared to the set of their corresponding primum (70), and lastly that metastases exhibit *MSI* at the same loci as their primum (68,69).

However, there are some findings challenging this hypothesis. Since Palmieri et al. (70) was not able to show a relation between the AJCC stages I-III and the prevalence of *MSI* at exactly one of 11 loci, as well as no overall linear increase in the prevalence of *MSI* at ≥ 2 loci of 11 over the AJCC stage I-III. In a similar manner Talwalkar et al. (71) did not observe a correlation of Breslow thickness and the presence of *MSI* in primary melanoma.

Interestingly, even though metastases of a primum, harboring *MSI* at a specific locus, can exhibit *MSI* at the same locus (68,69) they may not (68).

This indicates an intertumoral heterogeneity of the distribution of loci exhibiting *MSI* within a given bulk tumor sample giving rise to subclonal metastases and resulting in an intermetastatic heterogeneity of the *MSI* pattern.

Findings validating this hypothesis have been provided by Rübben et al. (72) as they were able to show that different micro dissected areas of a primary melanoma did show a different pattern of loss of heterozygosity (:= *LOH*) at the observed *MS* loci, as well as metastatic lesions that mutually exclusively exhibited the same pattern of *LOH* . Using this information it was possible to create a genealogy of the metastatic neoplastic lesions of the primary *MM* (72). Adopting this genealogy, different kinds of *MSI* pattern can be observed in non-directly related metastatic lesions, as well as a complete inheritance of loci displaying *MSI* from parent to child lesions with additional new loci exhibiting *MSI* in the child lesions (72).

As has been discussed in the previous subchapter (see 1.1.5) the *MSI-H* phenotype is widely considered to be caused by impairments of the *MMR* among specific types of cancers. Therefore, the prevalence of the *MSI-H* phenotype in melanoma is of special interest considering the research questions of this thesis. So far, the prevalence of *MSI-H* ranges between 0 – 50 % of the investigated tumor samples using conventional PCR based fragment analysis methods. (see Table 2) This wide variations, might be due to the fact that different types (i.e. *motif class* and *motif type*) of *MS* loci and/or *MS* loci on different chromosomes have been investigated and/or the small sample sizes of most of the studies. A more robust

study, at least considering the sample size, has been conducted by Vanderwalde et al. (73), who did investigate the *MSI* status of 345 melanomas and did not find a "*MSI-H"* phenotype in any of the observed melanomas. However, direct comparisons of this result are rather difficult, as they did use an next generation sequencing (:= *NGS*) approach and investigated 7317 targeted *MS* loci, using a cut off of ≥ 46 altered *MS* loci per mega base (:= *Mb*) for the *"MSI-H"* phenotype (73). Although they were able to show that this new definition resulted in high sensitivity, specificity, positive predictive value and negative predictive value compared to the old PCR based fragment analysis method (73) this is a limitation when comparing their result to the older findings.

Nevertheless, it seems, especially when integrating the findings of Vanderwalde et al. (73) that the *MSI-H* does occur at a rather small percentage considering melanoma of any kind, but might occur in higher percentages in some subsets of melanoma (see Table 2).

Nevi			
benign			
Phenotype	**%**	**(+/n)**	**REF**
MSI-L	0 0	(0/9) (0/30)	(74) (53)
MSI-H	0 0	(0/9) (0/30)	(74) (53)
≥ 2 MSI positive loci out of 11 loci	0	(0/8)	(70)
1 MSI positive locus out of 11 loci	0	(0/8)	(70)
dysplastic			
Phenotype	**%**	**(+/n)**	**REF**
MSI-L	28	(17/60)	(53)
MSI-H	0	(0/60)	(53)
≥ 2 MSI positive loci out of 11 loci	9	(1/11)	(70)
1 MSI positive locus out of 11 loci	8	(2/11)	(70)

Primary Melanoma			
Phenotype	**%**	**(+/n)**	**REF**
MSI-L	2 20 20 25 18 24 62 32	(1/41) (8/40) (2/10) (4/16) (8/44) (5/21) (8/13) (7/22)	(75) (76) (68) (71) (77) (69) (52) (53)
MSI-H	0 0 10 0 0 0 0	(0/41) (0/40) (1/10) (0/16) (0/44) (0/21) (0/13)	(75) (76) (68) (71) (77) (69) (52)

	0	(0/22)	(53)
≥ 2 MSI positive loci out of 11 loci	11	(6/56)	(70)
≥ 1 MSI positive loci out of 4 loci:	29	(10/34)	(67)
1 MSI positive locus out of 11 loci	16	(9/56)	(70)

Metastatic Melanoma			
Phenotype	**%**	**(+/n)**	**REF**
MSI-L	20	(2/10)	(68)
	25	(1/4)	(71)
	0	(0/10)	(77)
	27	(3/11)	(49)
	25	(2/8)	(69)
MSI-H	50	(5/10)	(68)
	0	(0/4)	(71)
	0	(0/10)	(77)
	46	(5/11)	(49)
	0	(0/8)	(69)
≥ 2 MSI positive loci out of 11 loci	21	(9/46)	(70)
≥ 1 MSI positive loci out of 4 loci:	77	(10/13)	(67)
1 MSI positive locus out of 11 loci	31	(13/46)	(70)

Melanoma (metastatic and primary)			
Phenotype	**%**	**(+/n)**	**REF**
MSI-L	13	(4/32)	(78)
	16	(5/32)	(74)
MSI-H	6	(2/32)	(78)
	0	(0/32)	(74)

Table 2 Prevalence of the Different Kinds of *MSI* Phenotypes in Melanocytic Lesions.
The MSI-L phenotype is defined as the occurrence of MSI positive loci in > 0% and < 30% of the loci investigated in a given case. The MSI-H phenotype is defined as the occurrences of MSI positive loci in ≥ 30% of investigated loci in a given case. Abbreviation: % := prevalence as percentage (round to the nearest whole number), (+/n) := (positive cases of the particular phenotype/total number of cases investigated), REF := study reference.

1.1.5.2 The Relationship of the *MMR* System and *MSI* in Human Melanoma

To our knowledge only four studies have investigated the relationship of the *MSI* phenotype and the *MMR* system in human melanoma (29,49,52,78). Of those studies Alvino et al. (29) were able to show, that the *MSI-H* phenotype did occur with a loss of protein expression of MSH2 and MSH6 as well as concomitant highly reduced *MMR* activity in the melanoma cell line PR-Mel. This provides evidence that disruptive changes in the *MMR* system might cause the *MSI-H* phenotype in human melanoma. However, Garcia et al. (49) did observe an *MSI-H* phenotype together with an IHC_{pos}-Status of MLH1, MSH2 and MSH6 in 40% (2 of 5) of the tested metastatic melanoma harboring this phenotype. Indicating that the *MSI-H* can occur in the absence of disruptive changes of the *MMR* system, at least on the protein staining level. Furthermore, Tomlinson et al. (78) observed an *MSI-H* phenotype in two patients without any single strand conformational polymorphisms within all exons of MSH2 nor MLH1. However, it must be stated that no other *MMR* proteins as well as no methylation

status nor protein expression status of some sort was assessed. Therefore, not ruling out the possibility that the observed *MSI-H* phenotype was either due to disruptive changes within other *MMR* proteins or altered methylation status of *MMR* genes. Hence final conclusions regarding the relationship between *MMR* proteins and the *MSI-H* phenotype cannot be drawn, especially as it has also been observed together with an IHC_{neg}-Status of all investigated *MMR* proteins (i.e. MLH1, MSH2, MSH6), as well as isolated IHC_{neg}-Status of MLH1 and MSH2 (49).

Considering the *MSI-L* phenotype, it has so far only been observed together with an isolated IHC_{neg}-Status of MSH2 or MLH1 (49) as well as in the presence of an preserved protein expression of MSH2, MSH6, MLH1 and PMS2 (29) or IHC_{pos}-Status of MSH2, MSH6 and MLH1 (52). Interestingly, the melanoma cells displaying an *MSI-L* phenotype in the presence of preserved *MMR* protein expression did show normal as well as reduced *MMR* activity compared to the control (29). However, the cells of the melanoma SN-Mel harboring an *MSS* phenotype in combination with preserved *MMR* protein expression did also exhibit a reduced *MMR* activity (29). This raises the question whether the observed reduction of the *MMR* activity measured by the study assay also translates into the *in vivo* environment. Lastly, no differences in the $\%_{IHC\_pos}$ between the *MSS* and *MSI-L* phenotype have been observed in primary radial growth phase melanoma (52).

Integrating the above-mentioned findings, it seems that it is rather difficult do draw definitive conclusions on the existence of disruptive changes of the *MMR* system solely based on the type of *MSI* phenotype and studies with larger sample sizes are needed to draw definitive conclusion regarding this question. However, it seems that disruptive changes are sufficient to cause an *MSI-L* or *MSI-H* phenotype, though they are not necessary.

This hypothesis is strengthened by the fact the *MSS* phenotype has so far only been observed together with preserved protein expression of the *MMR* proteins (29) as well as without an IHC_{neg}-Status of MSH2, MSH6 or MLH1 (49,52).

1.1.6 The Relationship of Tumor Mutational Burden and Immune-Checkpoint Inhibitors in Human Melanoma

1.1.6.1 The Tumor Mutational Burden

In a first step it seems of importance to clearly define the term *tumor mutational burden* (:= *TMB*) within this thesis, since this term remains to be inconsistently defined.

Within the dictionary of cancer terms by the National Cancer Institute *TMB* is defined as:

"The total number of mutations (changes) found in the DNA of cancer cells." (79)

However, this definition seems to be problematic, and rather impractical for concrete translational scientific research, as it implies the complete sequencing of the entire genome of cancer cells. Therefore, we consider the definition provided by Meléndez et al. as more suitable:

"[The] TMB is a quantitative measure of the total number of somatic nonsynonymous mutations per coding area of a tumor genome." (80)

This term allows to restrict the sequencing of tumor cells to the human exome limiting the amount of sequenced bases to approximately 30 to 50 megabases (:= *Mb*) or less than 2% of the entire genome (80). Nevertheless, when using this approach in a clinical setting as a diagnostic tool or predictive biomarker this may still be challenging for a set of reasons stated by Meléndez at al. (80):

- a test must be able to be performed on routine samples (limiting the amount of DNA, especially in biopsies)
- the results must be delivered in an adequate amount of time
- the price of the diagnostic tool must be affordable
- test results must be accurate to facilitate decision-making in clinical practice.

Considering these statements, gene panels might be preferable to perform *TMB* testing, since their total cost is lower, the turnaround time is shorter, they require lower DNA input, and can generate deeper sequencing on the same amount of DNA compared to whole exome sequencing (:= *WES*) (80). In line with this, there are currently different gene panels that have been used to investigate the *TMB* (81,82). However, using the definition stated earlier, the term *TMB* can no longer be used to refer to the measurement results obtained from these tests. Since, firstly not the entire coding area of the tumor cells was investigated, and secondly the results were normalized by the length of the observed coding region, resulting in the rate of mutations per *Mb*. Although it could be shown that the number of mutations per *Mb* measured using these target gene panels was highly related to the count obtained

from *WES* (81,82), the problem remains. Since the set of genes investigated differed between the two panels and one panel did count non-synonymous as well as synonymous mutations (81) whereas the other did only count non-synonymous (82). These reasons make it difficult to compare the results of the two panels, especially cut off values for clinical decision making. Therefore, we will maintain the definition of *TMB* as stated, however, will not refer to the results of gene panel tests with the term *TMB*. The results of these test will be described as *mutations per mega base* (:= *mut/mB*).

1.1.6.2 The *TMB* as a Biomarker in Melanoma Patients Treated with *ICI*

As it could be shown that somatic mutations can give rise to *neo-epitopes* (83) which may serve as *neo-antigens* (84,85) and *MM* appear to have high *TMB* (86) Snyder et al. conducted a study which, to our knowledge, was the first to investigate whether the *TMB* could serve as a predictive as well as prognostic biomarker in patients treated with CTLA-4 blocking agents (87). In this study it was shown that the *TMB* was indeed significantly associated with the long-term benefit from *ICI*. Shortly thereafter, Van Allen et al. could reproduce this finding and was also able to show, that the number of neo-antigens was directly related to the *TMB* within the observed cancer cells (88). Subsequently this has also been shown for *MM* patients treated with PD-L1/PD-1 blocking agents (89). However, the investigation in this study has been conducted using a gene panel and the *TMB h*as been calculated by extrapolating from the observed *mut/mB*. In the same manner a gene panel was used in another study, which investigated the *mut/mB* in various cancers including melanoma, treated with a variety of immune system related therapeutic agents (i.e. anti-PD-1/ PD-L1, anti-CTLA4, combination anti-CTLA4/anti-PD-1/PD-L1, high-dose IL2, OX40, anti-CD73, Talimogene laherparepvec, OX40 þ anti-PD-L1, IDO þ anti-PD-1) and found that the *mut/mB* pooled for all investigated cancers was significantly associated with the treatment response (90).

It is noteworthy that the findings by Snyder et al.(82) and Van Allen et al. (88) could not be reproduced in a study published by Campesato et al. (91), however, it is not entirely clear given the information provided by the authors, whether the analysis was performed using a WES and gene panel or gene panel only approach, making direct comparisons rather difficult.

1.1.6.3 The Tumor Mutation Load Essay

As the Oncomine Tumor Mutation Load Essay (ThermoFisher Scientific) (92,93) has been used within this study, this essay will be discussed briefly within this paragraph. This essay comprises of an *PCR*-based target enrichment panel that investigates 409 cancer related genes covering approximately 1.7 *mB* of the genome (93). The essay requires only 20 ng of target DNA and can be performed on a turn-around time of two days (93). *NGS* is performed using a high throughput semiconductor platform (93). The assay does not require matched normal tissue and can therefore be performed also when only tumor tissue is available (93). It has been shown that the essay archives a sensitivity of >90% and specificity of > 95% when the panel was performed in silico on The Cancer Genome Atlas (93). Furthermore, residuals of germ-line variants have been shown to be less then < 3 % on matched tumor and normal samples (93).

1.1.7 *MSI*, *dMMR* and *TMB* in the Context of *ICI* in *MM*

Vanderwalde et al. (94) performed a study comprising of 345 melanoma patients, investigating the *MSI* status together with the *TMB*. In their investigation they did not find any melanoma harboring an *MSI-H*, despite 36.5 % of the patients exhibiting a TMB high status (cut off: 17 *mut/Mb*) (94). Which indicates that a high TMB (adopting the study cut off) can occur in the absence of *MSI-H* thereby, most likely being *MMR* proficient, from which can be deduced that *dMMR* plays a rather small role as etiologic agent of TMB, if any. However, as has been previously stated, a *NGS* approach was used to measure the *MSI-H* status, posing a major limitation on the translation of previous findings regarding the *dMMR* and its relation to the *MSI-H* phenotype in the context of these results. Furthermore, beside the fact, that they did investigate the IHC_{pos} status of *MMR* proteins, they did not report any findings regarding melanoma patients, hence, only indirect conclusion regarding the *dMMR* status can be draw on the basis of the observed *MSI-H* phenotype.

Regarding the question whether *dMMR* is sufficient to induce an increase of the *TMB* as well as an increase in *MSI* among *MS,* Mandal et al. (95) performed an elegant study using the poorly immunogenic mouse melanoma cell line B16F10 within a mouse model. In this model MSH2 knock out B16F10 cells were engineered and serially passaged over the curse of 12 weeks (95). Cells were obtained at different time points (i.e. parental cells, after 4 weeks and after 12 weeks) and analyzed for novel non-synonymous short nucleotide variants (:= *SNVs*), novel coding indels and a genomic *MSI* score, compared to the parental cells (95). Using this model they were able to show that the genomic *MSI* score did significantly

increase from the parental to the 4 weeks as well as the 12 weeks group (95). Furthermore, they were able to show that the percentage of novel exonic indels within all novel mutations observed, did increase significantly from the 4 weeks to the 12 weeks group (95). These findings suggest that *dMMR* results in a state in which novel mutations accumulate over time, thereby increasing the number of mutations within a given tumor. As well that this state preferentially produces novel indel mutations increasing the number of *MS* exhibiting an *MSI* phenotype, which eventually leads to an *MSI-H* phenotype. Thus, providing evidence that *dMMR* is sufficient to cause an increase of *MSI* as well as *TMB,* at least in melanoma cells of the mouse.

In a next step, the cells of the different time points, were implanted into athymic nude mice, which were subsequently treated with an anti-PD1 antibody (95). Following the anti-PD1 treatment, a markedly pronounced decrease of the tumor volume within mice implanted with the 12-week cell group was observed compared to mice implanted with the 4-week or parental cell group (95). Indicating that melanoma harboring higher *TMB* as well as a greater genomic *MSI* score due to *dMMR* benefit more from anti-PD1 treatment, at least in mice.

Evidence strengthening this hypothesis has been provided by Ponti et al. (51) as they observed that the only patient harboring *dMMR* (i.e. IHC_{neg} of MSH6) exhibited the best response after anti PD-1 treatment within the observed cohort (n = 14).

Given these findings it can be concluded that *dMMR* is sufficient to produce an increase of *TMB* as well as in the rate of *MSI* (possibility resulting in an *MSI-H* phenotype) and that these changes are sufficient to increase the treatment outcome of patients treated with *ICI.*

However, the relevance of *dMMR* in the pathogenesis of a high *TMB* in human *MM* remains unclear.

1.2 *Research Motivation*

As stated previously the treatment of *MM* patients using *ICI* does constitute a feasible new therapeutic regiment in human melanoma (15), however, serious *irAE* are common (16). Taking this and the high costs of *ICI* therapy (17) into account it is of high interest to establish reliable predictive as well as prognostic biomarkers for the *ICI* treatment of *MM* patients.

These biomarkers must not only be cost efficient and reliable, but also implementable into the clinical routine. Furthermore, it is important that they can be performed on specimens obtained in the standard diagnostic routine. We, therefore, sought to reproduce previous findings using a new gene panel-based assay (Oncomine Tumor Mutational Load Assay), which can be performed using only very few amounts of DNA (i.e. 20 ng) as well as in the absence of normal non tumor tissue.

Besides this, we also aimed to validate whether the already established method used as a biomarker (i.e. evaluation of *dMMR-status* via *IHC*), in the routine setting of colorectal cancer at our institution, is applicable in *MM* patients as well.

1.3 *Hypotheses*

Based on the empirical data stated in the previous chapters, it can be inferred that:

- The effectiveness of *ICI* is related to the number of neo-epitopes expressed by tumor cells.
- The number of neo-epitopes is directly related to the *TMB*.
- The *TMB* is associated to the *treatment response* (:= *TR*) of *MM* patients treated with *ICI*.
- The *TMB* is directly related to the *mut/Mb.*
- The *mut/Mb* is associated to the *TR* of *MM* patients treated with *ICI*.
- Mutations within the *MMR* system results in a high number of mutations within *MM* cells.
- *MM* Patients suffering from cancer with known *MMR* gene mutations do benefit from *ICI*.

Therefore, the following hypotheses are stated:

1. The *mut/Mb* of *MM* patients, measured using the Oncomine Tumor Mutation Load Assay can be used to predict the *TR* of *ICI*.
2. A defective *MMR* system (i.e IHC_{neg} of *MMR* proteins and/or a *MSI-high* phenotype) can be found in *MM* patients especially within those, benefitting from *ICI*.

1.4 *Research Questions*

Based on the hypotheses stated in 1.3 this study seeks to answer the following research questions:

Identifier		Question
Main Question	**Sub question**	
Q_1 :=		Are there *dMMR* positive tumors in patients diagnosed with *CM* or *UP* treated with *ICI*?
	$Q_{1.1}$:=	Is a positive *dMMR-status* associated with the *TR*?
Q_2 :=		Are there tumors with an *MSI* phenotype in patients diagnosed with *CM* or *UP* treated with *ICI*?
Q_3 :=		Is there a statistically significant difference in the *TML-status* of *CM* or *UP* patients treated with *ICI* between patients with and without clinical benefit of *ICI*?
	$Q_{3.1}$:=	Is the *TML-status* a sufficient biomarker to predict *TR* in *CM* or *UP* patients treated with *ICI*?

Table 3 Research Questions of the Study.

2 Materials and Methods

2.1 *Comprising Study Description and Study Aim*

This study was designed as explorative retrospective pilot study to investigate the research questions stated in subchapter 1.4. To achieve this, a total of three different experiment types were performed. The performed experiments have been subsetted according to the following table:

Experiment Subset	Related Research Question	Experiment Type - Short Description
***E*$_{1.1}$ and *E*$_{1.2}$ (see 2.5)**	*Q*$_1$	Evaluation of the *MMR-status* via *IHC* (see. 2.5)
***E*$_2$ (see 2.6)**	*Q*$_2$	Evaluation of the *MSI-status* via *PCR* (see 2.6)
***E*$_3$ (see 2.7)**	*Q*$_3$	Evaluation of the *TML* via *NGS* (see 2.7)

Table 4 Overview of the Performed Experiment Subsets.

Each experiment process was modularized into modules stated in the following table:

Experiment Subset	Module Descriptor	Module – Name
E$_{1.1}$ and *E*$_{1.2}$ (see 2.5)	***E*$_{1.x}$M$_1$**	cohort generation (see 2.4.1)
	***E*$_{1.x}$M$_2$**	*IHC* (see 2.5)
	***E*$_{1.x}$M$_3$**	Microscopic evaluation (see 2.5.3)
E$_2$ (see 2.6)	***E*$_2$M$_1$**	cohort generation (see 2.4.2)
	***E*$_2$M$_2$**	*PCR* (see 2.6)
E$_3$ (see 2.7)	***E*$_3$M$_1$**	cohort generation (see 2.4.3)
	***E*$_3$M$_2$**	FFPE tissue cutting (see 2.7.1)
	***E*$_3$M$_3$**	HE staining (see 2.7.2)
	***E*$_3$M$_4$**	Microscopic evaluation (see 2.7.3)
	***E*$_3$M$_5$**	Marking the tumor area of interest (see 2.7.4)
	***E*$_3$M$_6$**	Digital image analysis (see 2.7.5)
	***E*$_3$M$_7$**	DNA extraction (see 2.7.6)
	***E*$_3$M$_8$**	DNA quality measurements (see 2.7.7)
	***E*$_3$M$_9$**	*TML* analysis (see 2.7.8)

Table 5 Overview of the Experiment Process Modules.

Due to the explorative character we also aimed to investigate methodological attributes (:= *inner module attributes*) within the modules to optimize further research projects. The motivation of investigation as well as the specification of the attributes are stated in the corresponding chapters.

2.2 *Study Process*

Originally, it was planned that the first two questions should be investigated by *SE*, however, *SE* did not finish the investigations and therefore the study was carried on and expanded by *MK*. It was decided that if the study showed promising results more complex studies (larger sample sizes, validation sets, prospective study design) should be performed. Therefore, experiment sets were performed in a sequential order (see Figure 7). The first two experiment sets ($E_{1.1}$ followed by E_2) were conducted by *SE*. After these, *MK* joined the study and reevaluated them (see 2.4.1). Subsequently, the last two experiments ($E_{1.2}$ and E_3) were performed by *MK,* followed by the characterization of the patients (see 2.3) and the statistical analysis (see 2.9). To minimize errors due to confounders, *outcome related attributes* and *potential outcome related attributes* were measured if possible (see 2.3).

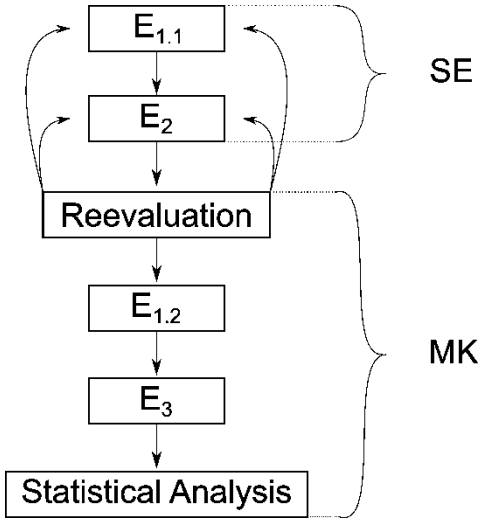

Figure 7 Study Sequence.

2.3 *Characterization of Patients*

Each patient was characterized based on the attributes specified in Table 6. The attributes were assessed by looking in the medical records of each patient. The data was obtained by *MK* and *MB*.

Patients Characteristics
Age at treatment initiation
Sex
Time between treatment initiation and diagnosis
ICI therapy
TNM status
Tumor stage
Breslow Thickness
Melanoma Type
LDH level
S100 level
CRP level
Neutrophil count
Lymphocyte count
Neutrophil to Lymphocyte Ratio
Eosinophil count
BRAF status
NRAS status
KIT status

Table 6 The Set of the Clinical Attributes Used for Patient Characterization.

2.4 *Cohort Generation and Tissue*

Due to the sequential nature of the this study the methods for the cohort generation modules of the experiment sets will be described together in this chapter in the following paragraphs. The overlapping patient sets have been visualized in Figure 8.

2.4.1 ($E_{1.1\text{-}2}M_1$) - $E_{1.1\text{-}2}$ Patient Set

In a first step a total of 27 patients, receiving a therapy with Pembrolizumab, Ipilimumab or Nivolumab in the time between 2012 and 2016 at the dermatology department of the medical university of Graz were included into the study by *SE*, as per protocol, based on the following inclusion criteria:

- Histologic diagnosis: cutaneous melanoma or melanoma of unknown primum
- Stage: III or IV
- Age: 18 – 90

Subsequently, tumor tissue of these patients was obtained from the *BioBank Graz* (96) for further analysis.

A set of patients (:= *stained-patients-set*) with a total number of 35 who had been stained immunohistochemically by *SE* (see 2.5), were found by *MK*. Since this exceeded the number of stained patients stated by *SE*, a revaluation of all the stained patients found was performed by *MK* for quality measurement. This was conducted using a list of all patients receiving Pembrolizumab, Ipilimumab or Nivolumab in the time between 2012 and 2018 at the department of dermatology of the medical university of Graz. In a first screening all patients with the following criteria were excluded from that list:

- Not clear whether patient received placebo or drug
- Patient switched between drugs
- Histological diagnosis different then cutaneous melanoma or melanoma with unknown primum
- Treatment initiation not within 2012 – 2016
- Age not within 18 - 90

After this screening, a total of 71 patients remained. In a second screening all possible tissue block histo-numbers found in the medical records were noted and patients for whom no tissue suitable for analysis, located in the *BioBank Graz,* could be identified, were excluded. A set (:= *possible-candidates-set*) of 57 patients remained after this screening. This set was then compared to the *stained-patients-set* (n=35). An intersection of 22 patients (:= *intersection-set*) could be found. From the remaining *stained-patients-complement-set* (*stained-patients-set* \ *possible-candidates-set,* n = 13) all patients meeting one or more exclusion criteria were excluded. Therefore, a total of 10 patients were excluded due to these reasons:

- Out of study time frame (n = 8)
- Non-CM or -*UP* (n = 1)
- No *ICI* therapy (n = 1)
- Not in medical records (n= 1)

The set of the remaining patients (n = 2), who met all inclusion criteria, was then united with the *intersection-set* resulting in a preliminary final set of patients (:= $E_{1.1}$-*patient-set*, n = 24). Since the E_3-*patient-set* was not entirely equal to the $E_{1.1}$-*patient-set* (see 4.2) it was decided to stain the complement of the E_3-*patient-set* ($E_{1.2}$-*patient-set* := E_3-*patient-set* \ $E_{1.1}$-*patient-set)* in the experiment $E_{1.2}$ ($E_{1.2}$-*patient-set* comprising of n = 3). The union of the $E_{1.1}$-*patient-set* and $E_{1.2}$-*patient-set* (:= $E_{1.1\text{-}2}$-*patient-set*, n = 27) was then used for further

microscopic analysis (see 2.5). After evaluating the stained slides (see 3.2) it was decided not to stain the remaining patients of the *possible-candidate-set* (see Discussion 4.2.1).

2.4.2 (E_2M_1) - E_2 Patient Set

As stated in the protocol, it was planned to evaluate the *MSI-status* in patients for whom a loss of expression in at least one of the stained *MMR* proteins was observed. The selection of the patient set for the E_2 was performed by *SE* before *MK* joint the study. A total of 10 patients were found to be examined by *SE.* This set (:= *initial-MSI-set*) was merged with the *possible-candidate-set* (see 2.4.1). A remaining *initial-MSI-complement-set* (*initial-MSI-set* \ *possible-candidates-set*) was found (n = 5). This set was excluded from the study to avoid inconsistencies and data corruption. Since the remaining intersection with the *possible-candidate-set* (:= E_2*-patient-set,* n =5) was a subset of the $E_{1.1}$*-patient-set,* with matching tissue block histo-numbers it was decided to include it into the study. It was decided not to examine the remaining complement set ($E_{1.1}$*-patient-set* \ E_2*-patient-set*) (see limitations 4.2).

2.4.3 (E_3M_1) - E_3 Patient Set

Due to the pilot character of this study and the costs of the *TML*-assay it was decided to evaluate only 15 patients using this method. Therefore, the medical records of all patients of the $E_{1.1}$*-patient-set* were reevaluated for their *TR* after *ICI.* This list was then reevaluated by *ER* to assure clinical validity and the patients were classified into a group benefiting from *ICI* treatment (:= *clinical-benefit group (CBG)*) and a *non-clinical benefit group* (for detailed explanation see 2.8.2). After this initial step, 3 patients classified as *CBG* (i.e. PAT 4, PAT 28, PAT 33) had been found. As, considering Q_3, it was planned to examine difference between the *CBG* and *non-CGB,* it was decided to increase the *CBG*. Therefore, the patients of the *possible-candidate-set* were reevaluated for their *TR* in the same manner as previously stated. After this we were able to identify 3 additional patients (i.e. PAT 10, PAT 22, PAT 30) being classified as *CBG*, and it was decided to include them into the E_3*-patient-set.* Subsequently, 9 patients of the $E_{1.1}$*-patient-set* who had been classified as *non-CBG,* were randomly selected and included into the E_3*-patient-set.* From these patients the most recent available tumor tissue was obtained and used for further analysis of their *TML-status*. It was decided not to limit the analysis to either primary or metastatic tissue only, but rather, to use the latest tumor tissue available, to reflect the actual clinical setting as closely as possible. In total the E_3*-patient-set* comprised of 15 patients, which intersected with the other patient sets as is depicted in Figure 8:

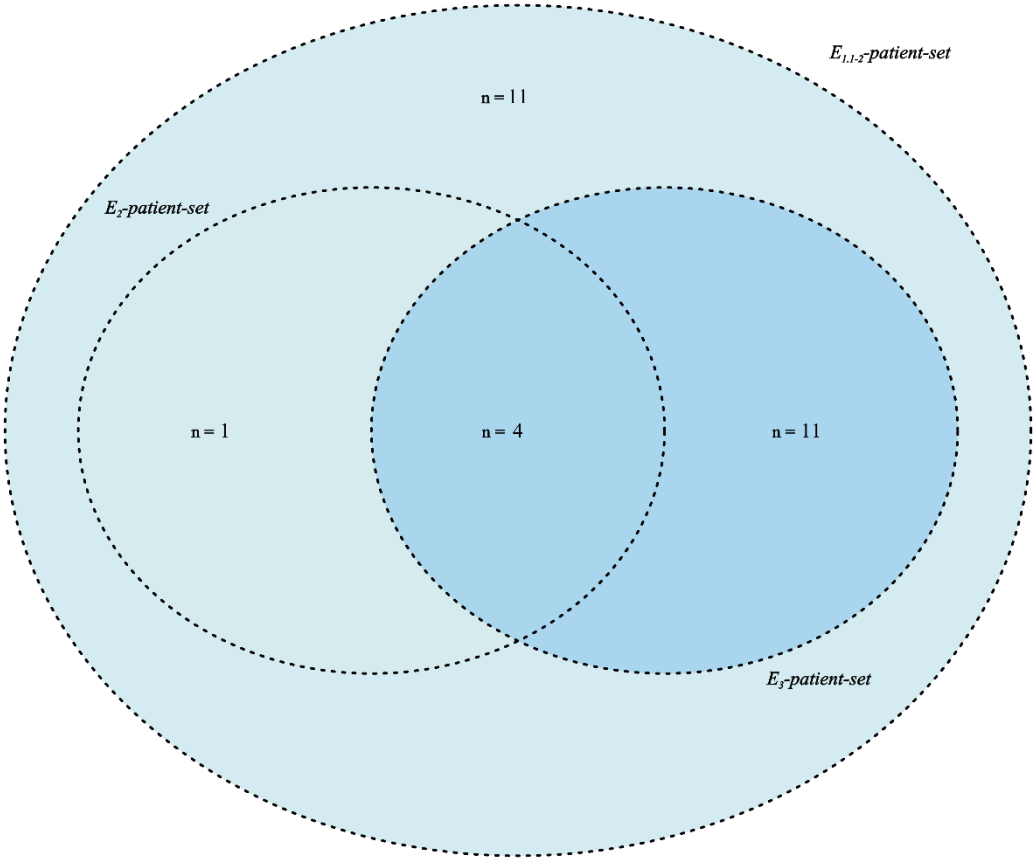

Figure 8 Venn Diagram of the Different Experimental Patient Sets.
This diagram depicts the different patient sets that have been investigated within this thesis, and their intersections. The number preceded by "n" refers to the sample size of the corresponding subset.

2.5 $E._{1.2}$ and $E_{1.1}$ - Immunohistochemistry (*dMMR-Status*)

2.5.1 $E._{1.x}M_2$ - Method and Materials

To investigate the *dMMR-status* (see 2.5.3) of a patient's tissue, all FFPE tissues of the $E_{1.1}$-*patient-set* and $E_{1.2}$-*patient-set* were stained immunohistochemically for the following four proteins MSH2, MSH6, MLH1 and PMS2. Tissues were cut at a thickness of 3-5 µm and stained using an automated stainer (i.e. Ventana Benchmark Ultra). The staining was performed using the VANTA MMR IHC Panel at the immunohistology-lab of the Diagnostic and Research Institute of Pathology (:= *DRI-Patho*). The slides were deparaffinized at 72°C and stained according to the following table:

Protein (Antibody)	Protocol
MLH1 (M1)	▪ Pretreatment with CC1 (FA. Ventana) for 40min at 100°C ▪ Application of Antibodies for 4min at 36°C ▪ Detection via OptiView DAB IHC Detection Kit (Productnr.760-700) + OptiView Amplification Kit (Productnr.760-099)
MSH2 (G219-1129)	▪ Pretreatment with CC1 for 64min at 100°C ▪ Application of Antibodies for 32min at 36°C ▪ Detection via OptiView DAB IHC Detection Kit (Productnr.760-700) + OptiView Amplification Kit (Productnr.760-099)
MSH6 (SP93)	▪ Pretreatment with CC1, 64min at 100°C ▪ Application of Antibodies for 24min at 36°C ▪ Detection via OptiView DAB IHC Detection Kit (Productnr.760-700) + OptiView Amplification Kit (Productnr.760-099)
PMS2 (A16-4)	▪ Pretreatment with CC1, 92min at 100°C ▪ Application of Antibodies for 36min at 36°C ▪ Detection via OptiView DAB IHC Detection Kit (Productnr.760-700) + OptiView Amplification Kit (Productnr.760-099)

Table 7 Technical Specifications of the Antibodies Used in the *IHC*-Module.

As positive control a FFPE tissue of a patient with colorectal cancer was stained in the $E_{1.1}$-*patient-set* (in the $E_{1.2}$-*patient-set* no positive control was stained see limitations 4.2).

2.5.2 Measured Inner Module Attributes

All stained slides were reviewed microscopically by *MK* on an optical microscope [A-Nikon Mikroskop E 600]. For each slide 3 non-overlapping, representative pictures (area with lowest positive staining pattern := $A_{IHC\text{-}low}$, area of highest pattern := $A_{IHC\text{-}high}$, area with most abundant pattern := $A_{IHC\text{-}most\ abundant}$) as well as one representative picture of positive internal controls (positively stained lymphocytes and normal tissue) in adjunction of the tumor tissue := $A_{control}$, were taken at a total magnification of 400 [x] (40 [x] objective, 10 [x] ocular) using a digital camera [ProgRes® SpeedXT core 3, JENOPTIK Optical Systems GmbH]. The pictures were digitally processed using the ProgRes® CapturePro 2.10.0.1 Software. To meet the picture observed by eye through the microscope, for each stained slide the following parameters were adjusted and kept the same for each sample:

- white value (documentation not possible, due to internal processing of the software)
- exposure time [ms]
- color temperature [K]
- colors (CMYK) [%]
- width of aperture
- light intensity (same for all pictures)

The images were then further analyzed using the digital image analysis software FiJI (97). First the files were converted to TIF files and then the following attributes were measured and computed for each Area:

Attribute name	Domain of values	Unit	Level of measure	Measurement/Computation instruction
[protein*] IHC-Ct-N_{total}	N_0	count	ratio	Compute using R: *[protein*] IHC-C_t-$N_{positve}$ +[protein*] IHC-C_t-$N_{positve}$*
[protein*] IHC-C_t-$N_{positive}$	N_0	count	ratio	Count cells manually using the cell counter plugin [FijI].
[protein*] IHC-C_t-$N_{negative}$	N_0	count	ratio	Count cells manually using the cell counter plugin [FijI].
[protein*] IHC-%-C_t-positive	{x: x ϵ R, 0 ≥ x ≤ 100}	percent	ratio	Compute using R*:* *[protein*] IHC-C_t-$N_{positve}$ / [protein*] IHC-Ct-N_{total} * 100*

[protein*] IHC-SI$_{[compartment**]}$	{none, weak, moderate, intense}		ordinal	Assign the value that is most appropriate considering all positive cells, to the whole area.
[protein*] IHC-SI-C$_{control}$	{none, weak, moderate, intense}		ordinal	Assign the value that is most appropriate considering all positive cells, to the whole area.
[protein*] IHC-R$_{SI(control,tumor)}$	{less, equal, greater}		ordinal	Assign the value that is most appropriate considering all positive cells, to the whole area.

Table 8 Specification of the Measured Inner Module Attributes of the *IHC* Module.
*the set of proteins for whom this attribute was measured was {MLH1, MSH2, MSH6, PMS2}.
**the set of cell compartments for whom this attribute was measured was {cytoplasmatic, nuclear}.

2.5.3 dMMR-Status

Each patient in the *$E_{1.1}$-patient-set* and *$E_{1.2}$-patient-set* was classified according to the following *dMMR-status* system:

Class	Definition
dMMR-positive	:= Patient for whom the *% [protein] positive tumor cells* in the protein set {PMS2, MSH2, MSH6, MLH1}was measured to be none in at least one of the proteins in ALL images.
dMMR-negative	:= Patient for whom the *% [protein] positive tumor cells* in the protein set {PMS2, MSH2, MSH6, MLH1}was measured to be convincingly NOT none in at least ONE of the images in all proteins.

Table 9 Definition of the *dMMR*-Status System.

2.6 *E_2 - Polymerase Chain Reaction (MSI-status, LOH-status)*

2.6.1 E_2M_2 - Methods and Materials

To investigate the *MSI-status* all patients of the *E2-patient-set* have been analyzed with a fluorescent *PCR*-based assay (MSI Analysis System, Version 1.2 Cat. No.:MD1641) and the AmpliTaq Gold® DNA Polymerase (Life Technologies Cat.No.: N8080242). The obtained *PCR* products were then further analyzed via capillary electrophoresis using the 3500 Genetic Analyzer (using: PowerPlex® C4 Matrix Standard (for "Spectral Calibration"), HiDi™ Formamide, GeneScan™ 500 ROX™ Size Standard, Performance Optimized Polymer Typ7 3500 Series, Anode Buffer Container 3500 Series, Cathode Buffer Container 3500 Series). In the *PCR* assay a set of seven genomic markers (five mononucleotide [BAT-25, BAT-26, NR-21, NR-24, MONO-27] and two pentanucleotide [Penta C and Penta D]) (see Table 10) were used to detect *MS*.

Marker name	GenBank Number	Major Repeat Sequence	Size Range (bp)	K562 Alleles (bp)
NE-21	XM_033393	$(A)_{21}$	94-101	101
BAT-26	U41210	$(A)_{26}$	103-115	113
BAT-25	L04143	$(A)_{25}$	114-124	122
NR-24	X60152	$(A)_{24}$	130-133	130
MONO-27	AC007684	$(A)_{27}$	142-154	150
Penta C	AL138752	$(AAAAG)_{3-15}$	143-194	163,174
Penta D	AC000014	$(AAAG)_{2-17}$	135-201	168,187

Table 10 Locus Information of the Seven Markers Used in the *MSI-Status* Analysis.
The information is obtained from the Promega MSI analysis system 1.2 technical manual (TM255) p. 2.

For each patient tissue an area with tumor and non-tumor tissue has been defined. The tissue of these areas has then been macro-dissected and analyzed separately with the assay.
The measured data has been viewed and analyzed using the Applied Biosystem GeneMapper 4.1 software.
To assure that the normal and tumor tissue are from the same patient, the data of the corresponding tissue samples (tumor ~ non tumor) has been aligned and the two pentanucleotide loci (Penta C and Penta D) have been compared for consistency in each patient.

2.6.2 MSI-Status

All analyzed patients were classified using the following *MSI-status* system:

Class	Subclass	Definition
MSS		:= Patient does not show any new allele in a mononucleotide locus in the tumor sample.
MSI		:= Patient exhibits a new allele in a mononucleotide locus in the tumor sample compared to the normal sample. The presence of a new allele is determined by either: ▪ a shift > 1 nucleotide (:= *nt*) of the location of the highest fluorescence peak of one mononucleotide locus in the tumor sample to the left or the right compared to the normal tissue sample. ▪ OR: increase of > 1 stutter peaks (all peaks being not the highest peak of the same fluorochrome, these peaks are caused by polymerase slippage) within the tumor sample compared to the normal tissue sample.
	MSI-H	:= Tumor sample shows ≥ 2 loci of the MSI class
	MSI-L	:= Tumor sample shows only 1 locus of the MSI class

Table 11 Definition of the *MSI*-Status System Used Within this Thesis.

2.6.3 LOH-Status

In addition to the *MSI-status* (see 2.6.2) we also investigated the *LOH* in all the analyzed patients. All patients were classified using the following *LOH-status* system:

Class	Definition
[locus*] LOH-positive	:= Patient shows an reduction of ≥ 50% of the fluorescence main peak signal in the observed locus in the tumor sample compared to normal tissue sample.
[locus*] LOH-negative	:= Patient shows a reduction of < 50% of the fluorescence main peak signal in observed locus in the tumor sample compared to normal tissue sample.

Table 12 Definition of the *LOH*-Status System.
The set of investigated loci was {BAT-25, BAT-26, NR-21, NR-24, MONO-27, Penta C, Penta D}

2.7 *E_3 - Next Generation Sequencing*

2.7.1 E_3M_2 - FFPE Tissue Cutting

2.7.1.1 Method and Materials

Each tissue block was cleaned from over standing bits of paraffin with a non-sharp knife to minimize random tilting and consequent loss of tissue due to increased trimming. The cutting was performed using a standard routine microtome [Microm HM440E]. To assure a *sufficient DNA yield* (Quality control 100 [ng], TML-analysis 20 [ng]) a *TML-required volume* was defined to be 5 [cm^2] · 5 [µm]. The *number of needed cuts* was estimated by:

$$n_{cuts} = 5\ [cm^2] / (Ø_{max\ assumed\ tumor\ area})^2\ [cm^2]$$

The maximal diameter of the *assumed tumor area* (defined as the macroscopically observable assumed tumor area) was measured using a cm scaled ruler. In one case (a biopsy) the *assumed tumor area* was estimated by multiplying the measured length and width.

Before cutting, the tissue blocks where placed on a cooling plate [PSI Medizin Technik Grünwald] for at least 30 [min] until the blocks reached a temperature of at least -1.1 [C°] The blocks remained on the plate and where not touched until the cutting process. The whole cutting process took 8:25 [h]. The blocks were cut at 5 – 10 [µm]. Before each new tissue block the whole microtome and all instruments as well as the working place where cleaned using a DNAse degrading agent [DNAse Away, Molecular BioProducts Cat.No. 7010]. After cutting, the tissue cuts where placed in distilled RNAse free water at room temperature to flatten out. The water was disposed after each block. One block was excluded since cutting could not be performed. The tissue of 15 patients was cut and a mean of 9.23 (*min*: 5, *max*: 34, *sd*: 8.17, n = 15) of cuts per block were performed. The flattened tissue slides were placed

on new glass slides to dry at room temperature. The dry slides were stored at 4 [C°] in a fridge until further processing. During the whole process as well as from this point onwards the cuts were only touched with clean gloves to avoid DNA contamination.

2.7.1.2 Measured Inner Module Attributes

The following attributes were measured by *MK*:

- ***Brownish coloration [tissue_block]***
- ***Brownish coloration [tissue_cut]***

Motivation

- To investigate whether brownish coloration of the tissue blocks, or tissue cuts is correlated with DNA yield.

Specification

Attribute name	Domain of values	Level of measure	Measurement instruction
Brownish coloration [sample_type]*	{none, +, ++, +++}	ordinal	none := no brownish coloration visible + := slight brownish coloration ++ := moderate brownish coloration +++ := strong brownish coloration

Table 13 Specification of the FFPE Tissue Cutting Module Inner Attributes.
Each sample was examined by *MK* for brownish coloration using a subjective ordinal measuring scale. The cut offs for the ordinal levels were defined in relation to the sample set itself, by comparing the samples side by side. *The set of sample_types contained {tissue_block, tissue_cut}.

2.7.2 E_3M_3 - HE Staining

2.7.2.1 Method and Materials

To assure that the tissue of interest could be found within the cut tissue, for each block the first cut of the cutting series were stained with hematoxylin and eosin (Mayer's) using the following protocol:

1. Incubate slides at for 30 min at 65 °C
2. Place in 100 % xylene for 15 min
3. Place in 100% ethanol for 2 min
4. Place in 90 % ethanol for 2 min
5. Place in 70 % ethanol for 2 min
6. Place in 50 % ethanol for 2 min
7. Rinse shortly in distillated water
8. Place in Mayer's hematoxylin for 3 min
9. Rinse with warm tab water for 3 min
10. Place in Eosin for 2 min
11. Place in 90% ethanol for 2 min
12. Place 100% ethanol for 2 min
13. Place in butyl acetate for 2 min
14. Mount with entellan

The cuts used for staining were cut to a thickness of 5 [µm] and after flattening in water at room temperature were placed in a warm water bath to flatten out even further. Before being stained as stated in the protocol, the flattened tissue cuts were placed on new slide to dry at room temperature. After drying the stained slides were microscopically evaluated (see 2.7.3) and the *tumour area of interest* was marked (see 2.7.4).

The stained slides were stored in the archive of the lab group.

2.7.3 E_3M_4 - Microscopic Evaluation

2.7.3.1 Method and Materials

Microscopic evaluation was performed by *MK* and *AA* using a standard light microscope used in the diagnostic routine by *AA*.

2.7.3.2 Measured Inner Module Attributes

All stained tissue slides were microscopically evaluated by *MK* for the following attributes:

- ***Availability of tumor tissue [E_3M_4]***
- ***% tumor cells***
- ***Melanin content [E_3M_4]***

Motivation

- ***Availability of tumor tissue [E_3M_4]*:** To assure, that the tumor tissue within the cut slides meets the *TML-required volume,* as to minimize unnecessary costs and data corruption.

- ***Melanin content [E_3M_4]*:** To validate if melanin content is related to DNA yield and success of NGS analysis

Specification

Attribute name	Domain of values	Level of measure	Measure instruction
Availability of tumor tissue [E_3M_4]	{available, not-available}	nominal	**not-available :=** no tumor tissue or found tumor tissue does not meet the *TML-required volume* **available :=** found tumor tissue meets *TML-required volume*
% tumor cells	{10%, 20%, 30%, 40%, 50%, 60%, 70%, 80%, 90%, 100%}	ratio	Choose the most appropriate value, considering the total tumor area.
Melanin content [E_3M_4]	{none, +, ++, +++}	ordinal	+ **:=** melanin can only be seen in 4x magnification ++ **:=** melanin can only by seen in 10x magnification +++ **:=** melanin can only be see in 40x magnification none **:=** melanin cannot be seen using either of the aforementioned magnifications

Table 14 Specification of the Microscopic Evaluation Module Inner Attributes.

2.7.4 E_3M_5 - Marking the Tumor Area of Interest

2.7.4.1 Methods and Materials

After microscopic evaluation of the HE stains the *tumor area of interest* was marked on each slide with a water-resistant pen. The *tumor area of interest* was defined as an area with densely packed malignant cells. The following areas were excluded from the *tumor area of interest* by drawing around them:

- areas of vast necrosis
- areas of high leucocytic invasion
- areas with high extracellular matrix and only a few tumor cells

These areas were excluded to minimize non-DNA substrate as well as non-tumor DNA.

2.7.5 E_3M_6 - Digital Image Analysis

2.7.5.1 Module Method and Materials

All tissue blocks and marked HE stains were photographed using an iPhone 7 on a white paper with a cm scaled ruler as length reference. The photos were obtained at an approximated distance of 30 [cm] parallel to the ground, using the integrated surface levelling software. The photos were then processed using the image analysis software FIJI. Each photo was converted to a cm scaled TIF file. These files were then used for image analysis.

2.7.5.2 Measured *Inner Module Attributes*

Motivation

- To evaluate the difference between the approximated *assumed tumor area* and the *d_assumed tumor area* as well as *tumor area of interest.*
- To answer the question whether the estimation of the *number of needed cuts* can be sufficiently calculated using the method stated in 2.7.1. or should be calculated based on a different approach.
- To investigate whether the DNA yield in [ng] can be sufficiently estimated by either of the measured variables (*tumor area of interest, d_assumed tumor area, assumed tumor area*) to optimize further research projects.

Specifications

The following attributes were measured by *MK*.

Attribute name	Domain of values	Level of measure	Measurement instruction
tumor area of interest	[cm^2]	ratio	Approximate the marked *tumor area of interest* on the HE stained slides with a polygon and measure the area of the polygon.
d_assumed tumor area	[cm^2]	ratio	Approximate the *assumed tumor area* on the tissue blocks with a polygon and measure the area of the polygon

Table 15 Inner Module Attribute Specification of the *NGS* Digital Analysis Module.

2.7.6 E_3M_7 - DNA Extraction

2.7.6.1 Method and Materials

Each tissue sample of the *E_3-patient-set* was brought to the *Molecular Diagnostic Lab* at the *DRI-Patho* (:= *Molecular Diagnostic Lab*) and was macro dissected for DNA extraction by *EW* in the presence of *MK*. The macro dissection was performed using a scalpel with a new clean unused blade for each new patient tissue sample. The tissue within the *tumor area of interest* was scraped of and placed in a clean 1.5 [ml] tube.

The tissue was then further processed on the Maxwell RSC Promega using the Maxwell RSC DNA FFPE Kit (A51450) according to the manufacturer protocol.

2.7.6.2 Measured Inner Module Attributes

Motivation

- To investigate whether brownish coloration after DNA extraction is correlated to melanin content.
- To investigate whether brownish coloration after DNA extraction is correlated with DNA yield.
- To investigate whether brownish coloration after DNA extraction is correlated to success in *NGS* analysis.

Specification

Attribute name	Domain of values	Level of measure	Measurement instruction
Brownish coloration [E_3M_7]*	{none, +, ++, +++}	ordinal	none := no brownish coloration visible + := slight brownish coloration ++ := moderate brownish coloration +++ := strong brownish coloration
Total area [measurement]**	[cm^2]	ratio	the value was computed using the following formula: *tumor area of interest* · number of used slides [n]

Table 16 Specification of the DNA Extraction Inner Module Attributes.

*Each sample was examined by *MK* for brownish coloration using a subjective ordinal measuring scale. The cut offs for the ordinal levels were defined in relation to the sample set itself, by comparing the samples side by side.

**The set of measurements contains {*tumor-area-of-interest, assumed-tumor-area,d_assumed-tumor-area*}

2.7.7 E_3M_8 - DNA Quality Measurements

To validate DNA quality, in a first step, the *DNA concentration* [ng/µl] was measured using a fluorometer (Quantus™ Fluorometer, Promega, E6150) and the Quant-iT™ PicoGreen® dsDNA Assay Kit (ThermoFisher, MP 07581). For this measurement, an amount of 40 [µl] of each sample was used. The measurement was performed as stated in the manufactures protocol (Promega Application Note #AN221). A mean DNA concentration of 40.27 [ng / µl] (*min*: 0.973, *max*: 80, sd: 31.2) was measured. It was decided to exclude all samples with less than 10 [ng / µl] from the following quality measurements, to assure to have enough DNA for the planned *NGS* analysis. Therefore, a total of 4 samples was excluded (i.e. PAT 1, PAT2, PAT 28, PAT 30). The remaining 10 samples were then used to measure the DNA segment length distribution. This was performed by conducting a *PCR* and subsequent gel electrophoresis. The IdentiClone™ BCL2/JH Gene Clonality Assay (Invivoscribe) and its primers were used for *PCR*. Two control size ladders (Gel Pilot 100 bp plus ladder (100) Qiagen cat. no. 239045, 100 bp ladder NEB #N0551S) were used to measure the *bp*-length. For gel electrophoresis 100 [ml] 1xTBE, 3% Agarose (3 [g]) as gel with 6 [µl] HDGreen plus (INTAS Science Imaging) as dye were used. 15 [µl] of each sample DNA together with 3 [µl] (100 bp ladder NEB) and 2 times 5 [µl] (Gel Pilot 100 bp plus) was placed on the gel. Electrophoresis was performed at 100 [V] for 40 [min]. Seven out of ten of the samples showed a *bp*-length of at least ~ 100 [*bp*] (highest measured *bp*-length was 300 [*bp*], n = 6 see Figure 9).

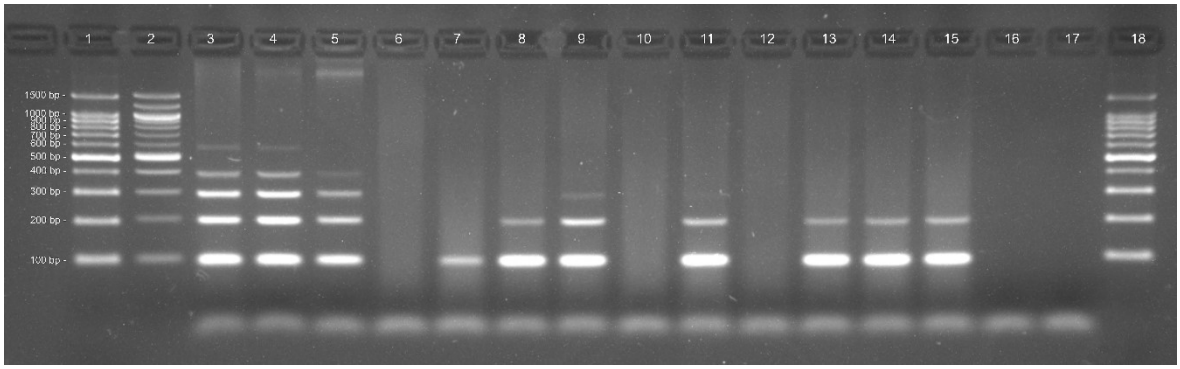

Figure 9 Photograph of the Control Size Ladders and DNA Segment Lengths.
The lanes 1 to 18 were loaded with probes according to the following list: (1) Gel Pilot Plus 100bp Qiagen, (2) 100 bp ladder NEB (#N0551S), (3) 0/0 control, (4) Pat DNA high qual. (a sample with known high quality DNA) , (5) Pat DNA low qual. (a sample with known low quality DNA), (6) PAT 26, (7) PAT 34, (8) PAT 9, (9) PAT 35, (10) PAT 14, (11) PAT 2, (12) PAT 33, (13) PAT 10, (14) PAT 4, (15) PAT 22, (16) blank extraction, (17) blank PCR, (18) Gel Pilot Plus 100bp Qiagen; The scale on the left hand side of the photograph depicts the fragment length [bp] in ascending order (i.e. 100 bp, 200 bp, 300 bp, 400 bp, 500 bp, 600 bp, 700 bp, 800 bp, 900 bp, 1000 bp, 1500 bp)

Three of the ten analyzed samples did not show any positive bands. It was decided to perform a Cancer Hot Spot Panel PCR (Ion Ampliseq Kit, ThermoFisher) using 10 [ng] DNA to determine whether the loss of amplification measured in the electrophoresis was due to

insufficient DNA or sample ~ kit interactions (possibly due to high melanin content see 3.1). As all three samples could be analyzed using this assay, it was decided to include them into the *TML* analysis as well. After the quality measurements, it was decided to include all 14 samples into the final *TML*-analysis. All quality measurements were performed at the *Molecular Diagnostic Lab* by *EW* and *ES*.

2.7.8 E_3M_9 - TML Analysis

2.7.8.1 Method and Materials

The *tumor mutation load* (*:= TML*) was measured using a targeted *NGS* approach via an Ion Torrent Chip. The Oncomine Tumor Mutation Load Assay (ThermoFisher) was used to create a gen library. The Oncomine Tumor Mutation Load – w1.0 – DNA – Single Sample workflow was performed as stated in the manufacturers protocol. A total of 10 [ng] of each tissue sample was used in this assay. Templating was performed on the Ion Chef System (ThermoFisher). Subsequent sequencing was performed on the Ion S5 System (ThermoFisher). Data analysis was performed using the Ion Reporter Software with the TMB algorithm v.1.0 (ThermoFisher). The analysis was conducted by *ES, EW* and *KK* at the *Molecular Diagnostic Lab*.

2.8 *Outcome Data*

2.8.1 Overall Survival

To analyze overall survival the following attributes were computed or measured:

Attribute name	Domain of values	Level of measure	Measurement instruction
Vital Status	{deceased, censored, unknown}	nominal	Look into the medical records classify according to: ▪ Deceased: only if a death report can be found in the medical records ▪ Censored: if the patient was alive until the last follow up

Date of death	{dd.mm.jjjj}	interval	Only include dates that are written on an official death report. In case no death report can be found no value is assigned.
Date of last follow up	{dd.mm.jjjj}	interval	The date of the last contact with the patient which can be found within the medical records.
Δ*days*	N_0	ratio	The interval of days between treatment initiation and death or *date of last follow up.*

Table 17 Specification of the Overall Survival Attributes.

2.8.2 Clinical Outcome

The clinical outcome of each patient was assessed by reviewing the medical records of the patients and assigning them into preliminary categories similar to the Response Evaluation Criteria in Solid Tumors 1.1 (:= *RECIST 1.1*) (98) consisting of ({clinical Progression of Disease (c*PD*), clinical Stable Disease (c*SD*), clinical Partial Response (c*PR*), clinical Complete Remission (c*CR*)}). These categories were assigned according to the following definitions:

- *cPD :=* Occurrence of new metastases or progression of already known metastases documented in follow up CTs or clinical examinations
- *cSD :=* No occurrence of new metastases and no apparent growth of already known metastases documented in follow up CTs or clinical examinations, without reduction of those metastases
- *cPR :=* Reduction of already known metastases documented in follow up CTs or clinical examinations, without occurrence of new metastases
- *cCR :=* Complete disappearance of already known metastases documented in follow up CTs or clinical examinations, without occurrence of new metastases

The clinical outcome was assessed for each patient 6 months after the treatment initiation and thereafter. The list of all patients within this study containing the assigned outcome classes were then reviewed by *ER* to assure clinical validity and a binary classification system was then applied assigning patients into a clinical benefit group (:= *CBG*) and a clinical non-benefit group (:= *non-CBG*) incorporating the former clinical outcome system, laboratory measurements as well as the clinical expertise of *ER*.

2.8.3 RECIST 1.1

To measure an objective treatment outcome (: = *oTR*) it was decided to use the *RECIST 1.1* (98). The radiological evaluation was performed by *EJ*. For each patient within the *E_3-patient-set* their sum of diameter of target lesions (*SOD*) was measured according to *RECIST 1.1* at *baseline* (before treatment initiation), after three months of treatment initiation and after six months. According to change of *SOD* the patients were classified using the *RECIST 1.1* status system ({Progression of Disease (= *PD*), Stable Disease (:= *SD*), Partial Response (= *PR*), Complete Remission (= *CR*)}). Due to the large discrete time intervals of three months in this study, it was decided not to calculate progression free survival intervals.

2.9 *Statistical Analysis*

All data mutation, statistical analyses and data plotting was performed using R (Version 3.6.1). The following additional libraries were used in their newest version: dyplr, ggplot2, cowplot, readr, tidyr, lubridate, ggfortify, ggpubr, venndiagram, pROC, stringr, survival, survminer. The following paragraphs state the statistical methods used and the theoretical justification for the used statistical model.

2.9.1 Linear Regression Analysis

For linear regression analysis the theoretical assumptions for each data set were checked by regression diagnostic plots (residual vs fitted, normal Q-Q, Scale-Location, Residuals vs Leverage). The plots are provided in the supplement (see 6.2.1).

2.9.2 Non-parametric Tests

In all situations where the distribution of the data was unknown, non-parametric test were performed. The Mann-Whitney-U Test was used to test unpaired data with factor level = 2. Kruskal Wallis Test was used for unpaired data with a factor level > 2. The Friedman's Test was used to compare paired data with a factor level > 2.

3 Results

3.1 *Inner Module Attributes*

3.1.1.1 Estimation of Tissue Area

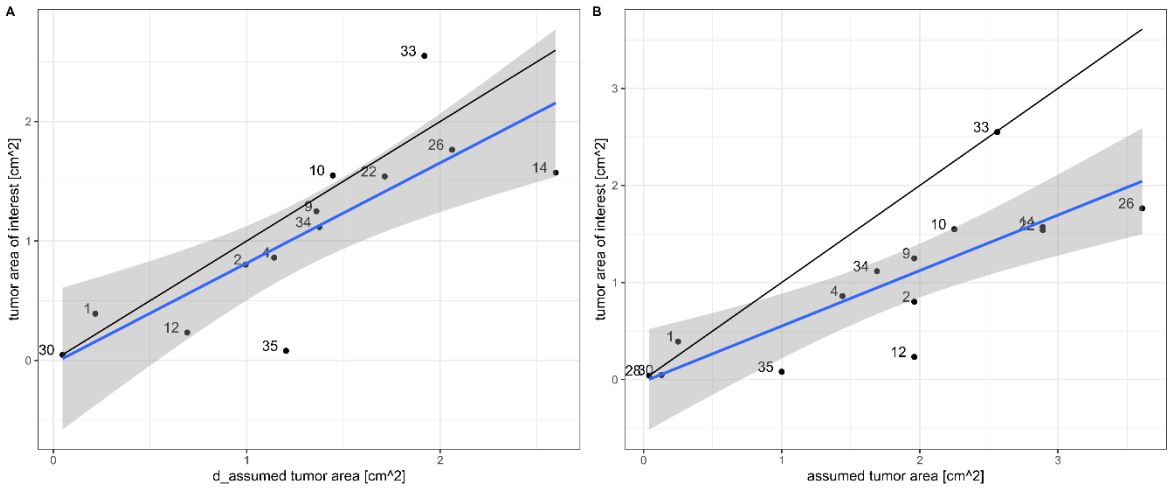

Figure 10 Estimation of *tumor area of interest* Using the *assumed tumor area* and *d_assumed tumor area.*

We were able to observe a statistically significant linear relationship between the *tumor-area-of-interest* and the *assumed-tumor-area* (p-value = 0.0003927, F-statistic = 23.6 on 1 and 12 DF, residual SE = 0.4641 on 12 DF, adjusted $R^2 = 0.6349$) and the *d_assumed-tumor-area* (p-values = 0.001037, F-statistic 19.49 on 1 and 11, residual SE = 0.469 on 11 DF, adjusted $R^2 = 0.6065$) validating that both measurement approaches can be used to predict the *tumor-area-of-interest*. Based on our findings the mean *tumor-area-of-interest* can be predicted using the following formulas (see Figure 10):

Equation 1

$$tumor\text{-}area\text{-}of\text{-}interest_{mean} = -0.02512 + 0.83956 * d\_assumed\text{-}tumor\text{-}area$$

Equation 2

$$tumor\text{-}area\text{-}of\text{-}interest_{mean} = -0.02042 + 0.57165 * assumed\text{-}tumor\text{-}area$$

3.1.1.2 Estimation of DNA yield

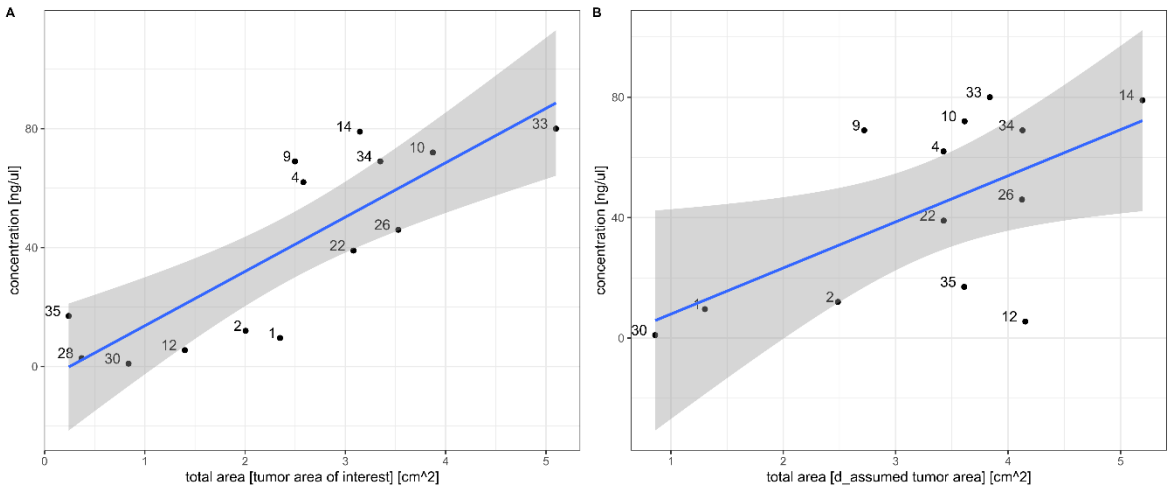

Figure 11 The Relationship Between the Total Area of Tumor Tissue and DNA Concentration.

The *total area [tumor-area-of-interest]* as well as the *total area [d_assumed-tumor-area]* were both significantly related to the DNA concentration of the samples tested with a *p-value* = 0.0004167 (F-statistic 23.26 on 1 and 12 DF, adjusted R^2 = 0.6314, residual SE = 18.96 on 12 DF) and *p-value* = 0.03022 (F-statistic = 6.183 on 1 and 11 DF, adjusted R^2 = 0.3016, residual SE = 25.5 on 11 DF) respectively (see Figure 11). No statistically significant relationship between the *assumed-tumor-area* and the DNA concentration was observed (p-value = 0.4933, F-statistic = 0.4992 on 1 and 12 DF, adjusted R^2 = -0.04007, residual SE = 31.85 on 12 DF). The investigation of the relationship was performed using a simple linear regression model. Based on our data, the mean DNA concentration can be estimated using the following formulas:

Equation 3

$$DNA\text{-}concentration_{mean}\ [\text{ng/ul}] = -4.587 + 18.285 * total\ area\ [tumor\text{-}area\text{-}of\text{-}interest]$$

Equation 4

$$DNA\text{-}concentration_{mean}\ [\text{ng/ul}] = -7.372 + 15.318 * total\ area\ [d\_assumed\text{-}tumor\text{-}area]$$

In a next step we evaluated the relationship between *DNA-concentration* and the *dissected tumor area of interest.* Since we were able to relate the *total area [tumor area of interest]* to the *DNA-concentration*, the DNA-concentration was normalized regarding to the *total area [tumor area of interest]*.

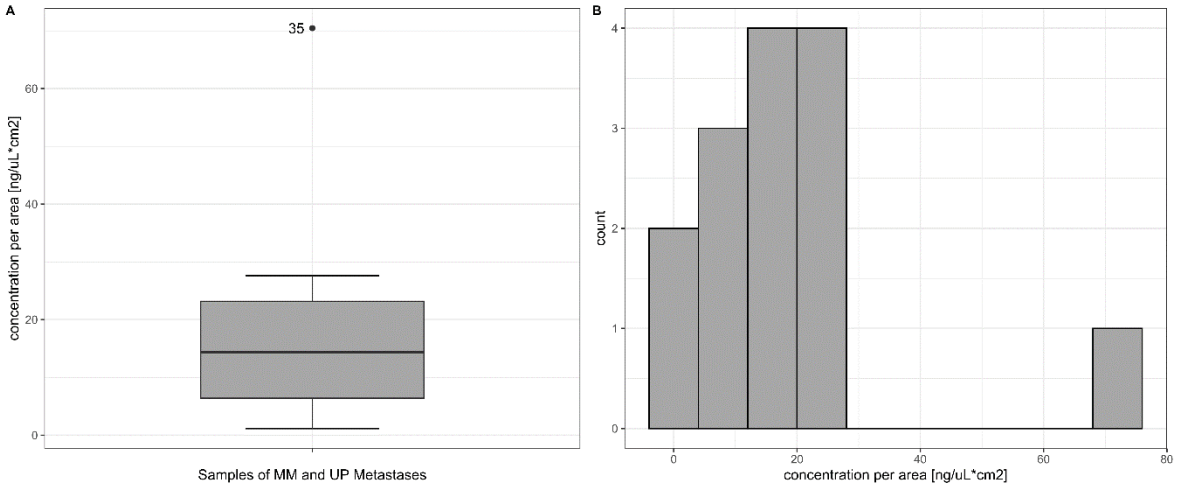

Figure 12 Distribution of the *DNA-concentration per Area* of Tumor Tissue Samples from Metastases of *MM* and *UP* Patients

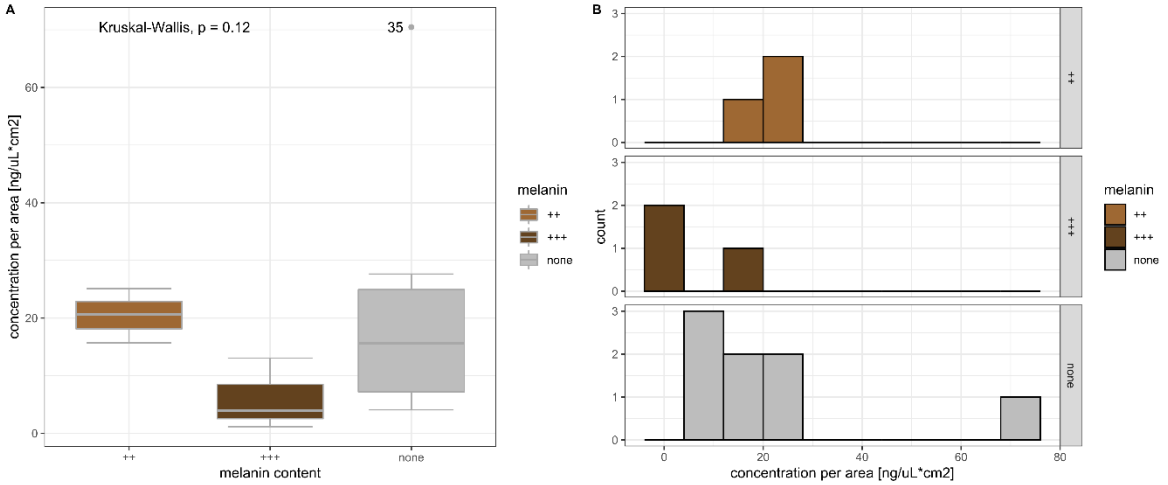

Figure 13 Impact of the Melanin Content on the *DNA-Concentration per Area.*

No statistically significant effect of melanin content regarding the DNA-concentration per area could be observed (p-value = 0.1209, Chi2 = 4.2262 on 2 DF) (see Figure 13).

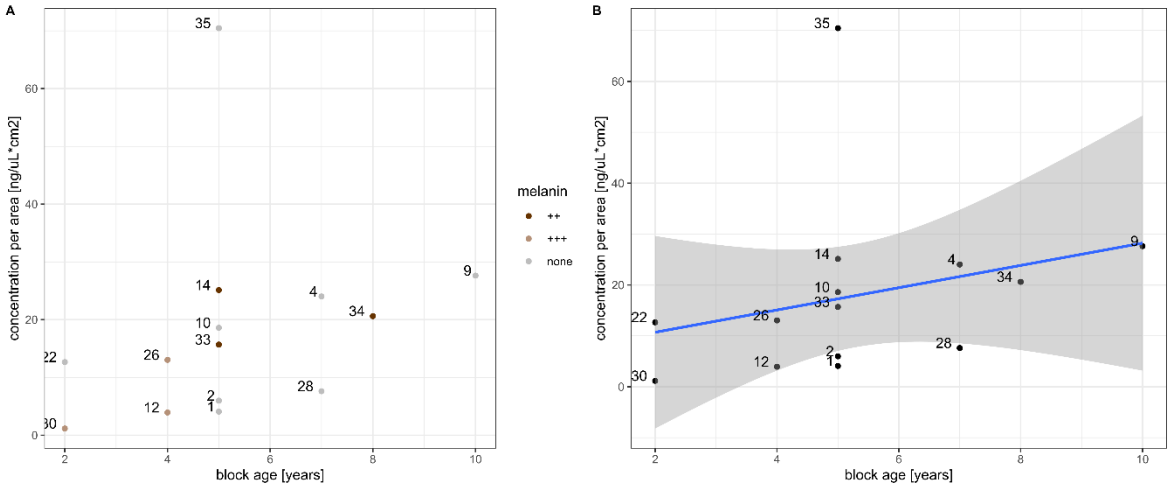

Figure 14 Block Age by Concentration per Area.

We were also not able to detect a relationship between block age and DNA concentration per area (p-value = 0.3457, F-statistic = 0.9633 on 1 and 12 DF) using a simple linear regression model (see Figure 18). Since one patient (i.e. 35) seemed to be an outlier concerning the *DNA-concentration per area*, this patient was reviewed again, however, no inconsistencies could be found, therefore, the patient was not excluded.

3.2 *Mismatch Repair Deficiency (dMMR)*

3.2.1 Results of the *$E_{1.1}$-patient-set*

3.2.1.1 Patients Characteristics

	Total (N = 24)
Melanoma Type	
CM	15 (62)
UP	9 (38)
Breslow Thickness	
median (*IQR*)	1.50 (0.95, 2.46)
mean (*sd*)	1.86 ± 1.28
Unknown	10/24 (42)
sex	
m	13 (54)
w	11 (46)
ICB Therapy	
Ipilimumab	15 (62)
Ipilimumab or Pembrolizumab	2 (8)
Nivolumab	4 (17)
Pembrolizumab	3 (12)
Tumor stage	
III C	1 (4)
IV	23 (96)
LDH baseline	
median (*IQR*)	201 (168.50, 320.50)
mean (*sd*)	276.00 ± 169.71
Unknown	1/24 (4)
S100 baseline	
median (*IQR*)	11.50 (6.75, 17.25)
mean (*sd*)	11.96 ± 6.64
BRAF	
K601E	1 (5)
none	11 (52)
V600E	9 (43)
Unknown	3/24 (12)
NRAS	
none	6 (67)
positive	3 (33)
Unknown	15/24 (62)
KIT	
none	8 (100)
Unknown	16/24 (67)

Table 18 Patient Characteristics of the *$E_{1.1}$-patient-set.*

3.2.1.2 *dMMR-Status*

After evaluating all samples of the *$E_{1.1}$-patient-set* (n = 24, plus 1 control), one sample (patient 4) had to be excluded since no tumor tissue could be found on the slides. Consecutively, 23 samples plus one control were analyzed and a total of 70682 cells were counted on a total of 288 images. In all stained slides tumor cells with convincingly positive staining status were found (see Figure 16).

> Therefore, we report a *dMMR-positive* status in 0% (0/23) [Clopper-Person *CI*: 0 – 14.81 %] patients tested.

The following figure depicts representative images of patient's stained tissue:

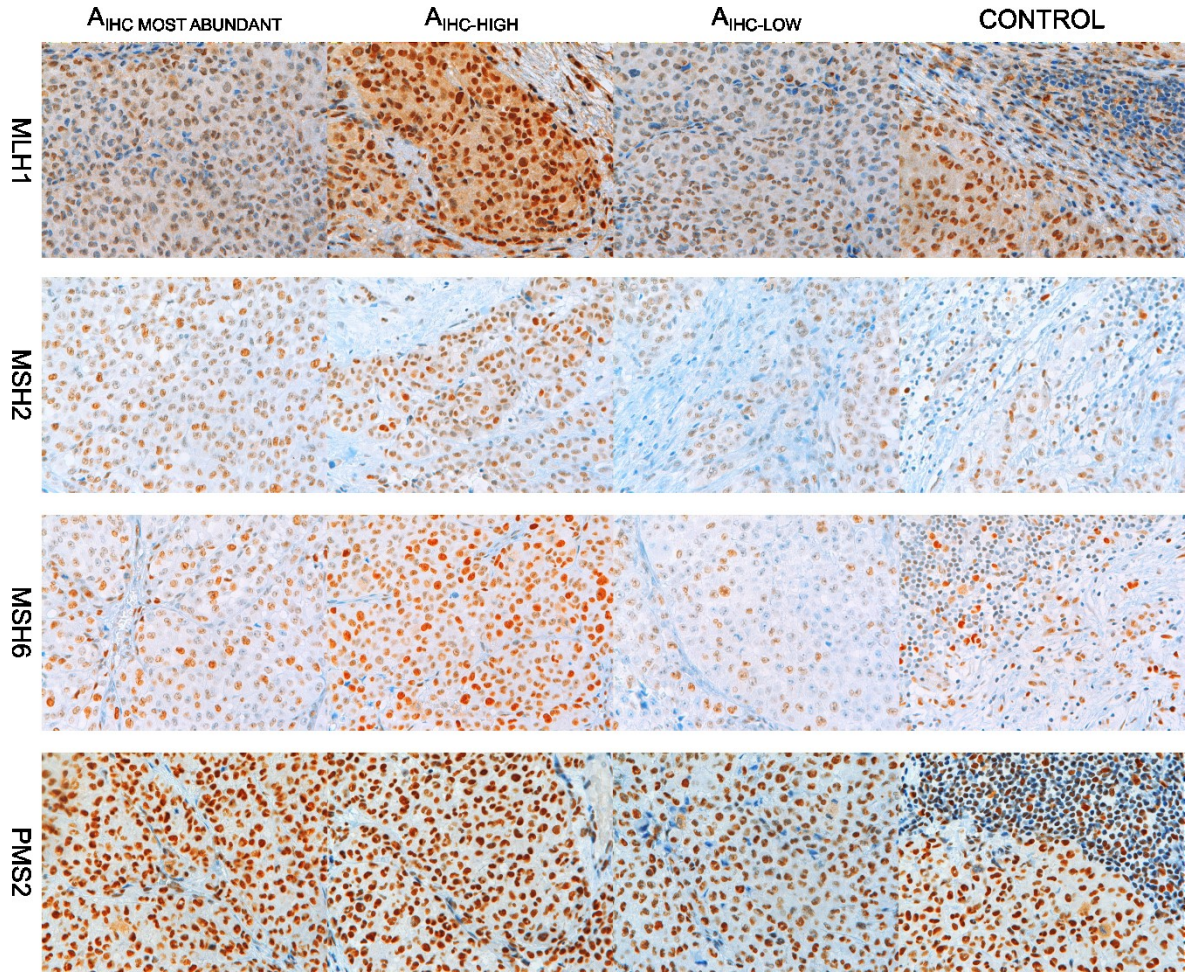

Figure 15 Representative Pictures of *MMR* Proteins Stained Via *IHC*.
The tumor tissue pictures are from the same patient (i.e. PAT 2). All images were taken at the same magnification (i.e. 400x), a scale bar was not included, due to a lack of a standardized length calibrator. The following technical specifications were used: exposure time 25 [ms], color temperature 3200 [K], width of aperture and light intensity were the same for all pictures, the white value was adjusted for each picture individually. Nuclear staining of lymphocytes or normal tissue were interpreted as positive internal control.

However, substantial differences in the percentages of positive cells between the evaluated areas ($A_{IHC\text{-}most\ abundant}$, $A_{IHC\text{-}low}$, $A_{IHC\text{-}high}$) were observed (see Figure 15 and Figure 16).

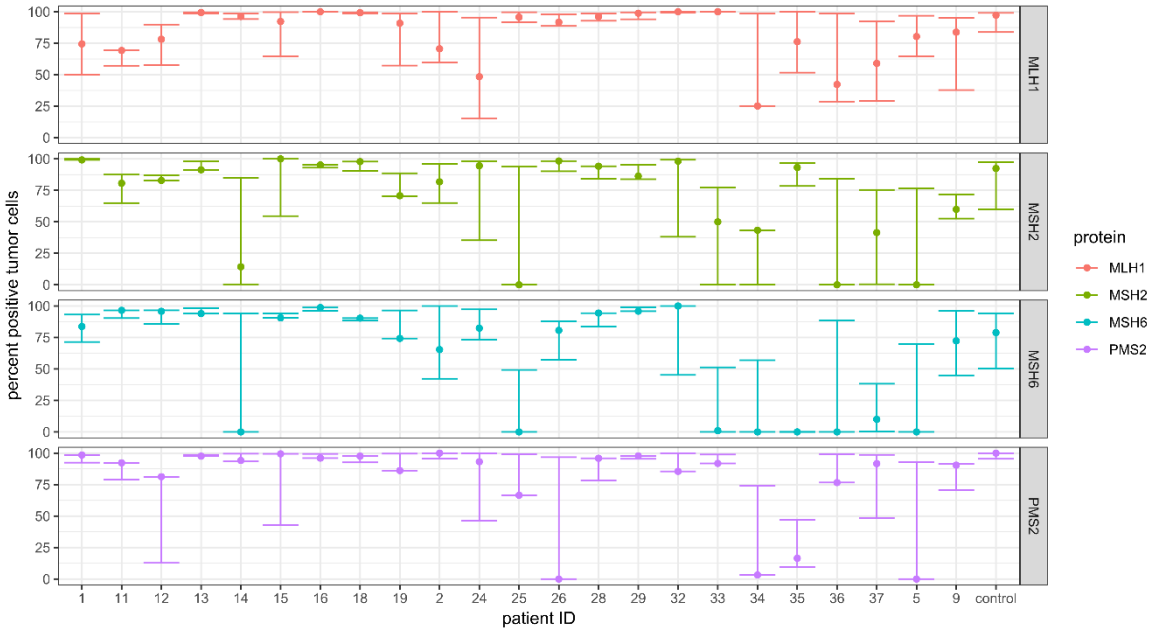

Figure 16 $\%_{IHC\_pos}$ within the *$E_{1.1}$-patient-set* by Stained Protein.
This figure depicts the $\%_{IHC\_pos}$ of the patient tissues examined within the E1.1-patient-set. The dot represents the value of the $A_{IHC\text{-}most\ abundant}$ and the error bars the $A_{IHC\text{-}low}$ and $A_{IHC\text{-}high}$.

Therefore, a subsequent in-depth analysis of the staining status considering the stained protein, the staining date and age of tumor blocks at staining was performed.

Since the distribution of the staining pattern within the tissue sample was not known, we considered the percentage of the most abundant pattern as the most appropriate for the further analysis. All subsequent analyses were therefore performed using the percentages of the $A_{IHC\text{-}most\ abundant}$.

3.2.1.3 In Depth Analysis of the Staining Pattern

Stained Proteins

The $\%_{IHC\_pos}$ did differ in the respect of the stained protein (see Table 19), with higher median percentages in in MLH1, PMS2 (90.91%, 91.83%) compared to MSH2 and MSH6 (82.85 %, 80.65 %). The variability did also differ substantially between the stained proteins with a high *IQR* in MSH6 (93.69 %), moderate in MSH2 (48.19 %) and rather low *IQR* in MLH1 and PMS2 (25.02%, 17.86%).

Protein	median [%]	*min* [%]	*max* [%]	*IQR* [%]
MLH1	90.91	25.14	100	25.02
MSH2	82.85	0	100	48.19
MSH6	80.65	0	100	93.69
PMS2	91.83	0	100	17.86

Table 19 Differences in the $\%_{IHC\_pos}$ Between the Stained Proteins.

The evaluation of the distribution of the percentage of positive tumor cells (:= $D_{\%, pos.ct}$) (see Table 20) appeared to be rather bimodal or U-shaped (see Figure 17A) for MSH2 and MSH6. The samples with low percentages in the patients stained for PMS2 (i.e. 35, 34, 26, 3) appeared to be outliers (values > 1.5 *IQR*), raising the question about technical errors in these samples especially patient 34, who appeared to be an outlier also in the MLH1 staining set. However, after reevaluation no differences could be found for those patients.

Interval / Protein	[0,10] %	(10,20] %	(20,30] %	(30,40] %	(40,50] %	(50,60] %	(60,70] %	(70,80] %	(80,90] %	(90-100] %
MLH1	0 (0)	0 (0)	1 (4.35)	0 (0)	2 (8.7)	1 (4.35)	1 (4.35)	4 (17.39)	2 (8.7)	12 (52.17)
MSH2	3 (13.04)	1 (4.35)	0 (0)	0 (0)	3 (13.04)	1 (4.35)	0 (0)	1 (4.35)	4 (17.39)	10 (43.48)
MSH6	8 (34.78)	0 (0)	0 (0)	0 (0)	0 (0)	0 (0)	1 (4.35)	2 (8.7)	3 (13.04)	9 (39.13)
PMS2	3 (13.04)	1 (4.35)	0 (0)	0 (0)	0 (0)	0 (0)	1 (4.35)	1 (4.35)	3 (13.04)	14 (60.87)

Table 20 Distribution of the $\%_{IHC\_pos}$ Cells for Each Stained Protein.
The number represents the total number of patients within the corresponding interval of a given Protein. The number in parentheses the percentage of patients within a given interval and protein.

The observed differences in the distributions between the *MMR* proteins were tested to be statistically significant (p-value = 0.01624, Friedman $Chi^2 = 10.291$ on 3 DF, n = 23) using

a non-parametric test for paired samples (Friedman's Test). This test was chosen since the $D_{\%,\ pos.ct}$ of the proteins remains unknown and did not show normality (see Figure 16A, no test performed). No post-hoc analysis was performed. In a next step the influence of staining date, and block age were analyzed.

Staining Date

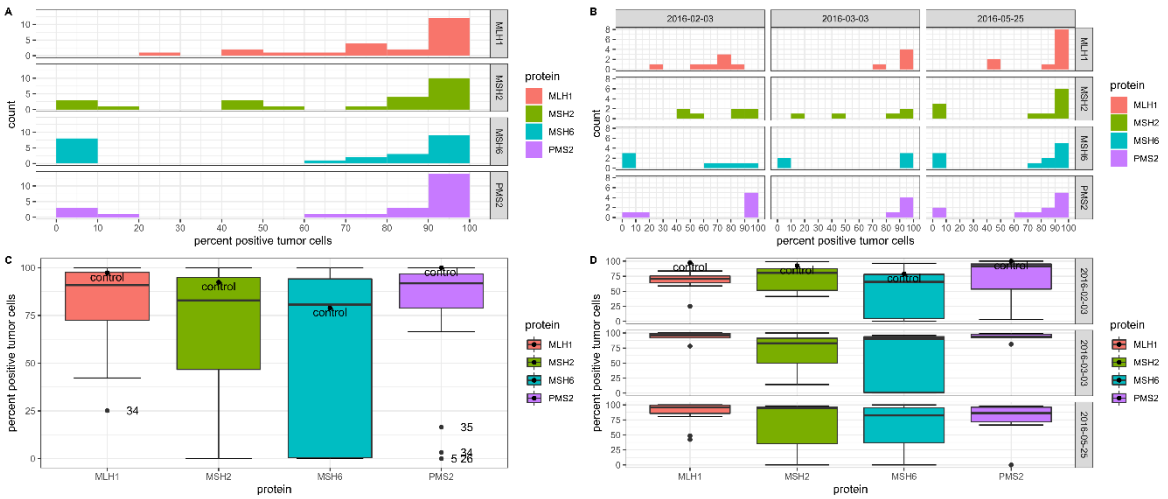

Figure 17 *%IHC_pos* within the *E1.1-patient-set* Subsetted by Stained Protein and Staining Date.

Considering the staining date, the plotted data suggested no strong effect, regarding the central tendency as well as the shape of the distributions (see Figure 17). However, since the sample sizes differed between the staining dates, (02.03.2016 n = 7, 03.03.2016 n = 5. 05.25.2016 n= 11) the Friedman's test could not be conducted, no other statistical analysis was performed.

Block Age

No statistical significant correlation between block age and the percentage of positive tumor cells considering the stained protein was found using a linear regression model (p-value = 0.449, F-statistic = 0.9833 on 7 and 84 degrees of freedom (:= *DF*), adjusted R^2 = -0.001285). Neither, by also considering the date of staining (p-value = 0.556, F-statistic = 0.9105 on 15 and 76 DF, adjusted R^2 = -0.01497). However, the analysis of the residuals revealed that the assumptions for linear regression might not be fulfilled (see 6.2.1). No further testing was performed.

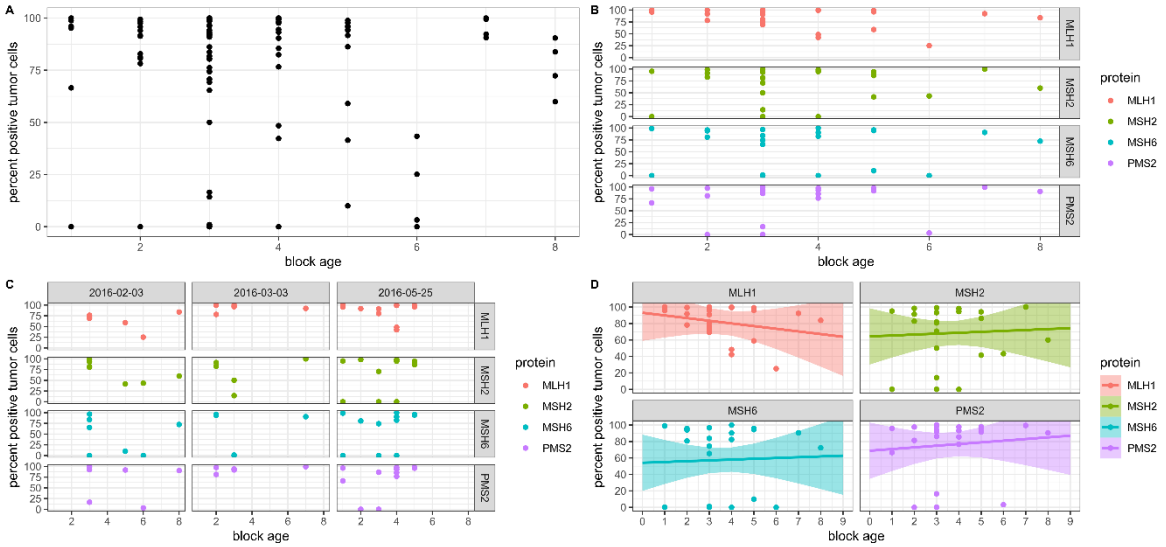

Figure 18 The Influence of Block Age on the $\%_{IHC\_pos}$

3.3 *Micro-Satellite Instability (MSI)*

In concordance with the results of the *$E_{1.1}$-patient-set* we were not able to observe any patient with an MSI phenotype (see Figure 19) within the investigated *E_2-patient-set*. However, a Penta-D positive *LOH-status* was observed in 40% (2 patients, n = 5) of the patients (see Figure 19).

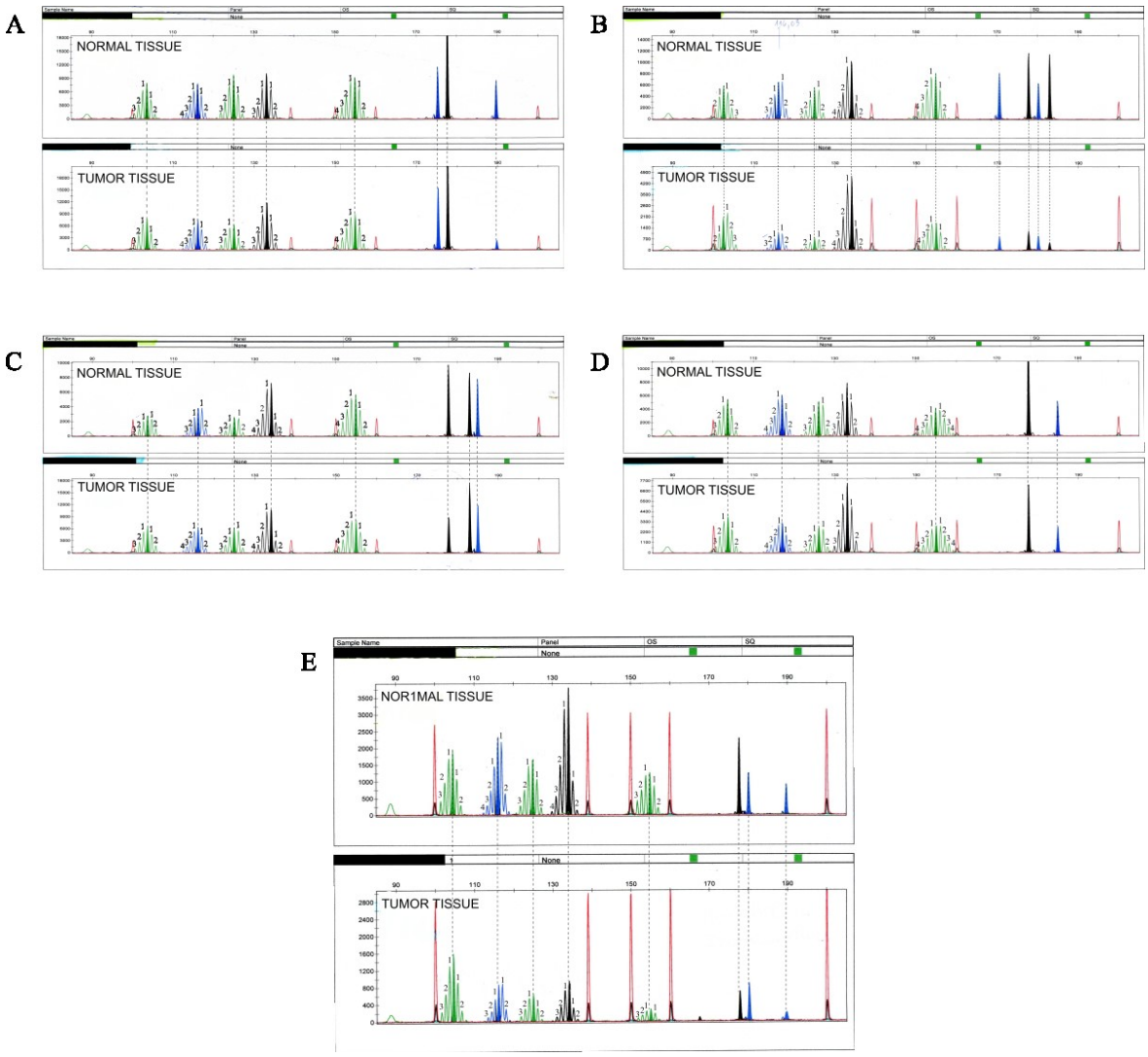

Figure 19 E_2 Results: *MSI*-Status and *LOH*-status of the Investigated Patients.
The figure depicts the results of the MSI analysis of the E_2-patient set. As there were no shifts of the highest peaks in any given locus nor an increase in the number of stutter peaks, we report an MSS phenotype in all investigated patients. The capital letters refer to the results of the following patients A = PAT 35, B = PAT 5, C = PAT 33, D = PAT 4, E = PAT 34. LOH was observed at the Penta D locus in 2 out of 5 patients (i.e. PAT 35 and PAT 34)

3.4 *Total mutational load (TML)*

3.4.1 Patient Characteristics

	CBG (N = 6)	non-CBG (N = 8)
Melanoma Type		
CM	3 (50)	7 (88)
UP	3 (50)	1 (12)
Breslow Thickness		
median (*IQR*)	1.60 (1.18, 1.90)	2.70 (1.25, 3.30)
mean (*sd*)	1.52 ± 0.73	2.51 ± 1.53
Unknown	3/6 (50)	1/8 (12)
Sex		
m	4 (67)	3 (38)
w	2 (33)	5 (62)
ICB Therapy		
Ipilimumab	3 (50)	6 (75)
Ipilimumab or Pembrolizumab	0 (0)	1 (12)
Nivolumab	2 (33)	0 (0)
Pembrolizumab	1 (17)	1 (12)
Tumor Stage		
III C	0 (0)	1 (12)
IV	6 (100)	7 (88)
LDH baseline		
median (*IQR*)	306.00 (238.00, 316.25)	205.50 (189.25, 268.25)
mean (*sd*)	286.83 ± 83.47	305.25 ± 241.15
S100 baseline		
median (*IQR*)	0.17 (0.08, 0.36)	0.10 (0.07, 0.42)
mean (*sd*)	0.22 ± 0.18	0.30 ± 0.38
BRAF		
none	2 (33)	3 (38)
V600E	2 (33)	4 (50)
V600K	1 (17)	0 (0)
Unknown	1 (17)	1 (12)
NRAS		
none	3 (50)	3 (38)
Q61	0 (0)	1 (12)
Unknown	3 (50)	4 (50)
KIT		
none	3 (50)	1 (12)
Unknown	3 (50)	7 (88)

Table 21 Patient Characteristics of the *E3-patient-set.*

The characteristics of the patients have been summarized in Table 21, for a more detailed summary table please consult STable 2.

3.4.2 Validation of Clinical Benefit Groups

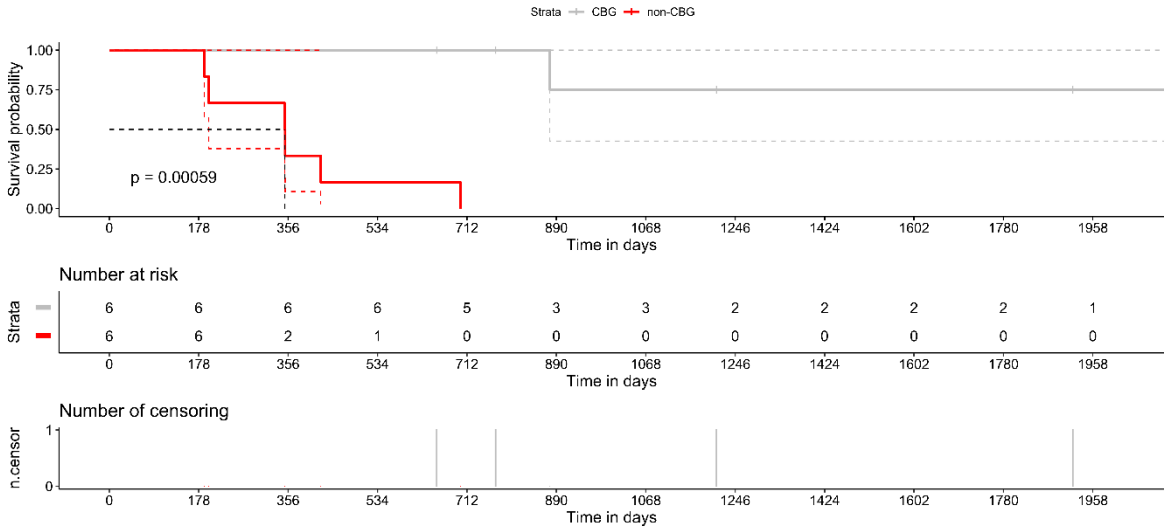

Figure 20 Kaplan Meier Curve of Patients within the *E3-patient-set* Stratified by *Clinical Benefit.*

In a first step we validated differences in *OS* (see Figure 23) between the *Clinical Benefit Groups*. Two patients were excluded from the statistical analysis due to the following reasons (the plot containing the two excluded patients can be seen in SFigure 3):

- Patient 34 (*non-CBG*): we were only able to obtain information about the last clinical follow-up, however, not whether the patient did die or not. The patient was excluded to minimize data corruption due to none-random censoring.
- Patient 26 (*non-CBG*): we knew that the patient did die, however, the exact date of death was unknown. Patient was excluded to minimize data corruption due to none-random censoring.

The *OS* between the two groups differed substantially, as only one *CBG* patient (i.e. 33) died within the observed time frame at day 877, wears no patients of the *non-CBG* lived longer than 699 days (median = 349.5 days, *min* = 189 days). The difference between the *OS* was tested to be statistically significant with a p-value = 0.00059 (Chi^2 = 11.8 on 1 DF, groups (n = 6, n = 6)) using a Log Rank Test.

In a second step we evaluated the *oTR* measured by *RECIST1.1* in the two groups.

Clinical Benefit	**3M (n = 8)**					**6M (n = 10)**				
	CR	PR	SD	PD	N group	CR	PR	SD	PD	N total
CBG	0 (0)	0 (0)	0 (0)	3 (100)	3 (100)	0 (0)	2 (50)	2 (50)	0 (0)	4 (100)
Non-CBG	0 (0)	1 (20)	1 (20)	3 (60)	5 (100)	0 (0)	0 (0)	1 (16.66)	5 (83.33)	6 (100)

Table 22 The Distribution of the *RECIST1.1-Status* in the *E3-patient-set.*

Due to incomplete data we were not able to measure the *RECIST1.1-status* in all patients consistently (see STable 3). Two patients (i.e. 26 (*non-CBG*), 30 (*CBG*)) were excluded from the analysis, since no sufficient radiological data was available in the medical data base. Six of the remaining patients (n =12) could be used in all follow-up time points (i.e. 2 (*non-CBG*), 4 (*CBG*), 12 (*non-CBG*), 33 (*CBG*), 34 (*non-CBG*), 35 (*non-CBG*)). Of the remaining six patients two could be used in the third month follow-up (i.e. 10 (*CBG*), 14 (non-CBG)) and four in the sixth month follow-up (i.e. 1 (*non-CBG*), 9 (*non-CBG*), 22 (*CBG*), 28 (*CBG*)). The reasons for exclusion are stated in STable 3.

In total we were able to investigate the *RECIST1.1* status of eight patients at three months and ten patients at 6 months. The exact distribution can be looked up in Table 22. The distribution of the *RECIST1.1*-status has been visualized in Figure 21.

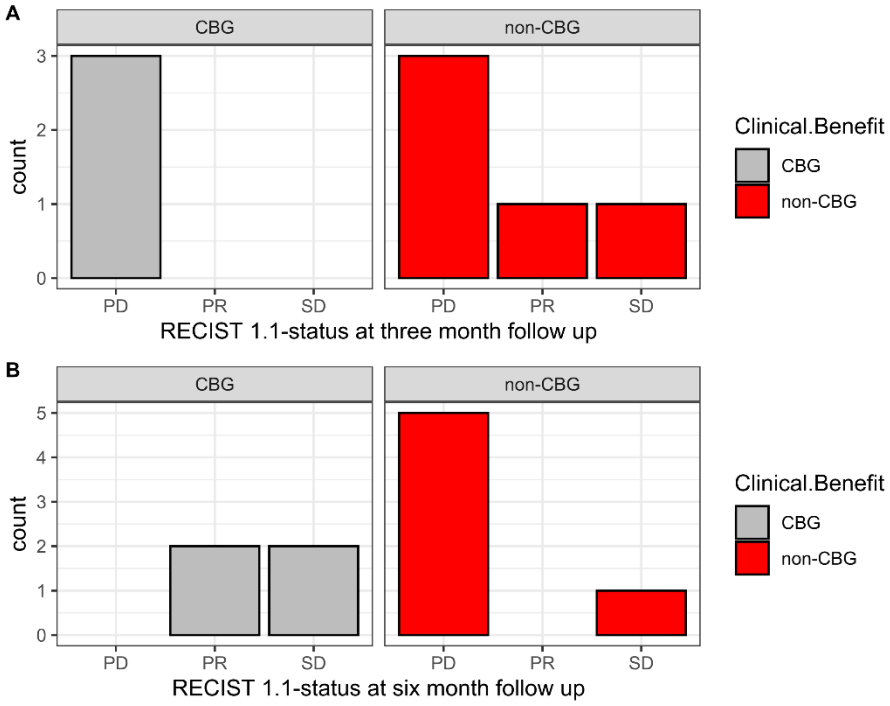

Figure 21 *RECIST1.1*-Status Distribution by *Clinical Benefit.*

The obtained results of the *oTR* at three months were rather unexpected, since 100% (3 / 3) of the patients showed a *PD* of disease. However, this result will be discussed later in this thesis (see 4.1).

3.4.3 TML-Status

A total of 14 samples was analyzed. In one patient (i.e. 34) *TML*-analysis did not yield any result. This patient was therefore excluded from further analyses. For the remaining samples, a mean average depth of coverage of 698 (*min* = 577, *max* = 1052, *sd* = 127) was achieved. The *TML-status* differed between the groups with a median 38.83 (*min* = 9.82, *max* = 171.71, *IQR* = 109.925) in the *CBG* and a median of 9.2 (*min* = 3.09, *max* = 68.74, *IQR* 12.72) in the *non-CBG*. This difference was tested to be statistically significant (p-value = 0.03671, W = 34, n = 13) using a one sided (CBG > non-CBG) Wilcoxon signed rank test (see Figure 22A).

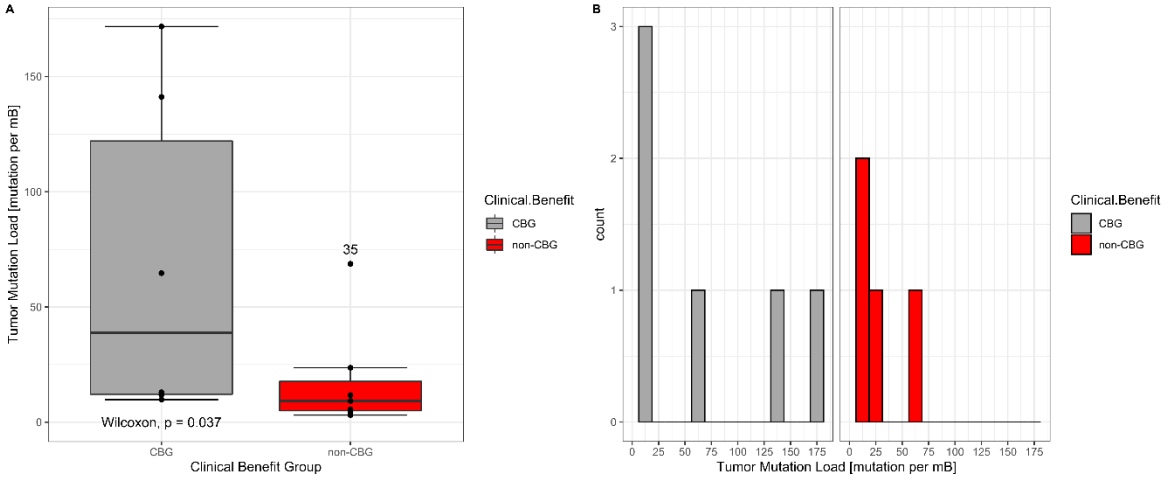

Figure 22 *TML*-Status by *Clinical Benefit*.

A receiver operating curve (:= *ROC*) was plotted (see Figure 23) to investigate the diagnostic ability of the *TML-status* as a binary classifier for *Clinical Benefit,* in the context of *CM* and *UP* patients treated with *ICI*. The predictive accuracy of the *TML-status* measured by the area under the curve (:= *AUC*) was 0.810 (*CI* 0.561 – 1.00) and the optimal cut-off point defined as Youden's J (99) was 9.51 [mutation/mB] (100 % sensitivity, 57.1 % specificity).

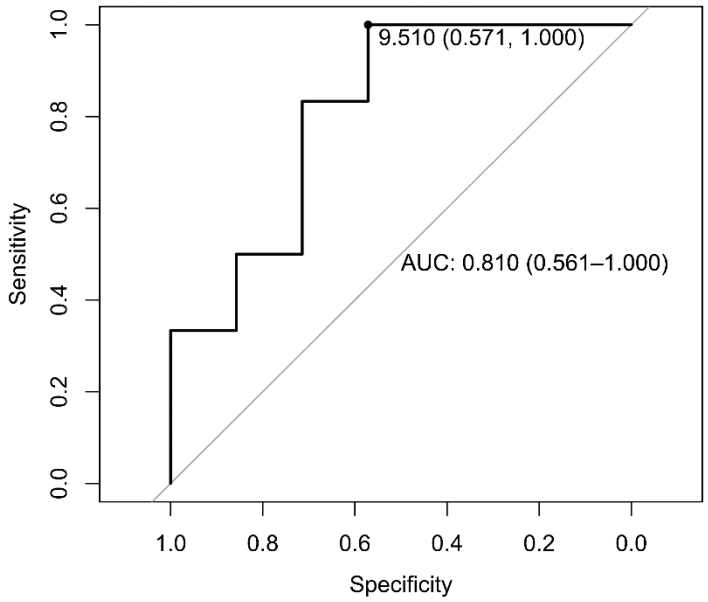

Figure 23 *ROC* of the *TML*-Status in *CM* and *UP* patients treated with *ICB*.

3.4.4 Relationship between *TML* Status and $\%_{IHC\_pos}$ of *MMR* proteins

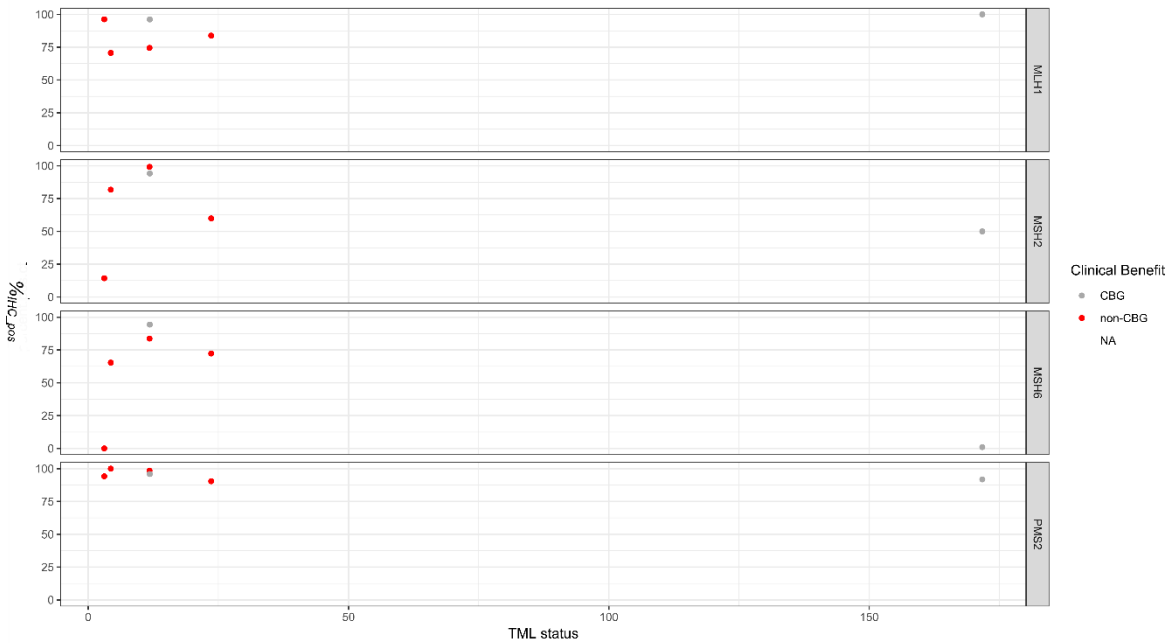

Figure 24 $\%_{IHC\_pos}$ in Relation to *TML* Status of the Investigated Proteins.
The figure depicts the $\%_{IHC\_pos}$ in Relation to TML status for each tested MMR protein. Only tissues with identical histo-numbers were used for this analysis (n = 7, PAT_1, PAT_2, PAT_9, PAT_13, PAT_14, PAT_28, PAT_33). All relationships between $\%_{IHC\_pos}$ and TML status showed no significant relation using a linear regression model (i.e. MLH1: p-value = 0.2994, MSH2: p-value = 0.667, MSH6: p-value = 0.2497, PMS2: p-value = 0.3162). Therefore, the regression functions were not plotted onto the data.

In a next step a possible relationship between the *TML status* and the $\%_{IHC\_pos}$ was investigated. (see Figure 24) Only the data of samples of the exact same histo-number for which the *TML status* and the $\%_{IHC\_pos}$ had been investigated were used for this analysis. Resulting in a sample size of n = 7 (i.e. PAT_1, PAT_2, PAT_9, PAT_13, PAT_14, PAT_28, PAT_33). No significant relation using a linear regression model was found between the $\%_{IHC\_pos}$ and *TML status* in the set of tested samples for each protein:

- **MLH1:** Adjusted R-squared: 0.07735 F-statistic: 1.419 on 1 and 4 DF, p-value: 0.2994,
- **MSH2:** Adjusted R-squared: -0.1862, F-statistic: 0.215 on 1 and 4 DF, p-value: 0.667
- **MSH6:** Adjusted R-squared: 0.1395, F-statistic: 1.811 on 1 and 4 DF, p-value: 0.2497
- **PMS2:** Adjusted R-squared: 0.05837 F-statistic: 1.31 on 1 and 4 DF, p-value: 0.3162)

Therefore, the regression functions are not displayed. No further testing using other regression models was performed.

3.5 $\%_{IHC\_pos}$ of MMR proteins and Clinical Benefit Groups

In a last step differences of the $\%_{IHC\_pos}$ of the stained *MMR* proteins between the *Clinical Benefit Groups* were analyzed. (see Figure 25) We report a significant difference in the central tendency of the $\%_{IHC\_pos}$ of MLH1 between the two *Clinical Benefit Groups* with *CBG* patients displaying a higher central tendency of $\%_{IHC\_pos}$ compared to *non-CBG* (i.e. Wilcoxon test: p-value = 0.00168). No significant difference of the central tendency between the *Clinical Benefit Groups* was observed for the other *MMR* proteins tested (i.e. MSH2: p-value = 0.345, MSH6: p-value = 0.4757, PMS2: p-value = 0.182).

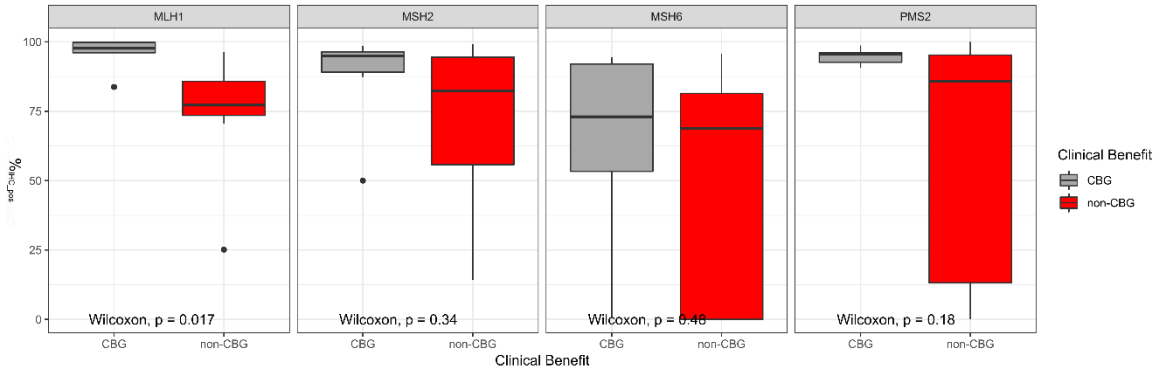

Figure 25 Differences in the $\%_{IHC\_pso}$ Between the *Clinical Benefit Groups.*
The figure depicts boxplots of the $\%_{IHC\_pos}$ values subsetted by the Clinical Benefit Group. A significant difference between the $_{IHC\_pos}$ between the CBG and non-CBG was found for MLH1 (i.e. p-value = 0.00168, using a Wilcoxon test) which shows a higher central tendency in the CBG compared to the non-CBG. No significant difference was found for the other MMR protein tested (p > 0.05).

A *ROC* was plotted (see Figure 26) to investigate the diagnostic ability of the $\%_{IHC\_pos}$ of MLH1 as a binary classifier for *Clinical Benefit,* in the context of *CM* and *UP* patients treated with *ICI*. The predictive accuracy of the $\%_{IHC\_pos}$ of MLH1 measured by the *AUC* was 0.896 (*CI* 0.726 – 1.00) and the optimal cut-off point defined as Youden's J was 93.888 [%] (87.5 % sensitivity, 83.3 % specificity).

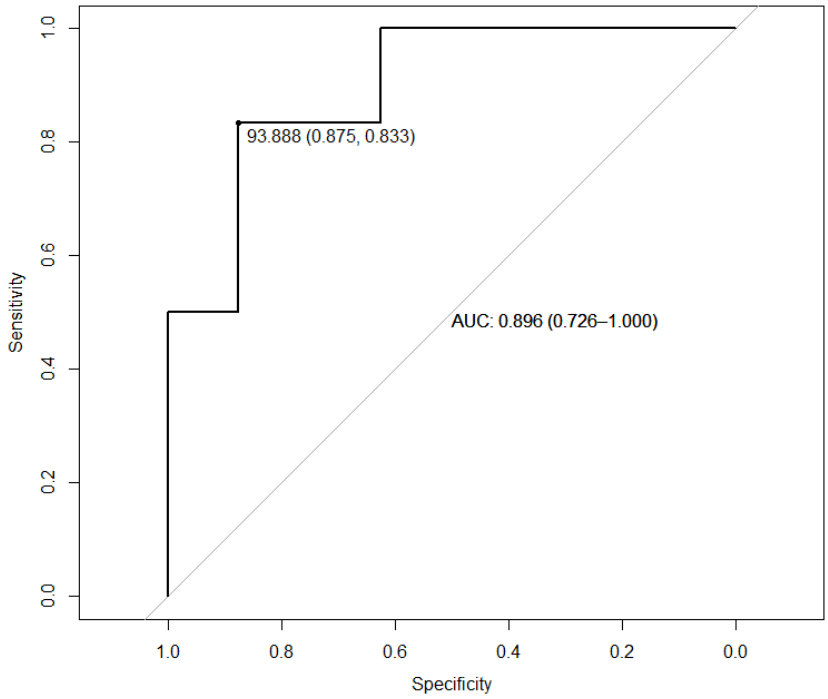

Figure 26 *ROC* of the $\%_{IHC\_pos}$ of MLH1 for *Clinical Benefit Group* Status.

4 Discussion

4.1 *Results in the Context of the Current Literature*

Given our patient set we did not find any disturbances of the *MMR* system in MLH1, MSH2, MSH6, PMS2 of patients treated with *ICI* (prevalence 0% (0/23) [Clopper-Pearson *CI*: 0 – 14.81%]. Our finding stands in line with previous studies which did also not detect any disruptive changes of the *MMR* system in human *MM* (40,52,57,100). However, it must be emphasized that none of these studies did investigate all *MMR* proteins, which were tested in this study. Considering the *dMMR* status of the individual proteins tested in this study, the same results have been observed by other authors that did find an *dMMR* in at least one other *MMR* protein, for MLH1, MSH2 and PMS2 (i.e. MLH1: (28,47,51,101), MSH2: (47,51,101), PMS2: (26,47,51)). Furthermore, when considering the *CI* of the observed prevalence of this study [0 – 14.81%], similar findings with a prevalence of *dMMR*, given a specific *MMR* protein, within the calculated study *CI* have also been found (i.e. MLH1: (46,48), MSH2: (28,46,48), MSH6: (47,51), PMS2 (26)). However, there are studies that did report substantially higher prevalence rates of *dMMR* in certain *MM* subsets, ranging between 32 – 42 % for the proteins MLH1 and MSH2 (26,41,48,49) as well as one study reporting a prevalence of *dMMR* of 20 % for MSH6 (49).

Nevertheless, the two studies with the largest sample sizes are in line with our findings, as Alvino et al. (47) reported a prevalence of *dMMR* of 0 % for the proteins MLH1, MSH2 and PMS2 as well as a prevalence of 6.18 % for MSH6 by investigating 91 – 101 patients for each stained protein. Furthermore, Song et al. (57) did report a prevalence of 0 % for the protein MSH2 incorporating 350 patients into their investigation. This suggests that the true prevalence of *dMMR* does not exceed the calculated study *CI* in *MM* patients.

So far only two studies have, to our knowledge, investigated the *MMR* status of *MM* patients treated with *ICI* (51,101). In concordance with our findings both studies did not detect any *dMMR* in the proteins MLH1 and MSH2 (51,101). Additionally Ponti et al. (51) did also not find any *dMMR* in the protein PMS2. Interestingly, they found a *dMMR* status of MSH6 in one of the investigated patients relating to a prevalence of 7.14 % (51) laying in a rather close proximity of the prevalence detected by Alvino et al. (47) (i.e. 6.18 %).

Hence it can be speculated that disturbances of the MSH6 protein may be of major interest in the context of *MM* patients treated with *ICI*, especially as it has been shown that a MSH6 low (cut off < 20 %) is significantly related to the *OS* in *MM* (47). However, we were not able to detect any differences in the $\%_{IHC\_pos}$ of MSH6 between the *CBG* and *non-CBG* of

our study. Though it must be emphasized that our study was not designed to test this hypothesis rigorously, as well as that the patients for whom this relation had been shown were not treated with *ICI* (47).

Nevertheless, we were able to show a highly significant difference ($p = 0.00168$) in the central tendency of the $\%_{IHC\_pos}$ of MLH1 between the *CBG* and *non-CBG* with the *CBG* patient set displaying a higher central tendency. This finding stands in contrast to the finding observed by Meyer et al. (56) in which a higher staining status of MLH1 measured via a semiquantitative scoring system had been shown to be related to a worse outcome in *MM* patients. However, the patients who had been investigated in this study did also not receive *ICI*, as well as a different measure had been used.

In concordance with the results of the *MMR* investigation we did not find any tumors harboring a *MSI* phenotype. This observation stands in line with previous observations that did also find a *MSS* phenotype only in the presence with an IHC_{pos}*-status of* MSH2, MSH6 or MLH1 (49,52). As well as previous studies that did not observe a *MSI-L* nor *MSI-H* phenotype (see Table 2).

Considering the *Clinical Benefit Groups* we were able to show that our classification did result in a highly significant difference in the *OS* (p-value = 0.00059) of the *CBG* compared to *non-CBG,* with patients of the *non-CBG* exhibiting a lower *OS* then the *CBG*, validating the approach of classification used within this thesis. Surprisingly, we observed an *oTR* of the *PD* type (*RECIST 1.1* (98)) in all patients of the *CBG* for whom the *oTR* was computable ($n = 3$) at the *3M* follow up. However, these seemed to be due to a phenomenon called "pseudo-progression" or "atypical progression" that can occur in melanoma patients treated with *ICI ,* when the *oTR* is measured via the *RECIST 1.1* (102). As some patients exhibit an initial increase of the size of their neoplastic lesions, which is then followed by a decreased in lesion size, thus being misclassified by using the *RECIST 1.1* classification (103). Therefore, a new standardized classification system for solid tumors treated with *ICI* - the immune-related response criteria - has been developed (103). We, therefore, interpret the initial *oTR* of the *PD* type in the *CBG* rather as technical artifacts/misclassification then as a real progression of disease, especially given the long *OS* of these patients observed in our study.

Lastly, consistent with previous findings (87–89) we were able to detect a significantly higher central tendency within a *TMB* related measure (i.e. *mut/Mb*) in patients benefiting from *ICI.* Furthermore, we were also not able to detect patients of the *MSI-H* phenotype within the subgroup of patients exhibiting an increased *mut/mB* similar to what has been

found by Vanderwalde et al. (94). Additionally, these patients did also not exhibit a *dMMR* (94).

4.2 *Limitations*

As this study was a pilot study, we must emphasize that this study has a set of limitations which will be discussed in the paragraphs below.

4.2.1 Sample Size

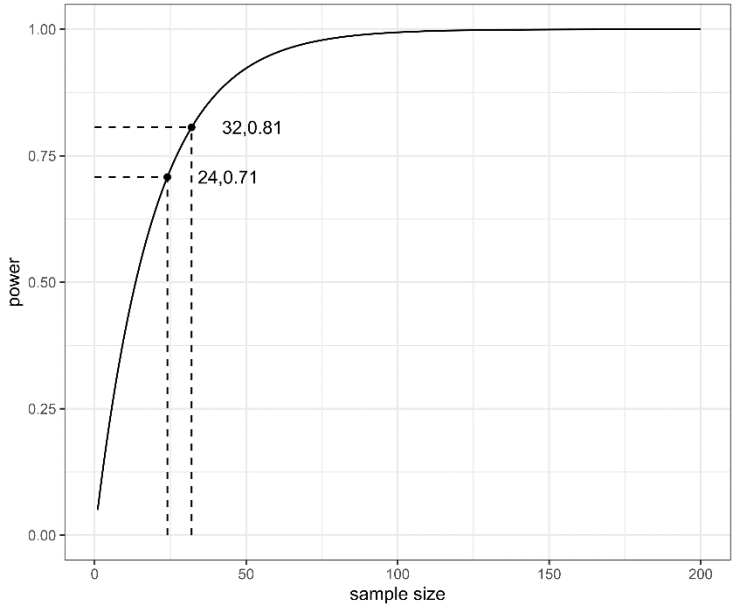

Figure 27 Power Calculation.

As the number of patients investigated was rather small, we evaluated the power of our study. This was performed using a probability of *dMMR* occurrence of 0.05, as this lays in close proximity to the prevalence of *dMMR* observed in melanoma using an appropriate sample size (i.e up to 101 (47)) as well as patients treated with *ICI* in which *dMMR* has been observed (51)). The limit of observed dMMR patients was set to 0. Given these assumptions we calculated a power of 0.71 given the number of investigated patients (n = 24) in our study. In a next step we calculated the minimum of patients required to yield a power of at least 0.80, which resulted in 32 patients (see Figure 27). Therefore, the power of our study seems to have a noteworthy limitation in the evaluation of *dMMR* in *MM* patients, assuming a similar probability of occurrence as has previously been reported.

4.2.2 Multiple Testing

Another limitation of this study might be the multiple tests performed at the same or at intersecting sets of patients (104). However, it was decided not to perform any Bonferroni Correction or other correction of some sort in this thesis.

4.2.3 Positive Control E_1 and Different Time Points

A limitation of this study is that only one positive control was stained at only one time point. Ideally an on-slide external positive control should have been stained for each stained tumor specimen. However, since we did not observe any loss of protein staining in any of the observed tissues with concomitant positive internal control, this limitation is rather technical, and the obtained results can still be accurately interpreted.

4.2.4 No Validation Set E_3

As the number of patients within our study was rather small, we were not able to create an internal validation set by splitting the patients into two sets.

Since internal validation as well as external validation are important for testing a biomarker-based risk prediction model (105), this is another limitation of our study. Since we were not able to investigate whether the observed optimal cut-off value is suitable for predicting *TR* also in a set of patients differing from the observed.

4.3 *Conclusion and Outlook*

4.3.1 No Definitive Conclusion About the Prevalence of dMMR in MM Patients Treated with ICI Can Be Drawn Based on the Findings of This Study

As it is rather unlikely that the true rate of *dMMR* exceeds 15% of melanoma patients treated with *ICI* given our findings, retrospective studies comprising of lager sample sizes should be performed, concomitantly testing for *MSI-H*, to establish a more precise estimate of the true rate of occurrence. Especially, to answer the question whether the IHC_{pos} status should be assessed in the routine setting.

4.3.2 The $\%_{IHC\_pos}$ of MLH1 Could Be a Potential Predictive Biomarker in MM Patients Treated with ICI

The findings observed within this study should be validated within prospective studies with optimized power based on the observed differences of the $\%_{IHC\_pos}$ of MLH1 within this study, incorporating a sufficient sample size to establish a test as well as a validation set and additionally measuring the *oTR* using the immune related response criteria (103).

4.3.3 The TML-status, Evaluated by the Oncomine TML Assay, Seems to Be a Potential Predictive Biomarker in MM Patients Treated With ICI

However, further prospective studies comprising of lager sample sizes, including an external validation set, and measuring the *oTR* using the immune related response criteria (103) should be conducted to further evaluate the diagnostic ability of this assay.

4.3.4 dMMR is No Major Etiologic Factor of a High TML-Status

Given our data, it seems that *dMMR* is not of major relevance within the pathogenesis of a high *TML*-status, however, this question should be addresses by studies especially designed to answer this question.

5 Bibliography

1. Medical Subject Headings [Internet]. U.S. National Library of Medicine; 2016 [cited 2020 Oct 14]. Available from: https://www.nlm.nih.gov/mesh/intro_preface.html#pref_rem
2. U.S. National Library of Medicine. Melanoma [MeSH Unique ID: D008545] [Internet]. [cited 2020 Oct 14]. Available from: https://www.ncbi.nlm.nih.gov/mesh/68008545
3. Leitlinienprogramm Onkologie (Deutsche Krebsgesellschaft Deutsche Krebshilfe AWMF). S3-Leitlinie Prävention von Hautkrebs, Langversion 1.1 2014, AWMF Registernummer: 032/052OL.
4. Armstrong BK, Kricker A. The epidemiology of UV induced skin cancer. J Photochem Photobiol B Biol. 2001 Oct;63(1–3):8–18.
5. Pleasance ED, Cheetham RK, Stephens PJ, McBride DJ, Humphray SJ, Greenman CD, et al. A comprehensive catalogue of somatic mutations from a human cancer genome. Nature. 2010 Jan 16;463(7278):191–6.
6. Maldonado JL, Fridlyand J, Patel H, Jain AN, Busam K, Kageshita T, et al. Determinants of BRAF Mutations in Primary Melanomas. JNCI J Natl Cancer Inst. 2003 Dec 17;95(24):1878–90.
7. Sondak VK, Smalley K. Targeting mutant BRAF and KIT in metastatic melanoma: ASCO 2009 meeting report. Pigment Cell Melanoma Res. 2009 Aug;22(4):386–7.
8. Udayakumar D, Mahato B, Gabree M, Tsao H. Genetic Determinants of Cutaneous Melanoma Predisposition. Semin Cutan Med Surg. 2010 Sep;29(3):190–5.
9. Goldstein AM, Chan M, Harland M, Hayward NK, Demenais F, Timothy Bishop D, et al. Features associated with germline CDKN2A mutations: a GenoMEL study of melanoma-prone families from three continents. J Med Genet. 2006 Aug 11;44(2):99–106.
10. Monshi B, Vujic M, Kivaranovic D, Sesti A, Oberaigner W, Vujic I, et al. The burden of malignant melanoma – Lessons to be learned from Austria. Eur J Cancer. 2016 Mar;56:45–53.
11. Duschek N, Skvara H, Kittler H, Delir G, Fink A, Pinkowicz A, et al. Melanoma epidemiology of Austria reveals gender-related differences. Eur J Dermatol. 2013;23(6):872–8.
12. Haluza D, Simic S, Moshammer H. Temporal and Spatial Melanoma Trends in

Austria: An Ecological Study. Int J Environ Res Public Health. 2014 Jan 6;11(1):734–48.

13. Brierley J, Gospodarowicz MK, Wittekind C, editors. TNM classification of malignant tumors. Eighth Edi. Oxford, UK: John Wiley & Sons, Inc.; 2017. 253 p.
14. Pasquali S, Chiarion-Sileni V, Rossi CR, Mocellin S. Immune checkpoint inhibitors and targeted therapies for metastatic melanoma: A network meta-analysis. Cancer Treat Rev. 2017 Mar;54:34–42.
15. Yun S, Vincelette ND, Green MR, Wahner Hendrickson AE, Abraham I. Targeting immune checkpoints in unresectable metastatic cutaneous melanoma: a systematic review and meta-analysis of anti-CTLA-4 and anti-PD-1 agents trials. Cancer Med. 2016;5(7):1481–91.
16. Khoja L, Day D, Wei-Wu Chen T, Siu LL, Hansen AR. Tumour- and class-specific patterns of immune-related adverse events of immune checkpoint inhibitors: a systematic review. Ann Oncol Off J Eur Soc Med Oncol. 2017 Oct 1;28(10):2377–85.
17. Verma V, Sprave T, Haque W, Simone CB, Chang JY, Welsh JW, et al. A systematic review of the cost and cost-effectiveness studies of immune checkpoint inhibitors 11 Medical and Health Sciences 1112 Oncology and Carcinogenesis. J Immunother Cancer. 2018;6(1).
18. Wu Y, Ju Q, Jia K, Yu J, Shi H, Wu H, et al. Correlation between sex and efficacy of immune checkpoint inhibitors (PD-1 and CTLA-4 inhibitors). Int J cancer. 2018;143(1):45–51.
19. Liu D, Keijzers G, Rasmussen LJ. DNA mismatch repair and its many roles in eukaryotic cells. Mutat Res. 2017 Jul;773:174–87.
20. Tamura K, Kaneda M, Futagawa M, Takeshita M, Kim S, Nakama M, et al. Genetic and genomic basis of the mismatch repair system involved in Lynch syndrome. Int J Clin Oncol. 2019 Sep 4;24(9):999–1011.
21. Korabiowska M, Brinck U, Stachura J, Jawien J, Hasse FM, Cordon-Cardos C, et al. Exonic deletions of mismatch repair genes MLH1 and MSH2 correlate with prognosis and protein expression levels in malignant melanomas. Anticancer Res. 2006;26(2A):1231–5.
22. Korabiowska M, Viehöver M, Schlott T, Berger H, Droese M, Brinck U. Relationship between DNA ploidy-related parameters and the deletions in mismatch repair genes MLH1 and MSH2 in lentigo maligna and malignant melanomas. Arch Dermatol Res.

2001 May;293(5):219–25.

23. Castiglia D, Bernardini S, Alvino E, Pagani E, De Luca N, Falcinelli S, et al. Concomitant activation of Wnt pathway and loss of mismatch repair function in human melanoma. Genes Chromosomes Cancer. 2008 Jul;47(7):614–24.
24. Castiglia D, Pagani E, Alvino E, Vernole P, Marra G, Cannavò E, et al. Biallelic somatic inactivation of the mismatch repair gene MLH1 in a primary skin melanoma. Genes Chromosomes Cancer. 2003 Jun;37(2):165–75.
25. Sharma G, Lian CG, Lin WM, Amin-Mansour A, Jané-Valbuena J, Garraway L, et al. Distinct genetic profiles of extracranial and intracranial acral melanoma metastases. J Cutan Pathol. 2016 Oct;43(10):884–91.
26. Korabiowska M, König F, Verheggen R, Schlott T, Cordon-Cardo C, Romeike B, et al. Altered expression and new mutations in DNA mismatch repair genes MLH1 and MSH2 in melanoma brain metastases. Anticancer Res. 2004;24(2B):981–6.
27. Hussein MR, Wood GS. hMLH1 and hMSH2 gene mutations are present in radial growth-phase cutaneous malignant melanoma cell lines and can be induced further by ultraviolet-B irradiation. Exp Dermatol. 2003 Dec;12(6):872–5.
28. Ponti G, Losi L, Pellacani G, Wannesson L, Cesinaro AM, Venesio T, et al. Malignant melanoma in patients with hereditary nonpolyposis colorectal cancer. Br J Dermatol. 2008 Jul;159(1):162–8.
29. Alvino E, Marra G, Pagani E, Falcinelli S, Pepponi R, Perrera C, et al. High-frequency microsatellite instability is associated with defective DNA mismatch repair in human melanoma. J Invest Dermatol. 2002 Jan;118(1):79–86.
30. Knudson AG. Hereditary cancer: two hits revisited. J Cancer Res Clin Oncol. 1996;122(3):135–40.
31. Murnyák B, Hortobágyi T. Immunohistochemical correlates of TP53 somatic mutations in cancer. Oncotarget. 2016;7(40):64910–20.
32. Cunningham JM, Christensen ER, Tester DJ, Kim CY, Roche PC, Burgart LJ, et al. Hypermethylation of the hMLH1 promoter in colon cancer with microsatellite instability. Cancer Res. 1998 Aug 1;58(15):3455–60.
33. Haraldsdottir S, Hampel H, Tomsic J, Frankel WL, Pearlman R, de la Chapelle A, et al. Colon and endometrial cancers with mismatch repair deficiency can arise from somatic, rather than germline, mutations. Gastroenterology. 2014 Dec;147(6):1308-1316.e1.
34. Xiong Z, Wu AH, Bender CM, Tsao JL, Blake C, Shibata D, et al. Mismatch repair

deficiency and CpG island hypermethylation in sporadic colon adenocarcinomas. Cancer Epidemiol Biomarkers Prev. 2001 Jul;10(7):799–803.

35. Lage H, Christmann M, Kern MA, Dietel M, Pick M, Kaina B, et al. Expression of DNA repair proteins hMSH2, hMSH6, hMLH1, O6-methylguanine-DNA methyltransferase and N-methylpurine-DNA glycosylase in melanoma cells with acquired drug resistance. Int J cancer. 1999 Mar 1;80(5):744–50.
36. Tellez CS, Shen L, Estécio MRH, Jelinek J, Gershenwald JE, Issa J-PJ. CpG island methylation profiling in human melanoma cell lines. Melanoma Res. 2009 Jun;19(3):146–55.
37. Clopper CJ, Pearson ES. The Use of Confidence or Fiducial Limits Illustrated in the Case of the Binomial. Biometrika. 1934 Dec;26(4):404.
38. Korabiowska M, Ruschenburg I, Schlott T, Kubitz A, Brinck U, Droese M. Relation between DNA ploidy status and the expression of the DNA-mismatch repair genes MLH1 and MSH2 in cytological specimens of melanoma lymph node and liver metastases. Diagn Cytopathol. 2001 Mar;24(3):157–62.
39. Seifert M, Scherer SJ, Edelmann W, Böhm M, Meineke V, Löbrich M, et al. The DNA-mismatch repair enzyme hMSH2 modulates UV-B-induced cell cycle arrest and apoptosis in melanoma cells. J Invest Dermatol. 2008;
40. Rass K, Gutwein P, Welter C, Meineke V, Tilgen W, Reichrath J. DNA mismatch repair enzyme hMSH2 in malignant melanoma: increased immunoreactivity as compared to acquired melanocytic nevi and strong mRNA expression in melanoma cell lines. Histochem J. 2001 Aug;33(8):459–67.
41. Korabiowska M, Cordon-Cardo C, Jaenckel F, Stachura J, Fischer G, Brinck U. Application of in situ hybridization probes for MLH-1 and MSH-2 in tissue microarrays of paraffin-embedded malignant melanomas: correlation with immunohistochemistry and tumor stage. Hum Pathol. 2004 Dec;35(12):1543–8.
42. Jewell R, Conway C, Mitra A, Randerson-Moor J, Lobo S, Nsengimana J, et al. Patterns of expression of DNA repair genes and relapse from melanoma. Clin Cancer Res. 2010 Nov 1;16(21):5211–21.
43. Ghasemi Basir HR, Alirezaei P, Ahovan S, Moradi A. The relationship between mitotic rate and depth of invasion in biopsies of malignant melanoma. Clin Cosmet Investig Dermatol. 2018 Mar;11:125–30.
44. Pepponi R, Marra G, Fuggetta MP, Falcinelli S, Pagani E, Bonmassar E, et al. The effect of O6-alkylguanine-DNA alkyltransferase and mismatch repair activities on the

sensitivity of human melanoma cells to temozolomide, 1,3-bis(2-chloroethyl)1-nitrosourea, and cisplatin. J Pharmacol Exp Ther. 2003 Feb;304(2):661–8.

45. Naumann SC, Roos WP, Jöst E, Belohlavek C, Lennerz V, Schmidt CW, et al. Temozolomide- and fotemustine-induced apoptosis in human malignant melanoma cells: response related to MGMT, MMR, DSBs, and p53. Br J Cancer. 2009 Jan 27;100(2):322–33.
46. Shpitz B, Klein E, Malinger P, Osmolovsky G, Gochberg S, Bomstein Y, et al. Altered expression of the DNA mismatch repair proteins hMLH1 and hMSH2 in cutaneous dysplastic nevi and malignant melanoma. Int J Biol Markers. 2005;20(1):65–8.
47. Alvino E, Passarelli F, Cannavò E, Fortes C, Mastroeni S, Caporali S, et al. High expression of the mismatch repair protein MSH6 is associated with poor patient survival in melanoma. Am J Clin Pathol. 2014 Jul;142(1):121–32.
48. Alonso SR, Ortiz P, Pollán M, Pérez-Gómez B, Sánchez L, Acuña MJ, et al. Progression in cutaneous malignant melanoma is associated with distinct expression profiles: a tissue microarray-based study. Am J Pathol. 2004 Jan;164(1):193–203.
49. Garcia JJ, Kramer MJ, O'Donnell RJ, Horvai AE. Mismatch repair protein expression and microsatellite instability: a comparison of clear cell sarcoma of soft parts and metastatic melanoma. Mod Pathol. 2006 Jul;19(7):950–7.
50. Korabiowska M, Dengler H, Kellner S, Stachura J, Schauer A. Decreased expression of MLH1, MSH2, PMS1 and PMS2 in pigmented lesions indicates accumulation of failed DNA repair along with malignant transformation and tumour progression. Oncol Rep. 1997;4(3):653–5.
51. Ponti G, Pellacani G, Tomasi A, Depenni R, Maccaferri M, Maiorana A, et al. Immunohistochemical mismatch repair proteins expression as a tool to predict the melanoma immunotherapy response. Mol Clin Oncol. 2020 Jan;12(1):3–8.
52. Hussein MR, Sun M, Roggero E, Sudilovsky EC, Tuthill RJ, Wood GS, et al. Loss of heterozygosity, microsatellite instability, and mismatch repair protein alterations in the radial growth phase of cutaneous malignant melanomas. Mol Carcinog. 2002 May;34(1):35–44.
53. Hussein MR, Sun M, Tuthill RJ, Roggero E, Monti JA, Sudilovsky EC, et al. Comprehensive analysis of 112 melanocytic skin lesions demonstrates microsatellite instability in melanomas and dysplastic nevi, but not in benign nevi. J Cutan Pathol. 2001 Aug;28(7):343–50.
54. Fontijn D, Adema AD, Bhakat KK, Pinedo HM, Peters GJ, Boven E. O6-

methylguanine-DNA-methyltransferase promoter demethylation is involved in basic fibroblast growth factor induced resistance against temozolomide in human melanoma cells. Mol Cancer Ther. 2007 Oct;6(10):2807–15.

55. Roos WP, Quiros S, Krumm A, Merz S, Switzeny OJ, Christmann M, et al. B-Raf inhibitor vemurafenib in combination with temozolomide and fotemustine in the killing response of malignant melanoma cells. Oncotarget. 2014 Dec 30;5(24):12607–20.
56. Meyer S, Fuchs TJ, Bosserhoff AK, Hofstädter F, Pauer A, Roth V, et al. A seven-marker signature and clinical outcome in malignant melanoma: a large-scale tissue-microarray study with two independent patient cohorts. Soyer HP, editor. PLoS One. 2012 Jun 7;7(6):e38222.
57. Song L, Robson T, Doig T, Brenn T, Mathers M, Brown ER, et al. DNA repair and replication proteins as prognostic markers in melanoma. Histopathology. 2013 Jan;62(2):343–50.
58. Avvaru AK, Saxena S, Sowpati DT, Mishra RK. MSDB: A Comprehensive Database of Simple Sequence Repeats. Genome Biol Evol. 2017 Jun 1;9(6):1797–802.
59. Hile SE, Shabashev S, Eckert KA. Tumor-specific microsatellite instability: Do distinct mechanisms underlie the MSI-L and EMAST phenotypes? Mutat Res - Fundam Mol Mech Mutagen. 2013;743–744:67–77.
60. Ellegren H. Microsatellites: simple sequences with complex evolution. Nat Rev Genet. 2004 Jun;5(6):435–45.
61. Weber JL, Wong C. Mutation of human short tandem repeats. Hum Mol Genet. 1993 Aug;2(8):1123–8.
62. Weber JL. Informativeness of human (dC-dA)n.(dG-dT)n polymorphisms. Genomics. 1990 Aug;7(4):524–30.
63. Kelkar YD, Tyekucheva S, Chiaromonte F, Makova KD. The genome-wide determinants of human and chimpanzee microsatellite evolution. Genome Res. 2008 Jan;18(1):30–8.
64. Levinson G, Gutman GA. Slipped-strand mispairing: a major mechanism for DNA sequence evolution. Mol Biol Evol. 1987 May;4(3):203–21.
65. De La Chapelle A, Hampel H. Clinical Relevance of Microsatellite Instability in Colorectal Cancer. J Clin Oncol. 2010;28:3380–7.
66. Pawlik TM, Raut CP, Rodriguez-Bigas MA. Colorectal carcinogenesis: MSI-H versus MSI-L. Dis Markers. 2004;20(4–5):199–206.

67. Richetta A, Ottini L, Falchetti M, Innocenzi D, Bottoni U, Faiola R, et al. Instability at sequence repeats in melanocytic tumours. Melanoma Res. 2001 Jun;11(3):283–9.
68. Richetta A, Silipo V, Calvieri S, Frati L, Ottini L, Cama A, et al. Microsatellite instability in primary and metastatic melanoma. J Invest Dermatol. 1997 Jul;109(1):119–20.
69. Massi D, Sardi I, Urso C, Franchi A, Borgognoni L, Salvadori A, et al. Microsatellite analysis in cutaneous malignant melanoma. Melanoma Res. 2002;12(6):577–84.
70. Palmieri G, Ascierto PA, Cossu A, Colombino M, Casula M, Botti G, et al. Assessment of genetic instability in melanocytic skin lesions through microsatellite analysis of benign naevi, dysplastic naevi, and primary melanomas and their metastases. Melanoma Res. 2003 Apr;13(2):167–70.
71. Talwalkar VR, Scheiner M, Hedges LK, Butler MG, Schwartz HS. Microsatellite instability in malignant melanoma. Cancer Genet Cytogenet. 1998 Jul 15;104(2):111–4.
72. Rübben A, Babilas P, Baron JM, Hofheinz A, Neis M, Sels F, et al. Analysis of tumor cell evolution in a melanoma: evidence of mutational and selective pressure for loss of p16ink4 and for microsatellite instability. J Invest Dermatol. 2000 Jan;114(1):14–20.
73. Vanderwalde A, Spetzler D, Xiao N, Gatalica Z, Marshall J. Microsatellite instability status determined by next-generation sequencing and compared with PD-L1 and tumor mutational burden in 11,348 patients. Cancer Med. 2018;7(3):746–56.
74. Kroiss MM, Vogt TM, Schlegel J, Landthaler M, Stolz W. Microsatellite instability in malignant melanomas. Acta Derm Venereol. 2001;81(4):242–5.
75. Quinn AG, Healy E, Rehman I, Sikkink S, Rees JL. Microsatellite instability in human non-melanoma and melanoma skin cancer. J Invest Dermatol. 1995 Mar;104(3):309–12.
76. Peris K, Keller G, Chimenti S, Amantea A, Kerl H, Höfler H. Microsatellite instability and loss of heterozygosity in melanoma. J Invest Dermatol. 1995 Oct;105(4):625–8.
77. Matsumura Y, Nishigori C, Yagi T, Imamura S, Takebe H. Mutations of p16 and p15 tumor suppressor genes and replication errors contribute independently to the pathogenesis of sporadic malignant melanoma. Arch Dermatol Res. 1998 Apr;290(4):175–80.
78. Tomlinson IP, Beck NE, Bodmer WF. Allele loss on chromosome 11q and microsatellite instability in malignant melanoma. Eur J Cancer. 1996

Sep;32A(10):1797–802.

79. National Cancer Institute. Definition of tumor mutational burden [Internet]. NCI Dictionary of Cancer Terms. [cited 2020 Oct 14]. Available from: https://www.cancer.gov/publications/dictionaries/cancer-terms/def/795825
80. Meléndez B, Van Campenhout C, Rorive S, Remmelink M, Salmon I, D'Haene N. Methods of measurement for tumor mutational burden in tumor tissue. Transl Lung Cancer Res. 2018 Dec;7(5):661–7.
81. Chalmers ZR, Connelly CF, Fabrizio D, Gay L, Ali SM, Ennis R, et al. Analysis of 100,000 human cancer genomes reveals the landscape of tumor mutational burden. Genome Med. 2017;9(1):34.
82. Rizvi H, Sanchez-Vega F, La K, Chatila W, Jonsson P, Halpenny D, et al. Molecular determinants of response to anti-programmed cell death (PD)-1 and anti-programmed death-ligand 1 (PD-L1) blockade in patients with non-small-cell lung cancer profiled with targeted next-generation sequencing. J Clin Oncol. 2018;36(7):633–41.
83. Segal NH, Parsons DW, Peggs KS, Velculescu V, Kinzler KW, Vogelstein B, et al. Epitope Landscape in Breast and Colorectal Cancer. Cancer Res. 2008 Feb 1;68(3):889–92.
84. Matsushita H, Vesely MD, Koboldt DC, Rickert CG, Uppaluri R, Magrini VJ, et al. Cancer exome analysis reveals a T-cell-dependent mechanism of cancer immunoediting. Nature. 2012 Feb 8;482(7385):400–4.
85. van Rooij N, van Buuren MM, Philips D, Velds A, Toebes M, Heemskerk B, et al. Tumor Exome Analysis Reveals Neoantigen-Specific T-Cell Reactivity in an Ipilimumab-Responsive Melanoma. J Clin Oncol. 2013 Nov 10;31(32):e439–42.
86. Alexandrov LB, Nik-Zainal S, Wedge DC, Aparicio SAJR, Behjati S, Biankin A V., et al. Signatures of mutational processes in human cancer. Nature. 2013 Aug 14;500(7463):415–21.
87. Snyder A, Makarov V, Merghoub T, Yuan J, Zaretsky JM, Desrichard A, et al. Genetic Basis for Clinical Response to CTLA-4 Blockade in Melanoma. N Engl J Med. 2014;371(23):2189–99.
88. Van Allen EM, Miao D, Schilling B, Shukla SA, Blank C, Zimmer L, et al. Genomic correlates of response to CTLA-4 blockade in metastatic melanoma. Science. 2015 Oct 9;350(6257):207–11.
89. Johnson DB, Frampton GM, Rioth MJ, Yusko E, Xu Y, Guo X, et al. Targeted Next Generation Sequencing Identifies Markers of Response to PD-1 Blockade. Cancer

Immunol Res. 2016 Nov 1;4(11):959–67.

90. Samstein RM, Lee C-H, Shoushtari AN, Hellmann MD, Shen R, Janjigian YY, et al. Tumor mutational load predicts survival after immunotherapy across multiple cancer types. Nat Genet. 2019 Feb 14;51(2):202–6.
91. Campesato LF, Barroso-Sousa R, Jimenez L, Correa BR, Sabbaga J, Hoff PM, et al. Comprehensive cancer-gene panels can be used to estimate mutational load and predict clinical benefit to PD-1 blockade in clinical practice. Oncotarget. 2015 Oct 27;6(33):34221–7.
92. ThermoFisher Scientific. Oncomine Tumor Mutation Load Assay [Internet]. [cited 2020 Oct 14]. Available from: https://www.thermofisher.com/at/en/home/clinical/preclinical-companion-diagnostic-development/oncomine-oncology/oncomine-tumor-mutation-load-assay.html
93. Chaudhary R, Bishop J, Broomer A, Cyanam D, Mandelman D, Nistala G, et al. Estimating tumor mutation burden using next-generation sequencing assay. J Clin Oncol. 2017 May 20;35(15_suppl):e14529–e14529.
94. Vanderwalde A, Spetzler D, Xiao N, Gatalica Z, Marshall J. Microsatellite instability status determined by next-generation sequencing and compared with PD-L1 and tumor mutational burden in 11,348 patients. Cancer Med. 2018;7(3):746–56.
95. Mandal R, Samstein RM, Lee K-W, Havel JJ, Wang H, Krishna C, et al. Genetic diversity of tumors with mismatch repair deficiency influences anti-PD-1 immunotherapy response. Science. 2019;364(6439):485–91.
96. Huppertz B, Bayer M, Macheiner T, Sargsyan K. Biobank Graz: The Hub for Innovative Biomedical Research. Open J Bioresour. 2016 Jul 22;3:1–6.
97. Schindelin J, Arganda-Carreras I, Frise E, Kaynig V, Longair M, Pietzsch T, et al. Fiji: an open-source platform for biological-image analysis. Nat Methods. 2012 Jul 28;9(7):676–82.
98. Eisenhauer EA, Therasse P, Bogaerts J, Schwartz LH, Sargent D, Ford R, et al. New response evaluation criteria in solid tumours: revised RECIST guideline (version 1.1). Eur J Cancer. 2009 Jan;45(2):228–47.
99. YOUDEN WJ. Index for rating diagnostic tests. Cancer. 1950 Jan;3(1):32–5.
100. Ponti G, Luppi G, Losi L, Cesinaro AM, Sartori G, Maiorana A, et al. p16 immunohistochemistry of multiple primary melanomas as screening to identify Familial Melanoma Syndrome. Int J Dermatol. 2012 Apr;51(4):488–92.

101. Kim ST, Klempner SJ, Park SH, Park JO, Park YS, Lim HY, et al. Correlating programmed death ligand 1 (PD-L1) expression, mismatch repair deficiency, and outcomes across tumor types: implications for immunotherapy. Oncotarget. 2017 Sep 29;8(44):77415–23.
102. Hodi FS, Hwu W-J, Kefford R, Weber JS, Daud A, Hamid O, et al. Evaluation of Immune-Related Response Criteria and RECIST v1.1 in Patients With Advanced Melanoma Treated With Pembrolizumab. J Clin Oncol. 2016;34(13):1510–7.
103. Wolchok JD, Hoos A, O'Day S, Weber JS, Hamid O, Lebbé C, et al. Guidelines for the evaluation of immune therapy activity in solid tumors: Immune-related response criteria. Clin Cancer Res. 2009;15(23):7412–20.
104. Benjamini Y, Hochberg Y. Controlling the False Discovery Rate: A Practical and Powerful Approach to Multiple Testing. J R Stat Soc Ser B. 1995;57(1):289–300.
105. Taylor JMG, Ankerst DP, Andridge RR. Validation of biomarker-based risk prediction models. Clin Cancer Res. 2008 Oct 1;14(19):5977–83.

6 Supplementary

6.1 *Results*

6.1.1 $E_{1.1}$-*patient-set* Patient Characteristics

	. (N = 24)
Melanoma Type	
CM	15 (62)
UP	9 (38)
Breslow Thickness	
minimum	0.50
median (*IQR*)	1.50 (0.95, 2.46)
mean (*sd*)	1.86 ± 1.28
maximum	5.00
Unknown	10/24 (42)
sex	
m	13 (54)
w	11 (46)
ICB Therapy	
Ipilimumab	15 (62)
Ipilimumab or Pembrolizumab (not clear which arm)	2 (8)
Nivolumab	4 (17)
Pembrolizumab	3 (12)
T	
pT1a	4 (17)
pT1b	1 (4)
pT2a	3 (12)
pT3a	2 (8)
pT3b	1 (4)
pT4a	1 (4)
pT4b	3 (12)
T2a	1 (4)
Tx	7 (29)
unknown	1 (4)
N	
N0	6 (25)
N1a	1 (4)
N1b	3 (12)
N2	1 (4)
N2b	1 (4)
N3	11 (46)
unknown	1 (4)
M	

M1a	6 (25)
M1b	6 (25)
M1c	11 (46)
unknown	1 (4)
Tumor stage	
III C	1 (4)
IV	23 (96)
LDH baseline	
minimum	144
median (*IQR*)	201 (168.50, 320.50)
mean (*sd*)	276.00 ± 169.71
maximum	868
Unknown	1/24 (4)
S100 baseline	
minimum	1.00
median (*IQR*)	11.50 (6.75, 17.25)
mean (*sd*)	11.96 ± 6.64
maximum	23.00
S100 3M	
minimum	1.00
median (*IQR*)	8.50 (2.75, 13.25)
mean (*sd*)	8.50 ± 6.04
maximum	19.00
S100 6M	
minimum	1.00
median (*IQR*)	7.50 (1.75, 13.25)
mean (*sd*)	8.12 ± 6.22
maximum	19.00
BRAF	
K601E	1 (5)
none	11 (52)
V600E	9 (43)
Unknown	3/24 (12)
NRAS	
none	6 (67)
positiv	3 (33)
Unknown	15/24 (62)
KIT	
none	8 (100)
Unknown	16/24 (67)
Eosinophils	
minimum	0.00
median (*IQR*)	0.10 (0.10, 0.25)
mean (*sd*)	0.24 ± 0.41
maximum	2.00
Unknown	1/24 (4)

Lymphocytes	
minimum	0.80
median (*IQR*)	1.40 (1.10, 2.05)
mean (*sd*)	1.60 ± 0.55
maximum	2.60
Unknown	1/24 (4)
Neutrophils	
minimum	2.20
median (*IQR*)	3.70 (3.20, 6.25)
mean (*sd*)	5.07 ± 2.99
maximum	13.40
Unknown	1/24 (4)

STable 1 Complete Patient Characteristics of the *$E_{1.1}$-patient-set*

6.1.2 *E_3-patient-set* Patient Characteristics

	CBG (N = 6)	non-CBG (N = 8)
Melanoma Type		
CM	3 (50)	7 (88)
UP	3 (50)	1 (12)
Breslow Thickness		
minimum	0.75	0.80
median (*IQR*)	1.60 (1.18, 1.90)	2.70 (1.25, 3.30)
mean (*sd*)	1.52 ± 0.73	2.51 ± 1.53
maximum	2.20	5.00
Unknown	3/6 (50)	1/8 (12)
Sex		
m	4 (67)	3 (38)
w	2 (33)	5 (62)
ICB Therapy		
Ipilimumab	3 (50)	6 (75)
Ipilimumab or Pembrolizumab (not clear which arm)	0 (0)	1 (12)
Nivolumab	2 (33)	0 (0)
Pembrolizumab	1 (17)	1 (12)
T		
pT1a	1 (17)	3 (38)
pT3a	0 (0)	2 (25)
pT3b	0 (0)	1 (12)
pT4b	1 (17)	1 (12)
T2a	1 (17)	0 (0)
Tx	3 (50)	0 (0)
Unknown	0 (0)	1 (12)
N		
N0	2 (33)	0 (0)
N1b	0 (0)	1 (12)
N2	1 (17)	0 (0)

N2b	1 (17)	1 (12)
N3	2 (33)	5 (62)
Unknown	0 (0)	1 (12)
M		
M1a	3 (50)	3 (38)
M1b	1 (17)	1 (12)
M1c	2 (33)	3 (38)
Unknown	0 (0)	1 (12)
Tumor Stage		
III C	0 (0)	1 (12)
IV	6 (100)	7 (88)
LDH baseline		
minimum	168	163
median (*IQR*)	306.00 (238.00, 316.25)	205.50 (189.25, 268.25)
mean (*sd*)	286.83 ± 83.47	305.25 ± 241.15
maximum	406	868
S100 baseline		
minimum	0.04	0.06
median (*IQR*)	0.17 (0.08, 0.36)	0.10 (0.07, 0.42)
mean (*sd*)	0.22 ± 0.18	0.30 ± 0.38
maximum	0.45	0.97
Unknown	0/6 (0)	1/8 (12)
S100 3M		
minimum	0.04	0.07
median (*IQR*)	0.06 (0.05, 0.07)	0.44 (0.11, 1,660.37)
mean (*sd*)	0.06 ± 0.02	960.21 ± 1,639.53
maximum	0.08	3,400.00
Unknown	2/6 (33)	1/8 (12)
S100 6M		
minimum	0.03	0.07
median (*IQR*)	0.05 (0.04, 0.07)	0.41 (0.39, 0.46)
mean (*sd*)	0.06 ± 0.02	622.26 ± 1,390.69
maximum	0.10	3,110.00
Unknown	0/6 (0)	3/8 (38)
BRAF		
none	2 (33)	3 (38)
Unknown	1 (17)	1 (12)
V600E	2 (33)	4 (50)
V600K	1 (17)	0 (0)
NRAS		
none	3 (50)	3 (38)
Q61	0 (0)	1 (12)
Unknown	3 (50)	4 (50)
KIT		
none	3 (50)	1 (12)

Unknown	3 (50)	7 (88)
Eosinophils		
minimum	0.00	0.10
median (*IQR*)	0.10 (0.10, 0.33)	0.10 (0.10, 0.20)
mean (*sd*)	0.20 ± 0.20	0.15 ± 0.08
maximum	0.50	0.30
Lymphocytes		
minimum	0.80	1.00
median (*IQR*)	1.10 (0.95, 1.77)	1.70 (1.17, 2.05)
mean (*sd*)	1.40 ± 0.69	1.68 ± 0.55
maximum	2.50	2.50
Neutrophils		
minimum	2.70	2.20
median (*IQR*)	4.55 (3.40, 5.47)	3.55 (3.13, 4.25)
mean (*sd*)	4.47 ± 1.42	3.81 ± 1.25
maximum	6.20	6.30

STable 2 Complete Patient Characteristics of the *E3-patient-set*

6.1.3 Radiologic Workup

Patient	Clinical Benefit	3M	6M	Reason of Exclusion
1	non-CBG	EXCLUDED	included	Insufficient baseline CT, however, compared to 3M a new lesion occurred at 6M, therefore patient was included at 6M
2	non-CBG	included	included	
4	CBG	included	included	
9	non-CBG	EXCLUDED	included	RECIST1.1-status remained unclear over 3M and 6M, however, a new lesion occurred in 6M, therefore, patient was included at 6M.
10	CBG	included	EXCLUDED	No data available within the 6M period.
12	non-CBG	included	included	
14	non-CBG	included	EXCLUDED	No data available within the 6M period
22	CBG	EXCLUDED	included	A PET-CT report stated that there was no evidence of any malignant process. However, we could not review it by our self, therefore, the patient was excluded from 3M.
26	non-CBG	EXCLUDED	EXCLUDED	No sufficient data available.

28	CBG	EXCLUDED	included	Time period between radiologic data and treatment initiation to long, therefore, patient was excluded at 3M. No progression of tumor or new lesions occurred between 3M and 6M, therefore patient was included in 6M.
30	CBG	EXCLUDED	EXCLUDED	No sufficient data available
33	CBG	included	included	included
34	non-CBG	included	included	included
35	non-CBG	included	included	included

STable 3 Sets of Included Patients for *RECIST1.1* Evaluation at 3M and 6M.

6.2 *Statistics*

6.2.1 Linear Regression Diagnostic Plots

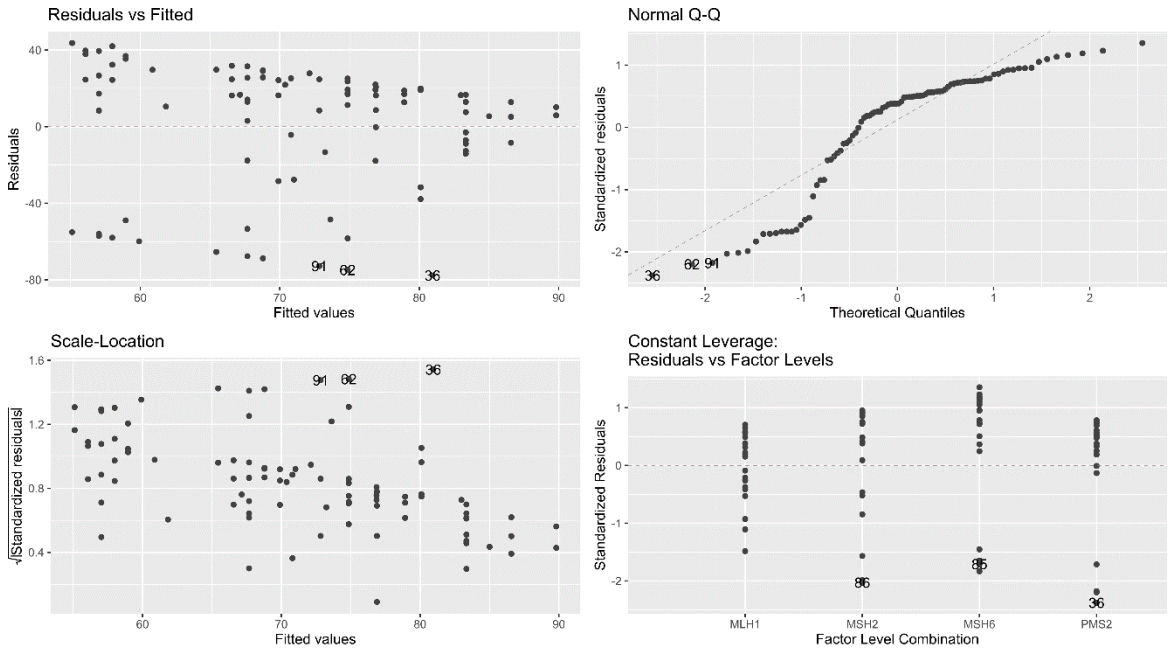

SFigure 1 Diagnostic Plots of the Linear Regression Model for the $\%_{IHC\_pos}$ in Relation to Block Age and *MMR* Protein

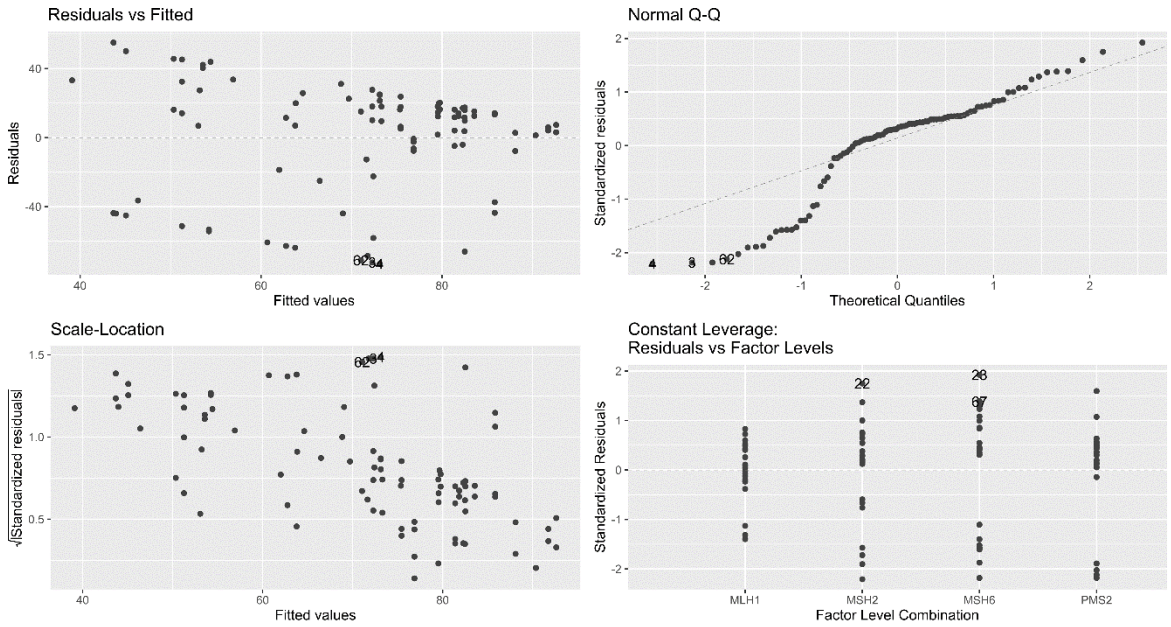

SFigure 2 Diagnostic Plots of the Linear Regression Model for the *%IHC_pos* in Relation to Block Age, Staining Date and *MMR* Protein

6.2.2 Survival Analysis

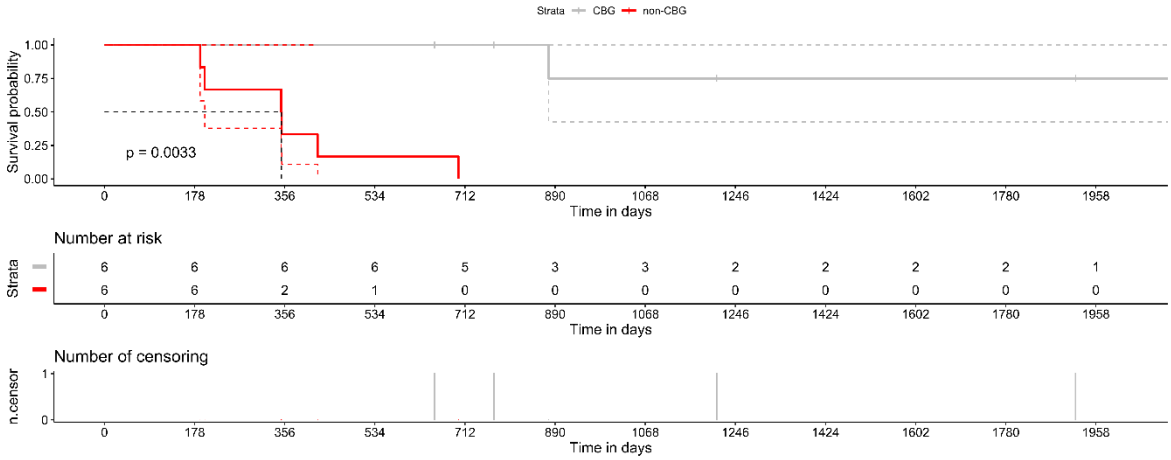

SFigure 3 Kaplan Meier Curve Including the Two Excluded Patients.